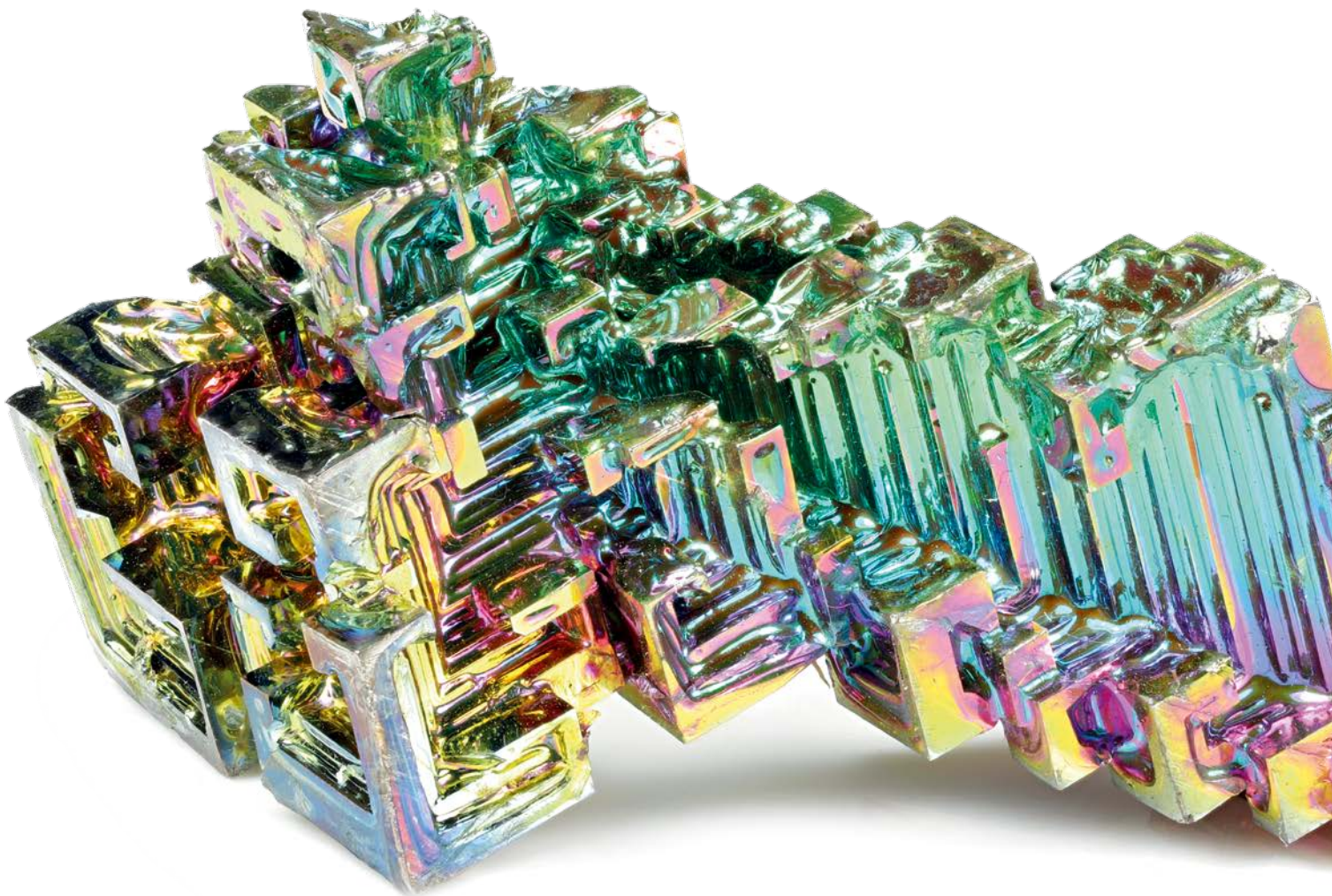


# NETZSCH

Proven Excellence.

## Thermal Properties of Metals and Alloys

Differential Scanning Calorimetry, Thermogravimetry, Simultaneous Thermal Analysis, Evolved Gas Analysis, *PulseTA*<sup>®</sup>, Dilatometry, Thermomechanical Analysis, Dynamic Mechanical Analysis, Laser Flash Analysis and Seebeck Analysis



# Introduction



## Metals and Alloys

The word "metal" originates from several different languages: "metallum" is found in Latin, "metallon" in Greek and in Old French "metal". Metals form a class of substances with various special properties. With a few exceptions, the atoms in metals form so called "metallic bonding" and feature delocalized electrons. This causes metals to feature high electrical and thermal conductivity properties. Metals are also known for their ductility and their metallic lustre. About 80% of all the chemical elements in the periodic table are metals. If a separating line is drawn in the periodic table between boron to astatine, all elements to the left of this line are metals. The transition from metals to non-metals via the metalloids is fluid.<sup>1</sup>

When metals are combined with each other, or when a metal is combined with another element, a so called "alloy" is formed. These materials often have improved properties compared to their pure components such as increased hardness, strength, ductility or corrosion resistance. Alloys can occur naturally or are man-made. A naturally occurring alloy, electum, is a mixture of gold and silver, which might also contain small amounts of copper and other metals. Bronze was one of the very first alloys created by mankind. It is obtained from a mixture of copper and tin. The types of alloys known today are very diverse as well and a large number of production processes exist. Alloys – just like metals – are indispensable in our everyday life and the range of metal and alloy applications is virtually endless.

Thermoanalytical methods play an important role in the characterization of both metals and alloys. For alloys, thermal analysis is especially important: the raw materials (base metals and/or alloying elements) can be examined, the production process can be monitored and optimized, as well as the final product being investigated. This provides the basis to tailor the specific properties of the alloy to meet the requirements of the respective application.

This booklet provides an insight into the wide range of applications of thermal analysis methods and their importance in the determination of the thermophysical properties of metals and alloys.

<sup>1</sup> <https://en.wikipedia.org/wiki/Metal>

## Methods

Differential Scanning Calorimetry (DSC) .....	8
Thermogravimetric Analysis (TGA) .....	9
Simultaneous Thermal Analysis (STA) .....	10
Hyphenated Techniques (Evolved Gas Analysis, EGA) .....	11
<i>PulseTA</i> ® – Calibration/Quantification .....	12
Dilatometry (DIL) .....	13
Thermomechanical Analysis (TMA) .....	14
Dynamic Mechanical Analysis (DMA) .....	15
Laser Flash Analysis (LFA) .....	16
Seebeck Analysis (SBA) .....	17

## Metals

### Non-Ferrous Metals

Measurement of the Mass Change of Titanium .....	20
Oxidation of Zirconium .....	22
Melting Point Determination of Vanadium .....	23
Thermophysical Properties of Pure Molybdenum .....	24
Thermal Expansion of Tungsten to the Highest Temperatures – Without Oxidation .....	28
Measurement of the Seebeck Coefficient of Pure Nickel .....	29
SBA 458 <i>Nemesis</i> ® – Expansion of the Temperature Range I – Ni and Pd .....	30
SBA 458 <i>Nemesis</i> ® – Expansion of the Temperature Range II – PbTe and Iron .....	32

### Ferrous Metals

Energy Release of Cold-Forged Iron .....	34
--	----



# Alloys

## Light Metal Alloys

Thermophysical Properties of Aluminum Alloy in the Solid and Liquid State .....	38
Volumetric Expansion of Aluminum Alloy into the Melt .....	39
Magnesium Alloys .....	40
Precise Determination of the Thermal Expansion of Aluminum Alloy 6061 .....	41

## Ferrous Alloys

Oxidation and Corrosion Studies on Large Metal Surfaces .....	42
Melting and Mass-Loss Behavior of a Steel Sample .....	43
Steel Corrosion under a Humid Atmosphere .....	44
Precise Determination of the Thermal Expansion of Type 304 Stainless Steel .....	45
Low-Alloyed Steel .....	46
Liquid Metals – Cast Iron .....	48

## High-Melting Alloys

Dental Alloy .....	50
Titanium Alloy .....	51
Titanium Alloy $\gamma$ -TiAl .....	52
Hydrogen Emission from Zircaloy BCR-176 Under Water Vapor .....	54
Copper Alloy .....	56
Silver Alloy SF928CH .....	57



## Superalloys

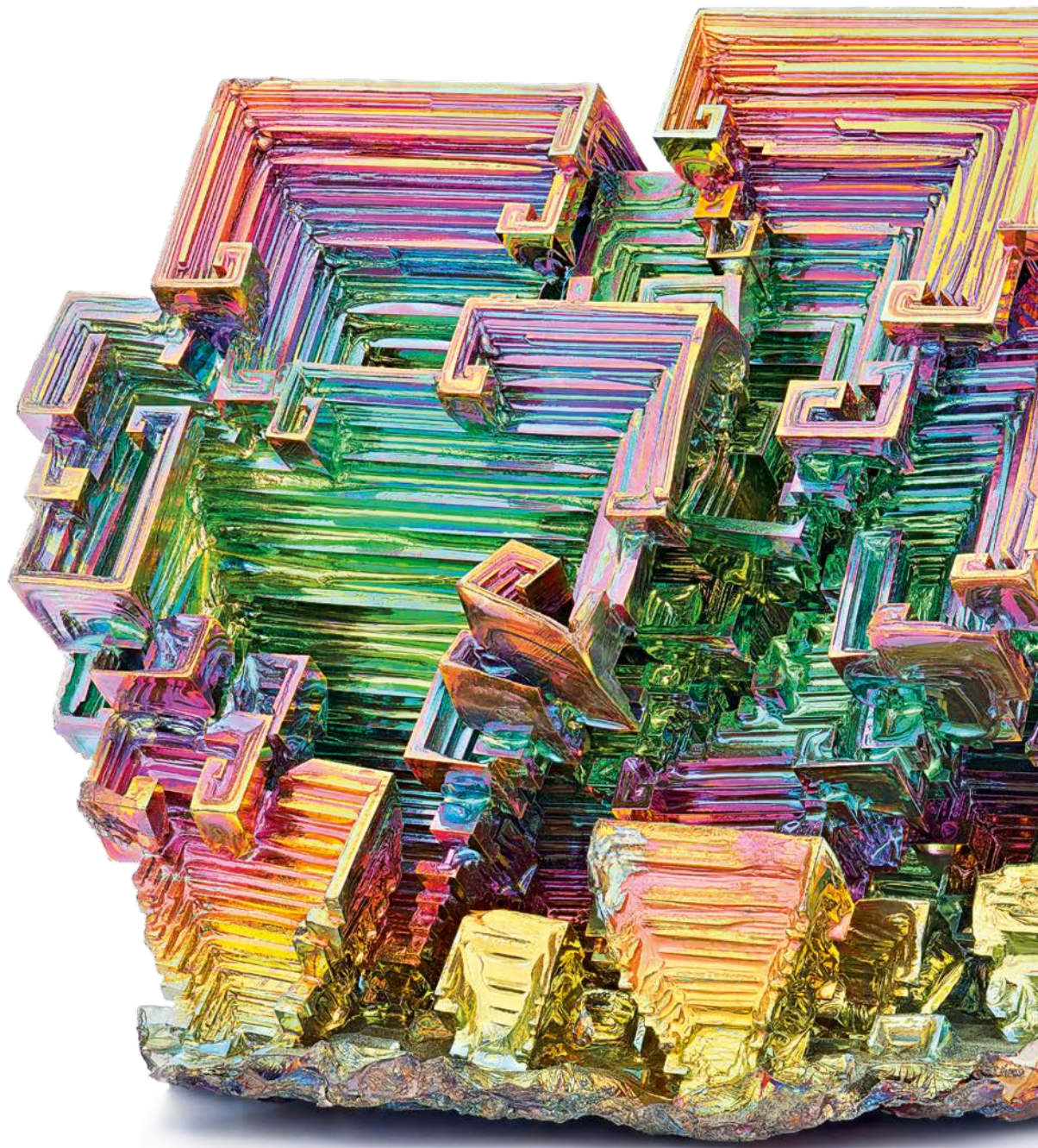
Nickel-Based Superalloy (Inconel 600) – DSC Measurements.....	58
Nickel-Based Superalloy (Inconel 600) – DIL Measurements.....	59
Nickel-Based Superalloy (Inconel 600) – LFA Measurements, Thermal Diffusivity.....	60
Highly Corrosion-Resistant Metal Alloy – Hastelloy.....	61

## Shape Memory Alloys

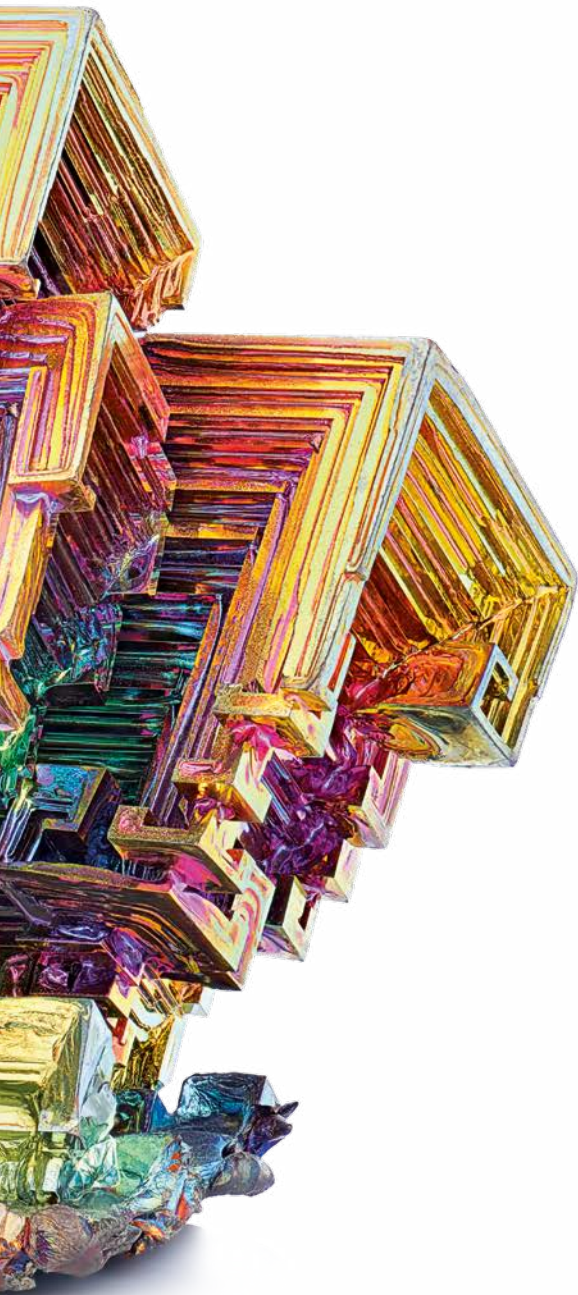
TiNiPd Alloys.....	62
NiTiNOL.....	63
Shape Memory Alloys –Viscoelastic Behavior.....	64
TiNi Memory Metal.....	65

## Related Materials and Other Applications

Metallic Foams – Al Foam.....	68
Amorphous Metals – Amorphous Fe Alloy.....	70
Minerals – High-Performance Material for Thermoelectrical Applications – Skutterudite.....	71
Metal Injection Molding (MIM) – Optimization of the Debinding Process of a Metal Green Body for Highest Product Quality.....	74



# Methods



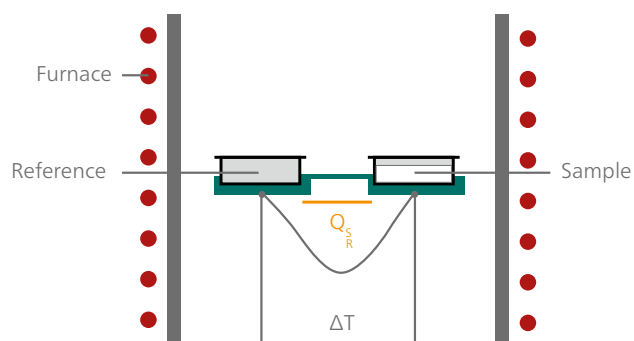


# Methods

## Differential Scanning Calorimetry (DSC)

In accordance with ISO 11357-1, a sample and a reference are subjected to a controlled temperature program (heating, cooling or isothermal). The actual measured properties are the temperature of the sample and the temperature difference between the sample and reference. From the raw data signals, the difference in heat flow between the sample and reference can be determined.

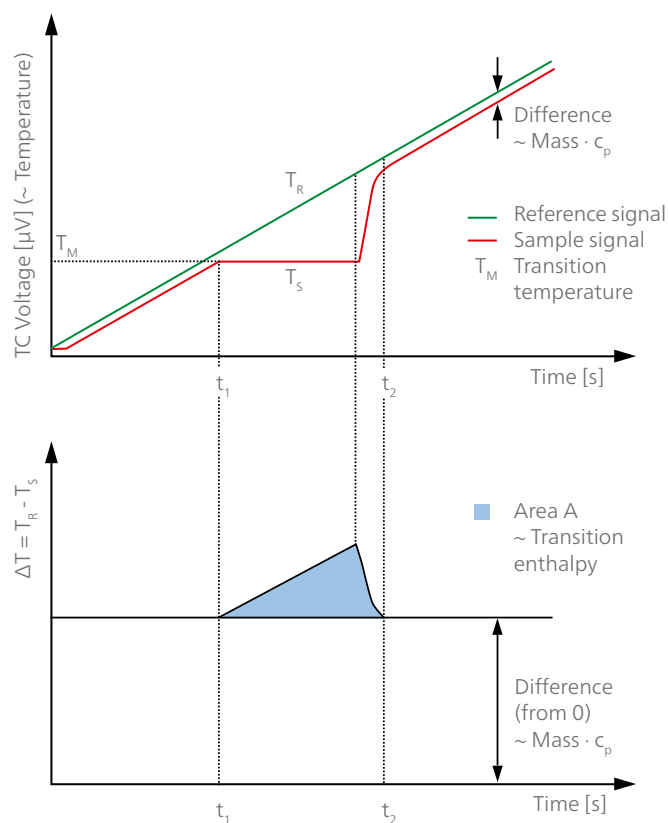
NETZSCH DSC systems are based on relevant instrument and application standards, e.g., ISO 11357, ASTM E793, ASTM D3895, ASTM D3417, ASTM D3418, DIN 51004, DIN 51007.



Schematic of a heat-flux DSC cell

### Measurement Results by DSC

- Melting temperatures and enthalpies (heat of fusion)
- Crystallization temperatures and enthalpies
- Post-crystallization
- Glass transition temperatures
- Oxidation Induction Time (OIT) and Oxidation Onset temperature (OOT)
- Degree of crystallinity
- Solid-solid transitions
- Decomposition onset
- Polymorphism
- Phase transitions
- Liquid crystal transitions
- Eutectic purity
- Purity Determination
- Reaction temperatures and enthalpies
- Cross-linking reactions (curing)
- Degree of curing
- Specific heat capacity ( $c_p$ )
- Molecular weight distribution (via melting peak shape, qualitative)
- Compatibility
- Kinetic studies
- Phase diagrams



Signal generation in a heat-flux DSC

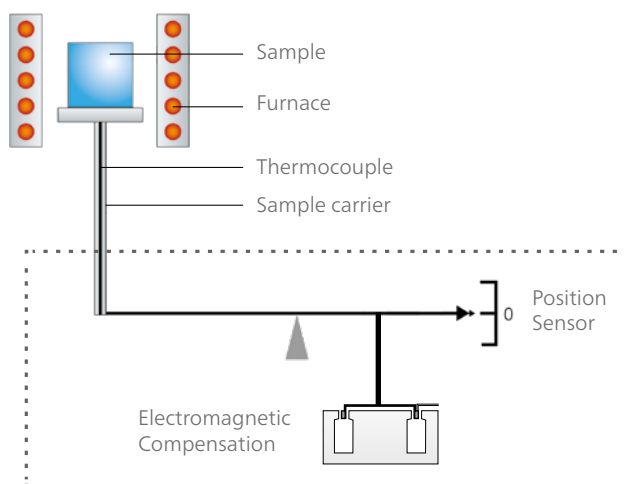
## Thermogravimetric Analysis (TGA)

Thermogravimetric analysis (or also called thermogravimetry, TG) is a method of thermal analysis in which the mass of a sample is measured versus time and/or temperature. This measurement provides information about physical phenomena, such as phase transitions, absorption and desorption; as well as chemical phenomena including thermal decomposition, and solid-gas reactions (e.g., oxidation or reduction).

NETZSCH thermobalances meet respective instrument and application standards including ISO 11358, ISO/DIS 9924, ASTM E1331, ASTM D3850 and DIN 51006.

### Measurement Results by TGA

- Mass changes
- Decomposition
- Reduction behavior
- Influence of aging
- Determination of ash content
- Reaction kinetics
- Identification
- Oxidation
- Corrosion studies
- Determination of plasticizer content and other additives
- Determination of added carbon black
- Purity Determination
- Compositional analysis
- Thermal stability
- Determination of filler content
- Determination of moisture content
- Curie temperatures



Measuring principle of the TG 209 **F1** Libra®

# Methods

## Simultaneous Thermal Analysis (STA)

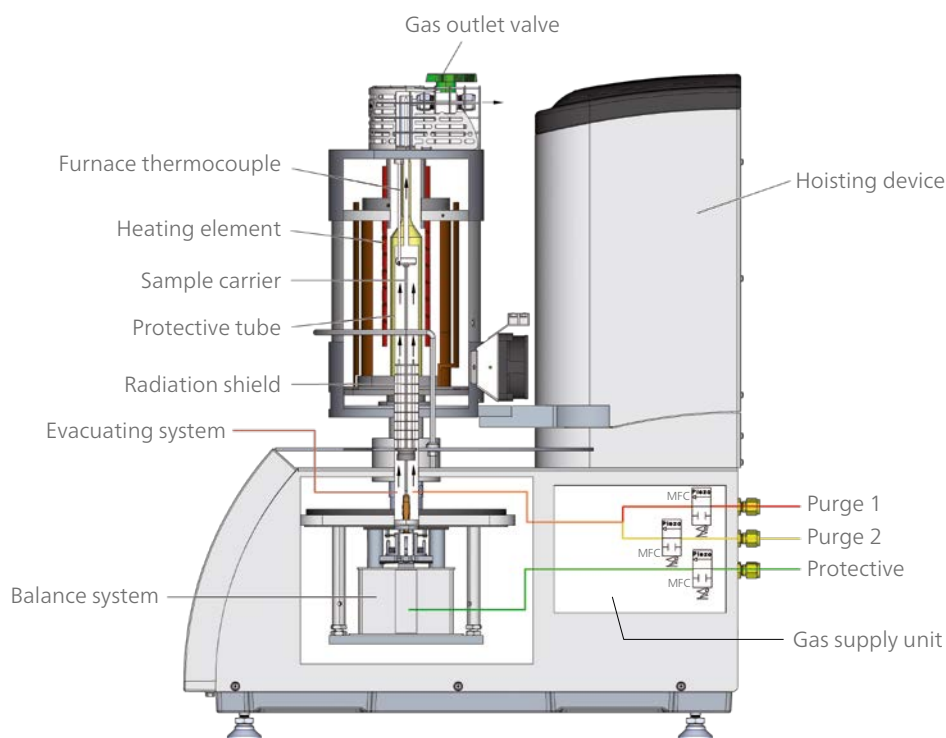
Simultaneous Thermal Analysis (STA) generally refers to the simultaneous application of Thermogravimetry (TGA) and Differential Scanning Calorimetry (DSC) to one and the same sample in a single instrument. The advantages are obvious: The test conditions are identical for both the TGA and DSC signals (same atmosphere, gas flow rate, water vapor pressure, heating rate, thermal contact with the sample crucible and sensor, radiation effect, etc.). Furthermore, sample throughput is improved as more information is gathered from each test run.

### Measurement Results by DSC

- Melting behavior
- Crystallization behavior
- Melting and crystallization enthalpy
- Solid-solid transitions
- Polymorphism
- Degree of crystallinity
- Glass transitions
- Cross-linking reactions
- Oxidative stability
- Purity Determination
- Specific heat capacity
- Kinetics Neo

### Measurement Results by TGA

- Mass changes
- Temperature stability
- Oxidation/reduction behavior
- Decomposition
- Corrosion studies
- Compositional analysis
- Kinetics Neo



Schematic of the STA 449 *F1 Jupiter*<sup>®</sup>



## Hyphenated Techniques (Evolved Gas Analysis – EGA)

By coupling a Thermobalance (TG, TGA), Simultaneous Thermal Analyzer (STA, TGA-DSC) or Dilatometer (DIL) with a Quadrupole Mass Spectrometer (QMS), it is possible to detect and identify evolved gases in exact time correlation with TGA or STA signals.

The combination with an FT-IR (Fourier Transform Infrared Spectrometer) has become a must, especially in the polymer, chemical and pharmaceutical producing industries.

A GC (gas chromatograph) separates gas mixtures based on the differences in component distribution between a stationary phase (e.g., inner coating of a capillary) and a mobile phase (e.g., He). The purge gas rapidly carries away gas components with a low affinity for the stationary phase. Gases with a high affinity for the stationary phase will follow with a significant time delay (“retention time”).

### Measurement Results by Hyphenated Techniques

- Decomposition
  - Dehydration
  - Stability
  - Residual solvent
  - Pyrolysis
- Solid-Gas Reactions
  - Combustion
  - Oxidation
  - Adsorption
  - Desorption
  - Catalysis
  - Corrosion
- Compositional Analysis
  - Polymer content
  - Proximate analysis
  - Binder burnout
  - Dewaxing
  - Ash content
  - Coal analysis
- Identification
  - Gas composition
  - Fingerprint
  - Partial pressure
  - Fragmentation
  - Solid-gas interactions
- Evaporation
  - Vapor pressure
  - Sublimation



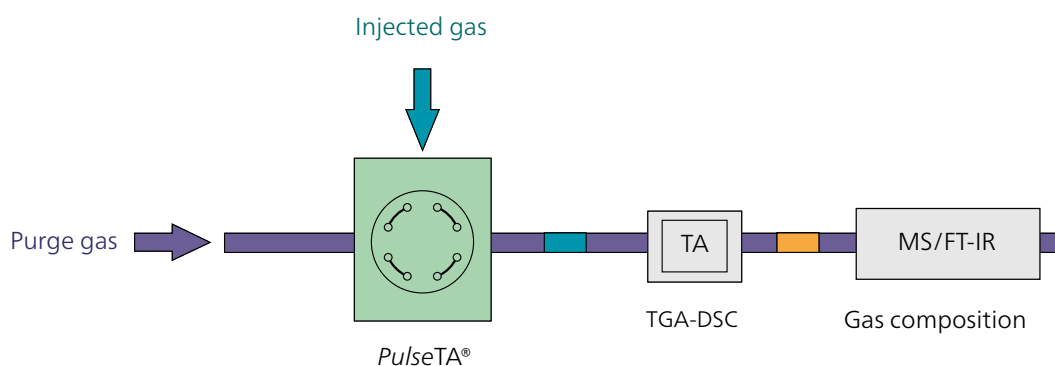
STA 449 F1 Jupiter® coupled to an FT-IR (left, BRUKER OPTICS) with external gas cell and QMS 403 Aëolos® Quadro (right)

# Methods

## PulseTA® – Calibration/Quantification

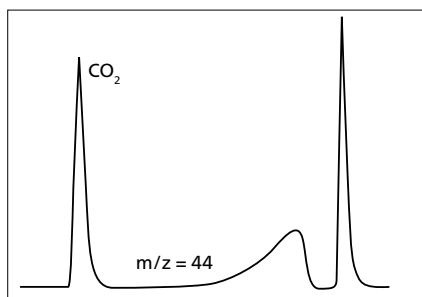
The quantification of MS signals requires calibration of the complete coupled system with a known type and amount of gas or solvent to control for the temperature-dependent flow properties. *PulseTA*® is a perfect tool for achieving quantitative gas detection in separate calibration runs or even online during a sample measurement. A known amount of gas is injected into the sample gas stream and the

registered signal of the resulting pulse is then integrated. The application of *PulseTA*® also allows for studying gas/solid reactions with stepwise control of the process via the injection of a reactive gas, and simplifies adsorption/desorption experiments and studies of catalytic reactions. The valve is controlled completely by the NETZSCH *Proteus*® software. It is no longer necessary to define the gas injection manually.



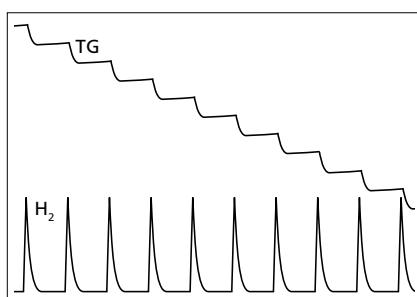
### Inert gas

CO<sub>2</sub> pulses for calibration of a carbonate decomposition



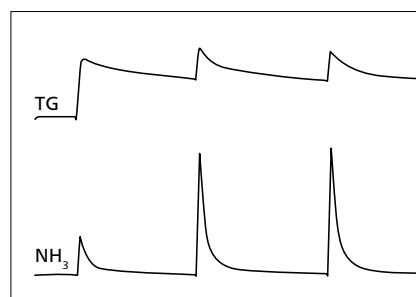
### Reactive gas (gas-solid reaction)

Reduction of metal oxide by H<sub>2</sub> pulses



### Reactive gas (adsorption)

NH<sub>3</sub> adsorption by a zeolite sample



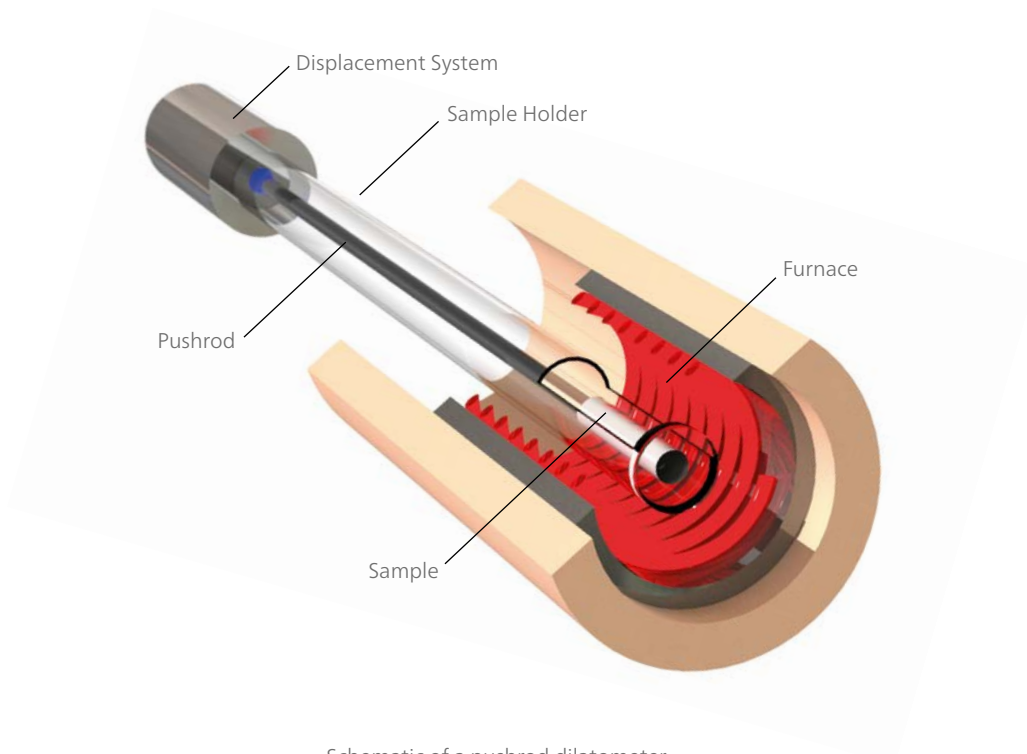
## Dilatometry (DIL)

Dilatometry (DIL) is the method of choice to study length change phenomena of ceramics, glasses, metals, composites, and polymers as well as other construction materials, thus revealing information regarding their thermal behavior and about process parameters or sintering (and curing) kinetics.

All NETZSCH dilatometers are based on, e.g., DIN EN 821, DIN 51045, ASTM E831, ASTM E228.

### Measurement Results by DIL

- Linear thermal expansion
- Coefficient of thermal expansion (CTE)
- Volumetric expansion
- Shrinkage steps
- Softening point
- Glass transition temperature
- Phase transitions
- Sintering temperatures and steps
- Density change
- Influence of additives and raw materials
- Decomposition temperature of, e.g., organic binders
- Anisotropic behavior
- Optimizing of firing processes
- Caloric effects by using *c-DTA*<sup>®</sup>
- Rate-Controlled Sintering (RCS)
- Kinetics Neo
- Debinding



Schematic of a pushrod dilatometer



# Methods

## Thermomechanical Analysis (TMA)

Thermomechanical Analysis (TMA) is a technique for determining the dimensional changes in solids, liquids or pasty materials as a function of temperature and/or time under a defined mechanical force (DIN 51005, ASTM E831, ASTM D696, ASTM D3386, ISO 11359 – Parts 1 to 3). It is closely related to dilatometry, which determines the length change of samples under negligible load (DIN 51045).

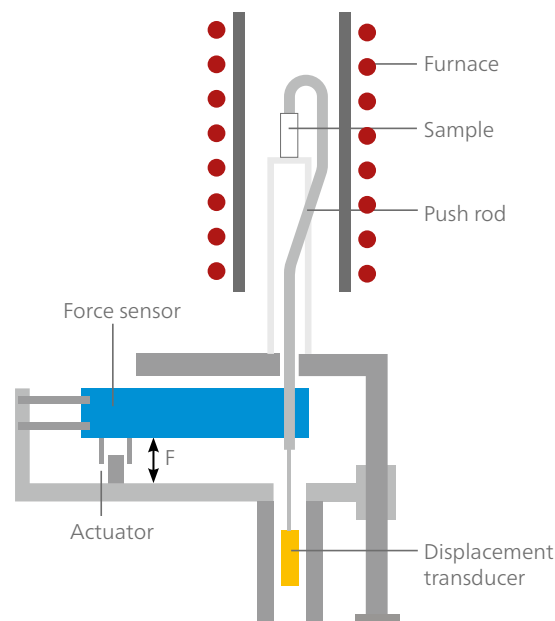
Many materials undergo changes in their thermomechanical properties during heating or cooling. For example, phase changes, sintering steps or softening can occur in addition to thermal expansion. Typical applications include plastics and elastomers, thermosets, composite materials, adhesives, films and fibers, ceramics, glass and metals.

Irrespective of the type of deformation selected (expansion, compression, penetration, tension or bending), every length change in the sample is communicated to a highly sensitive

linear variable displacement transducer (LVDT) via a pushrod and converted into a digital signal. The pushrod and corresponding sample holders of fused silica or aluminum oxide can be quickly and easily exchanged, in order to optimize the system for the respective application.

### Analysis Results by TMA

- Linear thermal expansion
- Coefficient of thermal expansion (CTE)
- Phase transition temperatures
- Sintering steps
- Dilatometric softening points
- Volumetric expansion
- Density changes
- Decomposition temperatures
- ...



#### Operating Principle

The pushrod and corresponding sample holders of fused silica or aluminum oxide can be quickly and easily exchanged, in order to optimize the system for the respective application.

## Dynamic Mechanical Analysis (DMA)

The Dynamic Mechanical Analyzer applies forced periodic loads to the sample and analyzes the phase shift between this primary excitation and the material's response. The response of an ideal elastic system (e.g., a spring) on a sinusoidal load at a given frequency is of the same frequency and exactly in phase with the excitation. The situation changes in a real system: A phase shift ( $\delta > 0^\circ$ ) between the primary excitation and response of the same frequency occurs in the case of linear visco-elastic materials (e.g., polymers); see Figure 1.

Elastic and non-elastic properties inherently describe the dynamic mechanical performance of the material. The storage modulus  $E'$ , the real part of the complex modulus  $E^*$ , represents the elastic component; the loss modulus  $E''$ , the dissipated part, is the imaginary part. Depicted in the complex plane, the loss and storage modulus are the projections of the complex modulus onto the real and imaginary axis (Figure 2). The tangent of the angle between the real axis and the complex modulus ( $E^*$ ) represents the phase shift ( $\tan \delta$ ) between the two.

### Measurement Results by DMA

- Dynamic modulus
- Damping factor ( $\tan \delta$ )
- Young's (static) modulus
- Frequency dependence
- Temperature dependence
- Glass transition
- Secondary transition
- Master curve
- Hysteresis representation
- Relaxation and retardation
- Creep testing
- Aging behavior
- Fatigue test
- Durability test
- Impact test
- Immersion test
- Predictive testing
- Tests under UV light
- Tests under controlled humid atmospheres
- Thermal expansion

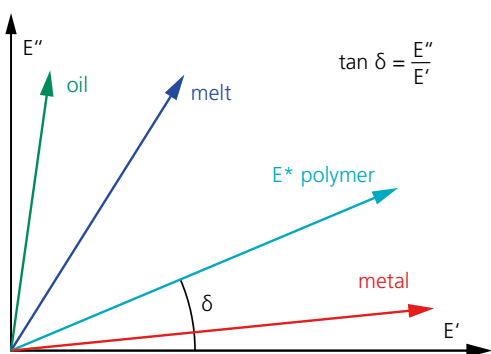


Figure 1. Example of an oscillatory stress on a sample in compression mode

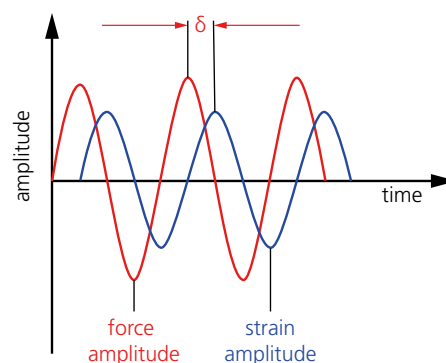


Figure 2. Schematic of the relationship between the dynamic force and strain for a visco-elastic sample,  $\delta$  stands for the phase shift between the two curves

# Methods

## Laser Flash Analysis (LFA)

The Laser or Light Flash Analysis (LFA) method dates back to studies by Parker et al.\* in 1961.

In carrying out a measurement, the lower surface of a plane-parallel sample (Figure 1) is first heated by a short energy pulse. The resulting temperature change on the upper surface of the sample is then measured with an infrared detector. The typical course of the signals is presented in the bottom picture (Figure 2). The higher the sample's thermal diffusivity, the steeper the signal increase.

Using the half time ( $t_{1/2}$ , time value at half signal height) and sample thickness ( $d$ ), the thermal diffusivity ( $a$ ) and finally the thermal conductivity ( $\lambda$ ) can be calculated by means of the formula below. Furthermore, the specific heat capacity ( $c_p$ ) of solids can be determined using the signal height ( $\Delta T_{max}$ ) compared to the signal height of a reference material.

$$\lambda(T) = a(T) \cdot c_p(T) \cdot \rho(T)$$

where

- $\lambda$  = thermal conductivity [W/(m·K)]
- $a$  = thermal diffusivity [mm<sup>2</sup>/s]
- $c_p$  = specific heat capacity [J/(g·K)]
- $\rho$  = bulk density [g/cm<sup>3</sup>].

LFA investigations generally take much less time than thermal conductivity measurements by means of GHP (Guarded Hot Plate) or HFM (Heat Flow Meter).

NETZSCH LFA instruments are based on the respective instrument and application standards for LFA, e.g., ASTM E1461, DIN EN 821, BS EN 1159-2, ASTM C714, etc.

\* W.J. Parker; R.J. Jenkins; C.P. Butler; G.L. Abbott (1961). "Method of Determining Thermal Diffusivity, Heat Capacity and Thermal Conductivity". Journal of Applied Physics. 32

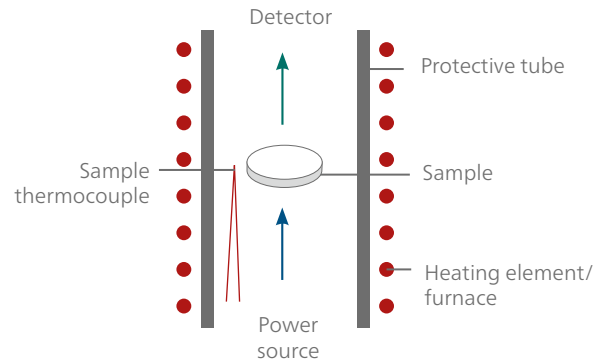


Figure 1. Flash technique

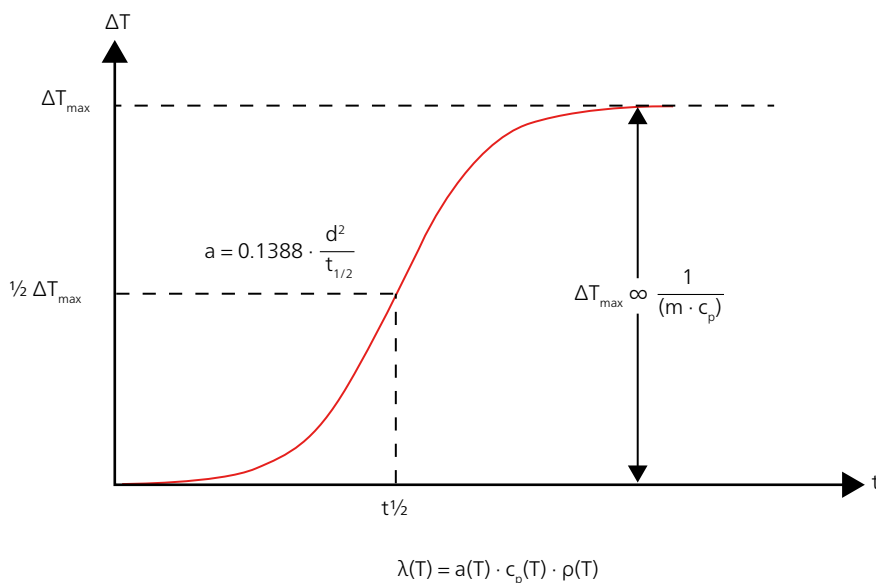


Figure 2. Typical course of the signals of an LFA



## Simultaneous Determination of the Seebeck Coefficient and Electrical Conductivity (SBA)

Thermoelectric materials with high working temperatures and optimized efficiency are being developed for the generation of electrical energy produced from heat. Traditionally this heat has been released into the environment. Therefore, precise knowledge of the thermal properties is of paramount importance in order to develop beneficial thermoelectrics with high electrical conductivities, large Seebeck coefficients, and low thermal conductivities.

The relative performance or efficiency of a thermoelectric material is described by the figure of merit ( $ZT$ ):

$$ZT = \left( \frac{S^2 \cdot \sigma}{\lambda} \right) T$$

where

$S$  = Seebeck coefficient or thermo power of the material [ $\mu\text{V}/\text{K}$ ]

$\sigma$  = electrical conductivity of the material [ $\text{S}/\text{cm}$ ]

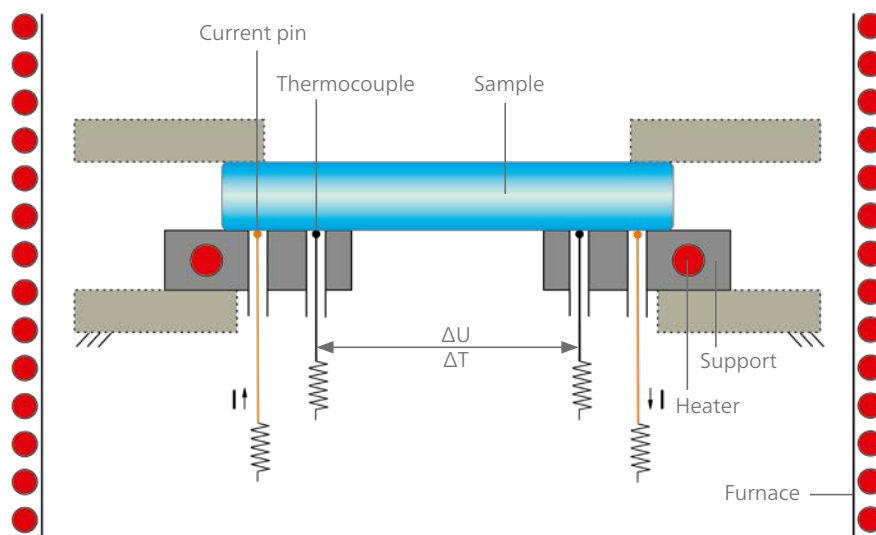
$\lambda$  = total thermal conductivity of the material [ $\text{W}/(\text{m}\cdot\text{K})$ ],

where  $\lambda = a \cdot c_p \cdot \rho$

$T$  = absolute temperature.

### A Clever New Setup

Using current pins and thermocouples on the sample's lower surface, the electrical conductivity is determined by the 4-point method. Micro heaters are placed below the two sample edges, creating temperature gradients in both sample directions for alternative heating of sample ends. The resulting voltage is measured by the thermocouple wires and then used for calculation of the Seebeck coefficient.



Measurement setup of the SBA 458 *Nemesis*® for the temperature range between RT and 800°C





# Metals



# Non-Ferrous Metals

## Measurement of the Mass Change of Titanium

### Introduction

Titanium is a light, lustrous, corrosion-resistant transition metal with white-silvery metallic color. It is often used in steels as an alloying element. Because of the high tensile strength to density ratio, corrosion resistance and ability to withstand moderately high temperatures without creeping, titanium alloys are used in aircrafts, armor plating, naval ships, spacecraft and missiles. Furthermore, consumer products like hammer heads, tennis rackets, golf clubs or jewelry can be made of titanium. Due to its biocompatibility, titanium is used for surgical implements and implants.

Fine titanium powder burns brightly and is used in fireworks for the silver sparks. Last but not least, titanium compounds also feature in very important applications: for example,  $\text{TiO}_2$  is a white permanent pigment for paints, paper, etc., and  $\text{TiN}$  is often used to coat cutting tools such as drill bits.

### Test Results

Figure 1 depicts the temperature-dependent mass change (TGA), rate of mass change (DTG) and DTA signal. The sample mass increased by 66% with a maximum rate of mass change at 858°C. The DTA signal exhibited an exothermic peak which is typical for oxidation. The mass spectrometer displayed a minimum for mass number 32 which reflects the consumption of  $\text{O}_2$  and thus confirms the oxidation (see Figure 2). The oxidation forms a protective layer on the metal.

Test Conditions	
Instrument	STA 449 Jupiter® – QMS Aëolos®
Sample	Titanium
Sample mass	71.60 mg
Temperature range	RT to 1500°C
Heating rate	10 K/min
Atmosphere	Synthetic air (70 ml/min)
Sample mass	71.60 mg
Crucible	$\text{Al}_2\text{O}_3$
Sensor	TGA-DTA, type S



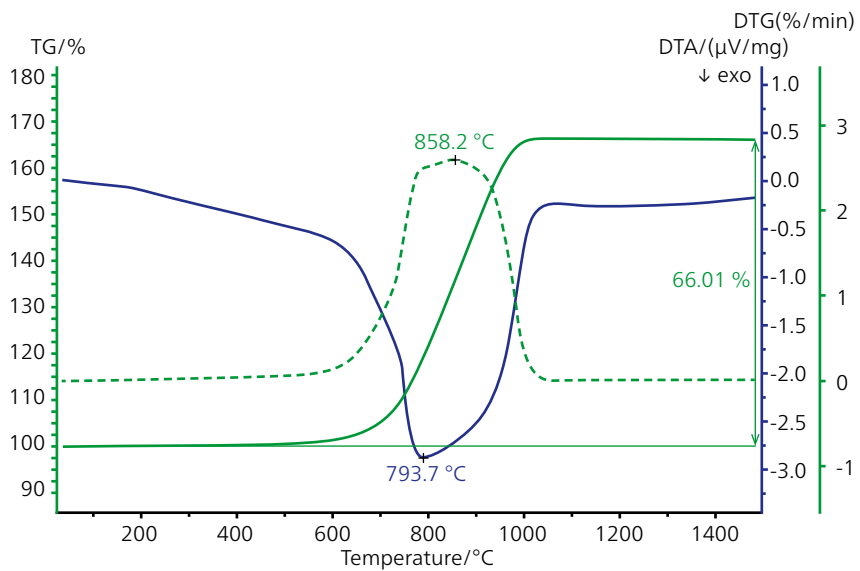


Figure 1. Temperature-dependent mass change of a Ti powder, rate of mass change and DTA signal

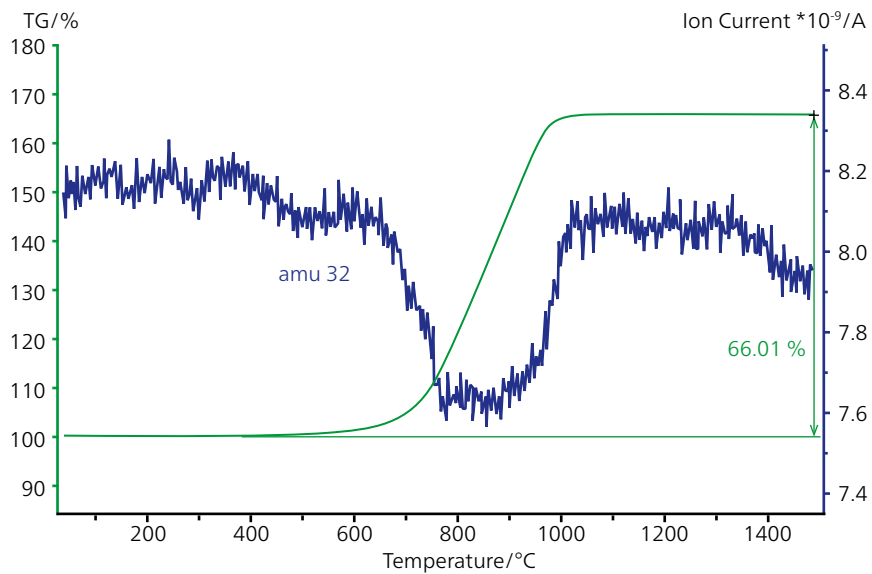


Figure 2. TGA curve and the simultaneously recorded ion current of amu 32 (oxygen) of the MS measurements

# Non-Ferrous Metals

## Oxidation of Zirconium

### Introduction

The oxygen trap system, *OTS*<sup>®</sup>, for the STA 449 **F1/F3 Jupiter**<sup>®</sup> and DSC 404 **F1/F3 Pegasus**<sup>®</sup> removes traces of residual oxygen in the gas atmosphere inside the instrument. A residual oxygen content of < 1ppm can be achieved.

A ceramic substrate bearing a getter ring is mounted on the sample carrier or in the sample carrier tube. This getter ring is capable of almost entirely eliminating the residual oxygen after evacuation.

Such low oxygen concentrations cannot be achieved unless the instrument is vacuum-tight and equipped with an evacuation system. Both of these requirements are fulfilled by the STA 449 **F1/F3 Jupiter**<sup>®</sup> and DSC 404 **F1/F3 Pegasus**<sup>®</sup> systems.

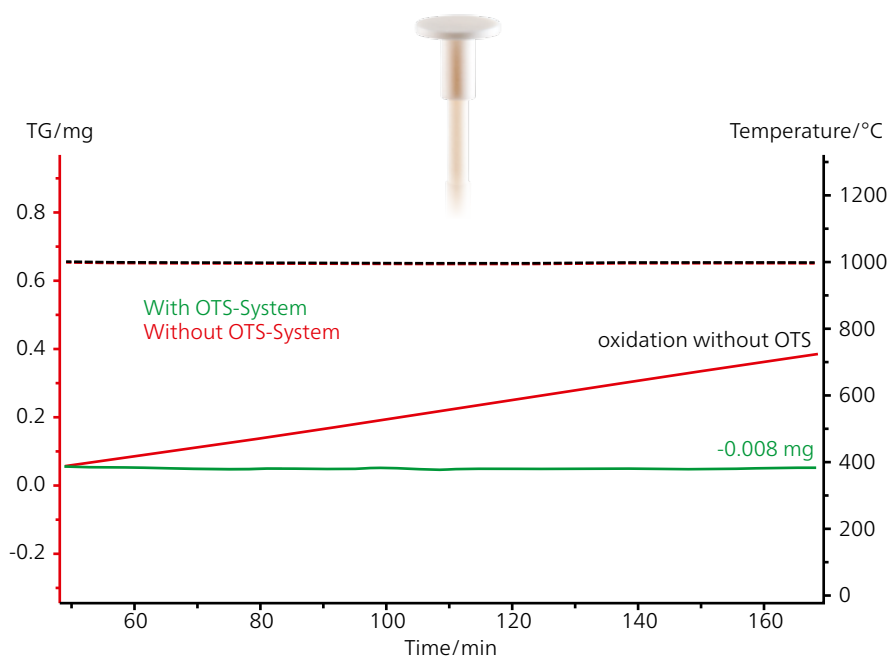
### Test Results

In this example, a zirconium sample was measured with the STA 449 **F1 Jupiter**<sup>®</sup> under isothermal conditions (1000°C).

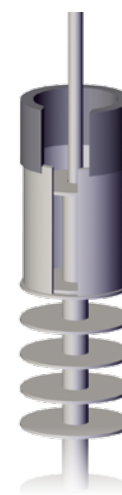
After two hours at 1000°C, an oxidation effect was observed in the sample, measured without *OTS*<sup>®</sup> system in the instrument.

Test Conditions	
Instrument	STA 449 <b>F1 Jupiter</b> <sup>®</sup> , equipped with the oxygen trap system, <i>OTS</i> <sup>®</sup>
Sample	Zirconium
Sample mass	109.09 mg
Temperature range	2h isothermal at 1000°C
Heating rate	20 K/min (RT up to 1000°C)
Atmosphere	Helium, dynamic, 50 ml/min
Crucible	Slip-on plate made of alumina
Sensor	TGA sample carrier

The mass increase amounts to 0.38 mg. Using a sample holder with integrated *OTS*<sup>®</sup>, however, no significant oxidation occurs which can be seen in the negligible mass loss (-0.008 mg).



TGA signal of the STA measurements on zirconium under isothermal conditions at 1000°C



*OTS*<sup>®</sup> Oxygen Trap System



## Melting Point Determination of Vanadium

### Introduction

For DTA and TGA measurement to very high temperatures, zirconia crucibles are available for tests up to 2000°C. These crucibles can be used for testing metals such as vanadium.

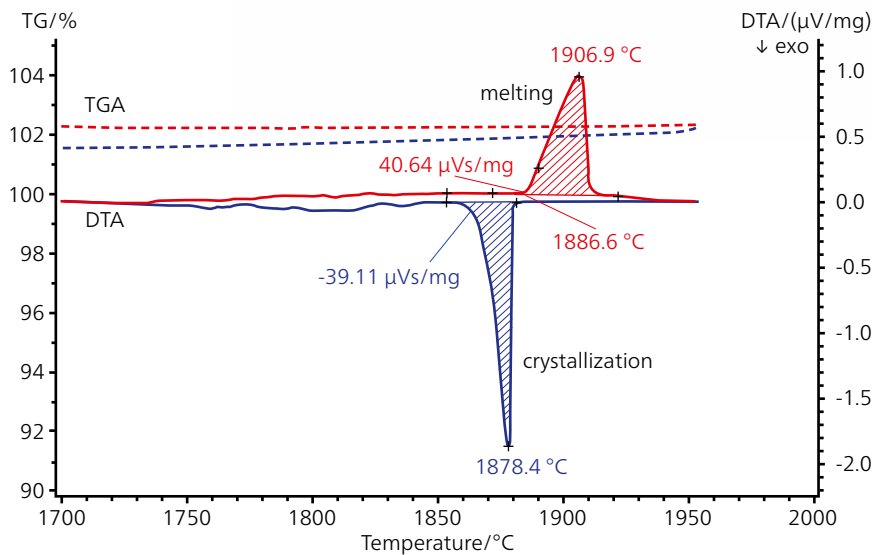
### Test Results

In this example, the melting point of a vanadium sample (99.7%) was determined with the STA 449 **F1 Jupiter**<sup>®</sup>. ZrO<sub>2</sub> crucibles were used. Melting occurs at an onset temperature of 1886°C. During cooling, the sample recrystallizes with only a small supercooling effect at 1878°C. The typical oxidation effects for vanadium (starting at 660°C in air) cannot be observed. Even in the liquid state above melting, neither the DSC nor the TGA curve shows effects or a mass increase. This proves the vacuum tightness of the instrument and the suitability of the zirconia crucible.

Test Conditions	
Instrument	STA 449 <b>F1 Jupiter</b> <sup>®</sup>
Temperature range	RT to 2000°C
Sample	Vanadium (99.7%)
Sample mass	21.13 mg
Heating rate	20 K/min
Cooling rate	75 K/min
Atmosphere	Helium
Crucibles	ZrO <sub>2</sub>



Crucible variety made of Au, Ag, Pt, Al<sub>2</sub>O<sub>3</sub>, BN for NETZSCH STA systems



Melting and crystallization of vanadium

# Non-Ferrous Metals

## Thermophysical Properties of Pure Molybdenum

### Introduction

Molybdenum has been available as a specific heat standard from NIST [1] for several decades. According to literature [1, 2, 3, 4], see page 27, pure molybdenum should not show any phase changes up to the melting point. This is, however, critical because it is sensitive to oxygen at elevated temperatures. Due to the high vapor pressure of the molybdenum oxides, the material does not generally change properties because of surface oxidation. The formed oxides simply evaporate from the surface. All these special properties of molybdenum make it a reasonable substance for a multi-property standard material.

Test Conditions	
Instruments	DIL, DSC, LFA
Sample	Molybdenum (99.99%)
Temperature range	-125°C to 1400°C
Dimensions	Length: 25 mm, Ø: 5 mm (DIL) Thickness: 5.5 mm and 1 mm (DSC) Thickness: 12.7 mm and 2 mm (LFA) (metal rod for sample preparation)
Atmospheres	He, Ar (50 ml/min)
Heating rates	5 K/min (DIL); 20 K/min (DSC)

### Experimental

Measurements of different thermophysical properties such as thermal expansion, density change, specific heat capacity and thermal diffusivity were carried out on a pure (99.99%) molybdenum material.

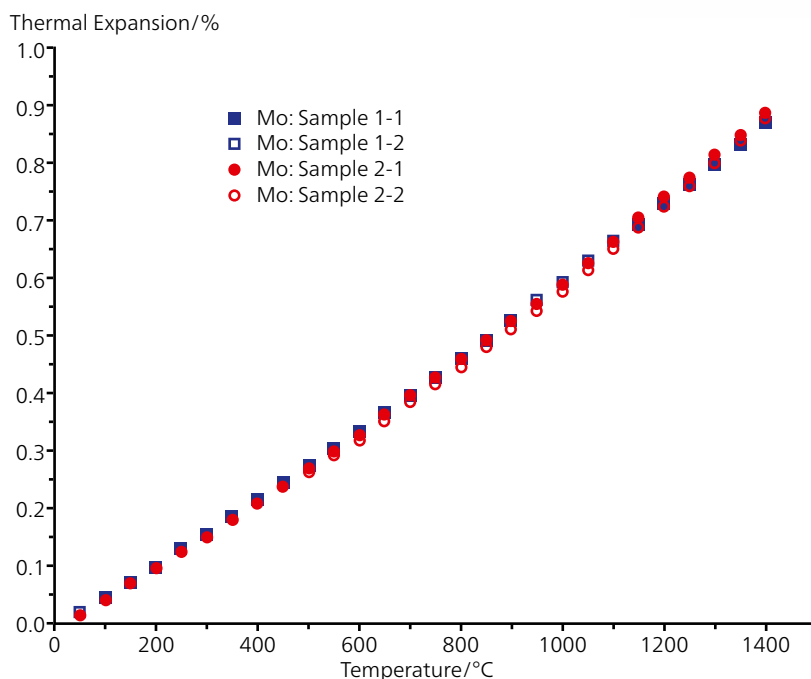


Figure 1. Thermal expansion for two different molybdenum samples, measured by dilatometry

## Dilatometry

Pushrod dilatometry (DIL) was employed for the measurement of the thermal expansion and determination of the density change.

The test results allow a detailed insight into the material's behavior under thermal treatment and it was also possible to determine the thermal conductivity of the sample. A comparison was made of all test results with available literature data.

Tests were carried out on different samples prepared from the original material and measured between  $-125^{\circ}\text{C}$  and  $1400^{\circ}\text{C}$ . It was therefore possible to evaluate this material as a potential candidate for a standard material for different thermophysical properties over a broad temperature range.

The pure molybdenum (99.99%) was supplied by Plansee SE, Reutte, Austria. A large block, 30 mm in diameter and 120 mm in length, was used for the analysis. From this cylindrical block, different samples were prepared for the various test techniques. For each measurement method, two samples were prepared and tested two to three times. The thermal stability and homogeneity of the material was checked and the repeatability of the test results was determined.

## Test Results

Presented in Figure 1 are the measured thermal expansion results for the two different molybdenum samples, measured twice. Data scattering between the samples and the different experiments are generally within  $\pm 1.5\%$ . Considering the accuracy and repeatability of the instrument employed, the influences of surface effects and the impact of the evaporation of oxides, scattering of the data is in an acceptable range. The results give no indication of material inhomogeneities or changes in the thermal expansion values between the different heating runs.

Depicted in Figure 2 are the volumetric expansion and the density change of molybdenum versus temperature. The volumetric expansion was determined from the measured thermal expansion assuming an isotropic behavior of the material and therefore, the same expansion behavior in all directions. Density calculation was based on the volumetric expansion and the room-temperature bulk density of  $10.216\text{ g}\cdot\text{cm}^{-3}$ . The room-temperature bulk density was determined from the original supplied sample block by measuring mass and volume.

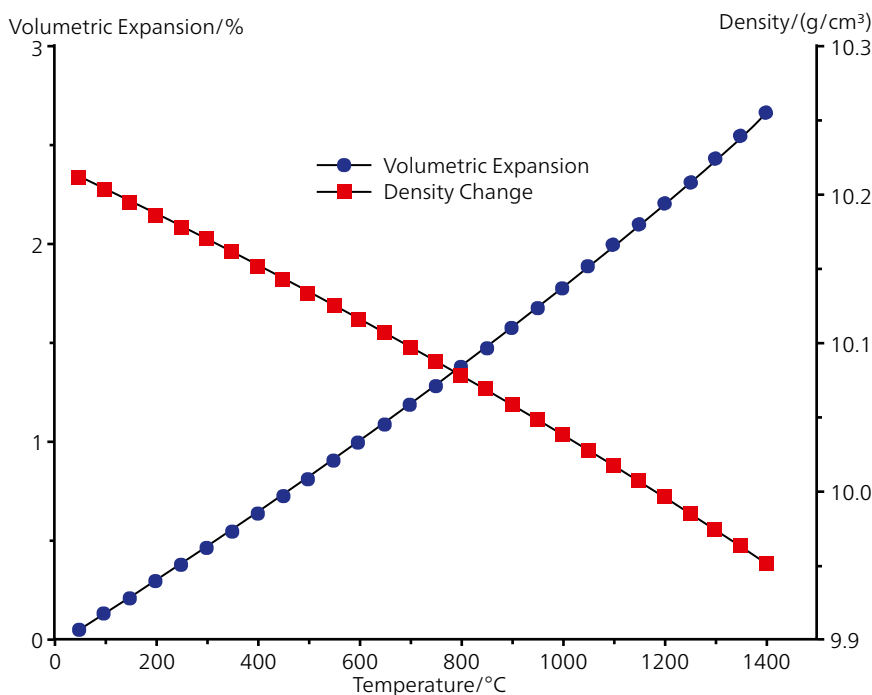


Figure 2. Volumetric expansion and density change, determined by dilatometer measurements

# Non-Ferrous Metals

## Differential Scanning Calorimetry

Figure 3 shows the specific heat capacity values measured with the differential scanning calorimeter (DSC). Again, both samples were measured twice in the low-temperature steel furnace (at the temperature range -125°C to 300°C) and in the high-temperature platinum furnace (at the temperature range 300°C to 1275°C) of the NETZSCH DSC 404 Pegasus®. The deviation between the individual results was within ±2.0% and therefore easily within the stated uncertainty of the instrument used for the tests. The values show a strong increase versus temperature in the low-temperature range. This behavior can be expected according to the well-known Debye theory [5]. At high temperatures, the increasing values are nearly linear. This is in perfect agreement with the solid-state physics (Rule of Dulong and Petit, [5]). No overlapping transition or other thermal effects were detected within this temperature range, clearly indicating that no phase change occurs in the material between -125°C and 1275°C. This fulfills the condition as a standard material since no structural changes occur in the temperature range of interest.

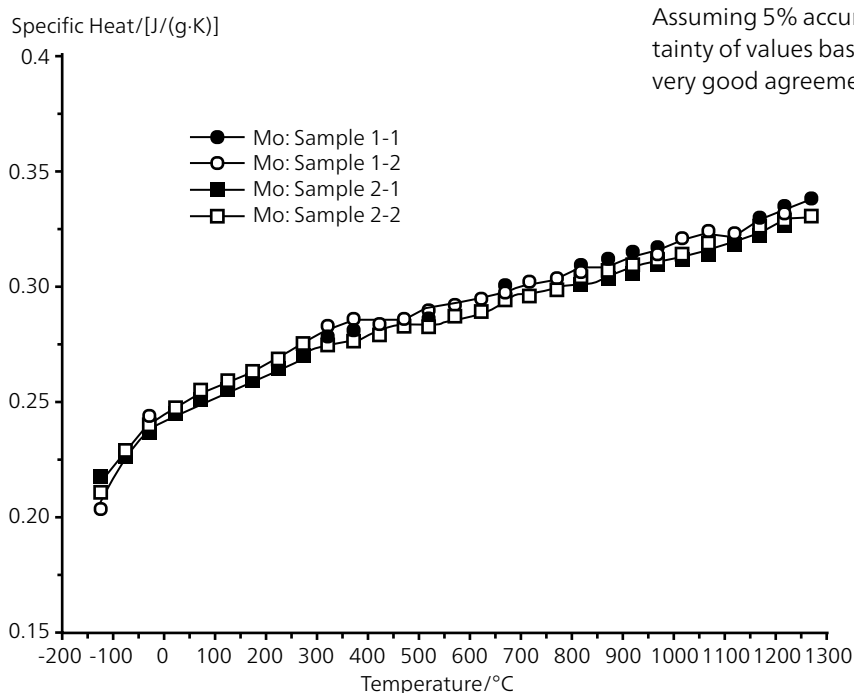


Figure 3. Specific heat capacity results

## Laser Flash Analysis

Figure 4 shows the measurement results for the thermal diffusivity gathered from the different Laser/Light Flash Analysers (LFA) used for the tests. It can clearly be seen that the thermal diffusivity decreases versus temperature. The decrease follows the  $T^{-1}$  behavior below 600°C resulting in a nearly linear decrease at higher temperatures. Such behavior is typical for predominately phonon-conducting materials such as ceramics or graphite materials. Therefore, it might be the case that the electron contribution to the heat transfer is small for this metallic material. Scattering of the measurement results from run to run and from sample to sample is generally within ±2%. Only at 1000°C, slightly higher scattering (±3%) was observed. A possible explanation for this might be the evaporation of molybdenum oxides in this temperature range influencing the sample's emissivity and therefore the absorption of laser light and emission of infrared light.

Presented in Figure 5 are the results of the thermal conductivity determined by multiplying the measured density, specific heat and thermal diffusivity. The density data below room temperature and the specific heat above 1275°C were determined by a linear extrapolation of the measured data. It can clearly be seen, that the thermal conductivity follows the temperature dependence of the thermal diffusivity. A comparison with literature values [6] was also made. Assuming 5% accuracy of the literature values and 3% uncertainty of values based on the measurement, the results are in very good agreement.

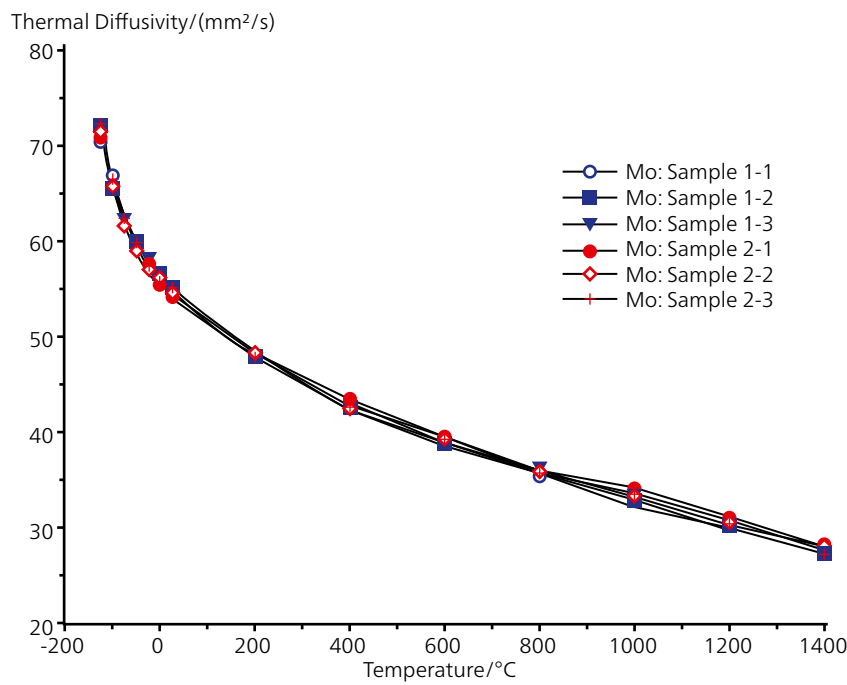


Figure 4. Thermal diffusivity results, obtained by LFA measurements

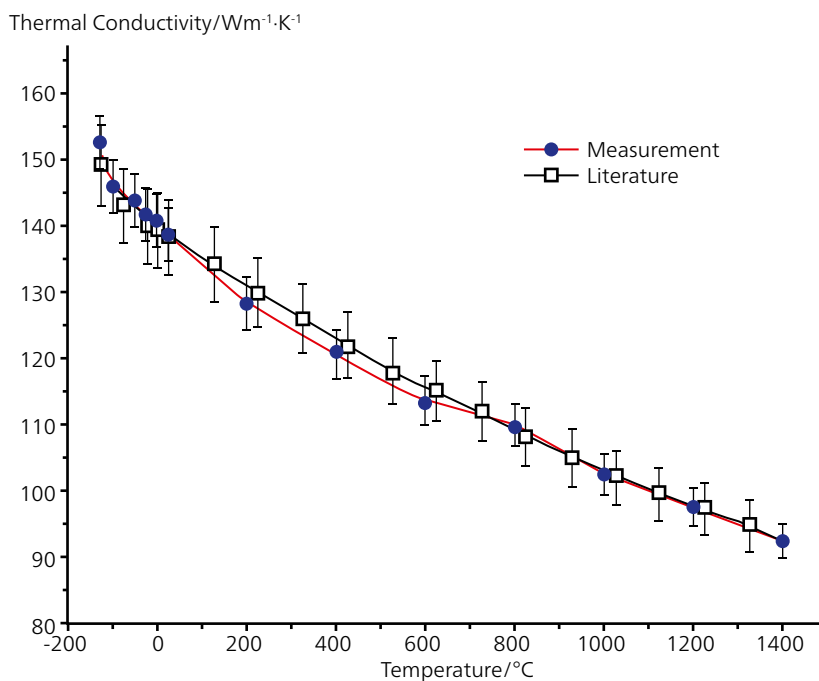


Figure 5. Thermal conductivity results of the LFA measurements on a pure Mo sample

## Conclusion

Various thermophysical properties (thermal expansion, density change, specific heat capacity, thermal diffusivity, thermal conductivity) were measured on high-purity molybdenum. The comparison with literature values indicated the quality of the measurement results and the reliability of the material. It can be assumed from the tests results that pure molybdenum might be a reasonable candidate to be used as a standard material up to high temperatures above 1200°C. It may be used as a calibration standard for various thermo-physical properties.

## Literature

- [1] P Cali, Certificate – Standard Reference Material 781, Molybdenum – Heat Capacity, National Bureau of Standards, Washington, 1977
- [2] d'Ans, Lax, Taschenbuch für Chemiker und Physiker, 3, Springer Verlag, Berlin, 2000
- [3] Y. S. Touloukian, R. K. Kirby, R. E. Taylor, P. D. Desai, Thermophysical Properties of Matter, Vol. 12, Thermal Expansion, Metallic Elements and Alloys, IFI Plenum, New York-Washington, 1977
- [4] Y. S. Touloukian, E. H. Buyco, Thermophysical Properties of Matter, Vol. 4, Specific Heat, Metallic Elements and Alloys, IFI Plenum, New York-Washington, 1970
- [5] C. Kittel, H. Krömer, Thermodynamik, 5. Auflage, Oldenburg Wissenschaftsverlag GmbH, München (2001)
- [6] Y. S. Touloukian, R. W. Powell, C. Y. Ho, M. C. Nicolaou, Thermophysical Properties of Matter, Vol. 10, Thermal Diffusivity, Metallic Elements and Alloys, IFI Plenum, New York-Washington, 1973

# Non-Ferrous Metals

## Thermal Expansion of Tungsten to the Highest Temperatures – Without Oxidation

Tungsten is a metal that is very sensitive to oxidation. However due to the vacuum-tight design of the DIL 402 *Expedis® Supreme*, the material can be measured in pure He atmosphere (in combination with *OTS®* – Oxygen Trap System) to determine its true expansion behavior. There is no need of a reducing atmosphere to suppress superficial oxidation (which would change the color of the sample).

### Comparison of Measurement and Literature Values

Measured CTE between 20°C and 1500°C  
 $5.143 \times 10^{-6} \text{ 1/K}$

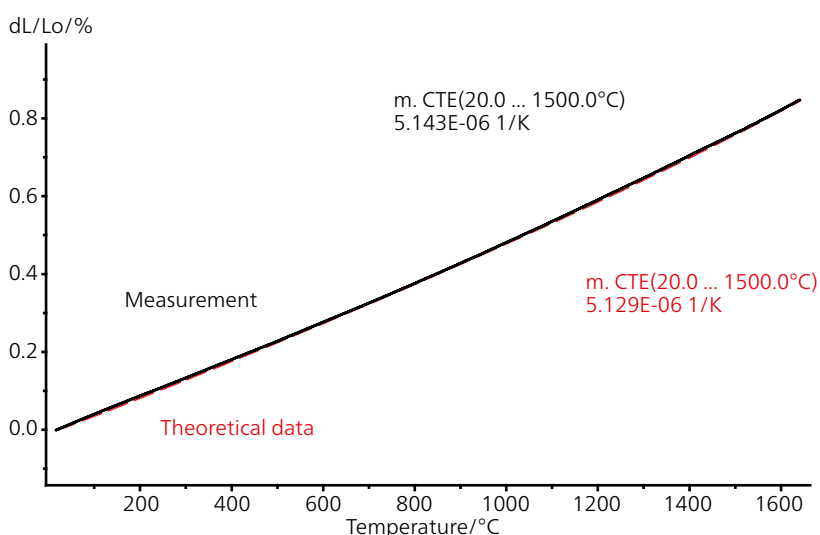
Literature values (NIST standard table)  
 $5.129 \times 10^{-6} \text{ 1/K}$

Difference between measurement and literature  
 $1.4 \times 10^{-8} \text{ 1/K}$

Test Conditions	
Instrument	DIL 402 <i>Expedis® Supreme</i>
Sample	Tungsten (W)
Sample length	25 mm
Heating rate	5 K/min
Atmosphere	He
Constant contact force	250 mN
Sample holder	Alumina
Sensor	DSC, type S



Left: Two tungsten samples after a measurement up to 1640°C. The sample on the left is corroded due to the oxygen-containing test atmosphere; the sample on the right still shines due to a measurement in an oxygen-free test atmosphere.



Thermal expansion of tungsten; displayed are the length change of the sample (black solid line) together with the tabulated theoretical data (red dashed line, NIST standard table).

## Measurement of the Seebeck Coefficient of Pure Nickel

### Introduction

In order to enhance and optimize thermoelectric materials, it is necessary to investigate their thermophysical and thermoelectric properties. Along with the laser flash instruments, NETZSCH also offers the SBA 458 *Nemesis*<sup>®</sup> for the simultaneous measurement of electrical conductivity and the Seebeck coefficient.

### Measurement

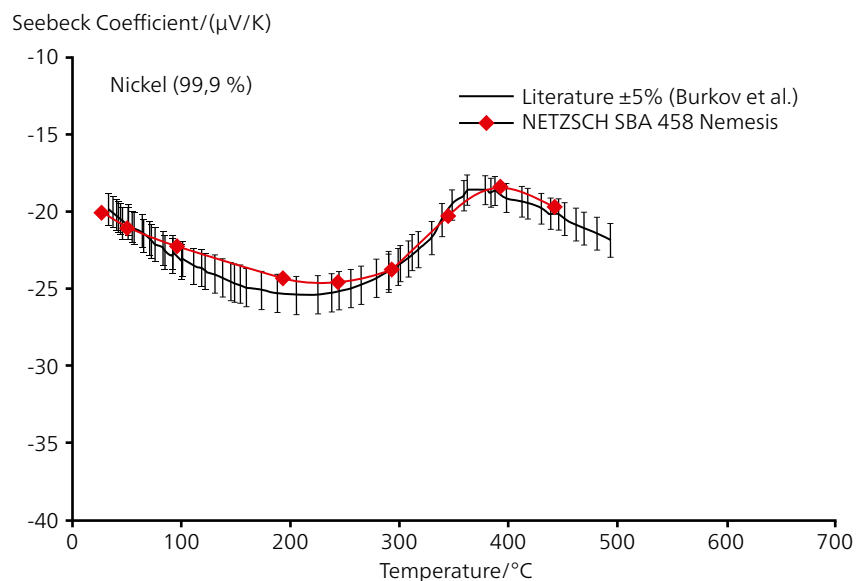
Thermoelectric materials should possess low thermal conductivity and high values for the electrical conductivity and Seebeck coefficient. The higher the measuring signal, the lower the edge effects. At the same time, the thermal conductivity of thermoelectrical materials is low, helping guarantee a homogeneous temperature distribution within the sample. However, if the sample is highly thermoconductive and exhibits only a small thermoelectrical effect, measurements are far more difficult to conduct. The smallest of asymmetries or poor thermal connection to the heaters may lead to inhomogeneous temperature profiles being formed within the sample, resulting in increased measurement uncertainties. In this respect, pure nickel is a material often used for precision tests on Seebeck instruments.

Test Conditions	
Instrument	SBA 458 <i>Nemesis</i> <sup>®</sup>
Sample	Nickel (Ni, 100.0%)
Sample dimensions	Thickness: 0.12 mm width: 5 mm length: 25 mm
Heating rate	Depending on the temperature step between 1 and 10 K/min
Atmosphere	Helium, 50 ml/min
Sensor	DSC, type S

The figure shows measurements on pure nickel in comparison with literature data. It is obvious that the measurement points determined by the SBA 458 are in very good agreement with literature data and all lie within the  $\pm 5\%$  range.

### Summary

Only by means of the complex measurement setup – with 2 additional heaters, current pins and sheathed thermocouples fixed from below and a defined contact pressure controlled by means of springs – is it now possible to also carry out measurements on materials with a very low Seebeck coefficient and comparatively high thermal conductivity.



Comparative measurements of the Seebeck coefficient on pure nickel (99.9%)



# Non-Ferrous Metals

## SBA 458 Nemesis® – Expansion of the Temperature Range I – Ni and Pd

### Introduction

The SBA 458 Nemesis® allows for measurements up to 1100°C using various sample geometries and dimensions.

The high-temperature sample carrier system is equipped with ceramic components and especially designed micro heaters. Furthermore, sensitive parts in the sample carrier system are also protected.

The high-temperature sample carrier system can be used – without additional mechanical or electrical adjustment – in the basic unit of the SBA 458 (plug and play). The software automatically recognizes the built-in sample carrier system so that the operator can start with the measurement directly.

### Test Results

Since there are no stable and certified thermoelectric materials available in the temperature range up to 1100°C, the measurements shown here with the high-temperature sample carrier system are on metals up to 1100°C as well as one additional measurement on certified lead telluride to 350°C.

Figures 1 and 2 show the measurements of the Seebeck coefficient and electrical conductivity of nickel and palladium to 1100°C. The deviations from the corresponding literature values are less than 5% for both the Seebeck coefficient and electrical conductivity.

Test Conditions	
Instrument	SBA 458 Nemesis®
Samples	Nickel (Ni, 99.99%) Palladium (Pd, 99.99%)
Sample dimensions	Thickness: 0.12 mm Width: 5 mm Length: 25 mm
Heating rate	Depending on the temperature step between 1 and 10 K/min
Atmosphere	Ar/H <sub>2</sub> (98%/2%), 100 ml/min
Sample	PbTe
Sample dimensions	Length: 25 mm Thickness: 0.2 mm Width: 5 mm
Atmosphere	Ar/H <sub>2</sub> (98.2%), 100 ml/min
Sample	Pure iron (99.99%)
Sample dimensions	Length: 25 mm Thickness: 0.1 mm Width: 5 mm
Atmosphere	Ar/H <sub>2</sub> (98%/2%), 100 ml/min



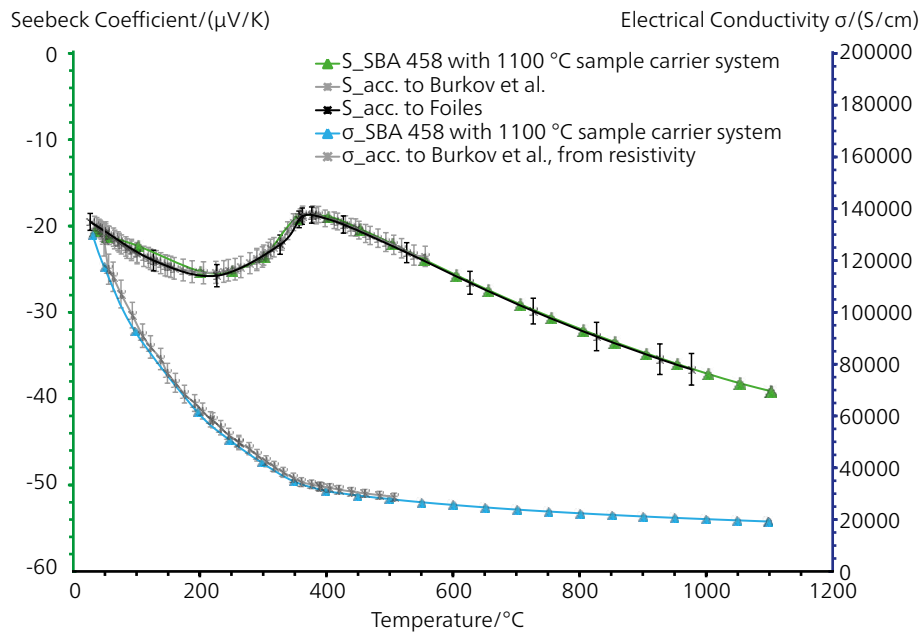


Figure 1. Measurement of the Seebeck coefficient and the electrical conductivity of nickel with the SBA 458 *Nemesis*® in comparison with literature – sources [1] and [2]

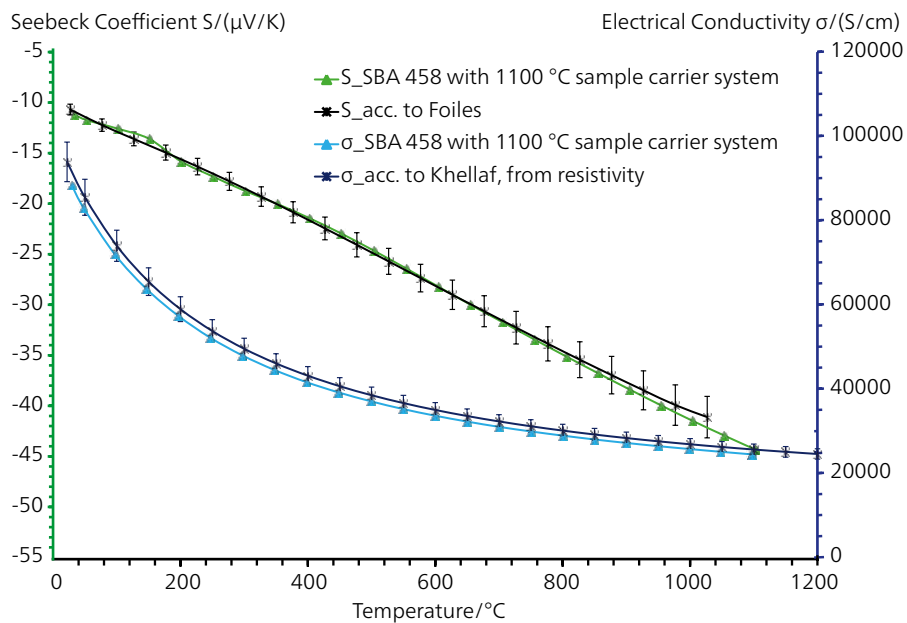


Figure 2. Measurement of the Seebeck coefficient and the electrical conductivity of palladium with the SBA 458 *Nemesis*® in comparison with literature – sources [2] and [3]

# Non-Ferrous Metals

## SBA 458 Nemesis® – Expansion of the Temperature Range II – PbTe and Iron

The lead telluride certified for the Seebeck coefficient was measured at a deviation of less than 7% (Figure 3).

Another example, demonstrating the high accuracy of the SBA 458 in the range to 1100°C, is shown with the measurement on pure iron.

Pure iron has a low Seebeck coefficient, which complicates the process of determining that value. Despite this, the measurement results of both the Seebeck coefficient and the electrical conductivity exhibit high measuring accuracy (see Figure 4).

At room temperature, pure iron exists in the  $\alpha$  modification (bcc, body-centered cubic crystal structure) and is transformed at 911°C into the  $\gamma$  modification (face-centered cubic crystal structure, or fcc). These transitions, as well as the Curie point, can be detected by means of thermal analysis (dilatometry and differential scanning calorimetry and also with the SBA 458 (see Figure 5).

### Literature

- [1] Burkov, A.T., Heinrich, A., Konstantinov, P.P, Experimental set-up for thermopower and resistivity measurements at 100-1300 K, Measurement science and technology 12, 2001
- [2] Foiles, C.L., Thermopower of pure metals and dilute alloys, in Landoldt-Börnstein, Group III, Band 15, 1985
- [3] Khellaf, A., Lattice Defect Studies of High Quality Single Crystal Platinum and Palladium, The University of Arizona, Faculty of the Department of Physics, 1987
- [4] Hust, J.G., Lankford, A.B., National Bureau of Standards, U.S. Department of Commerce, Standard Reference Material: Update of Thermal Conductivity and Electrical Resistivity of Electrolytic Iron, Tungsten and Stainless Steel, NBS Special Publication 260-90, 1984

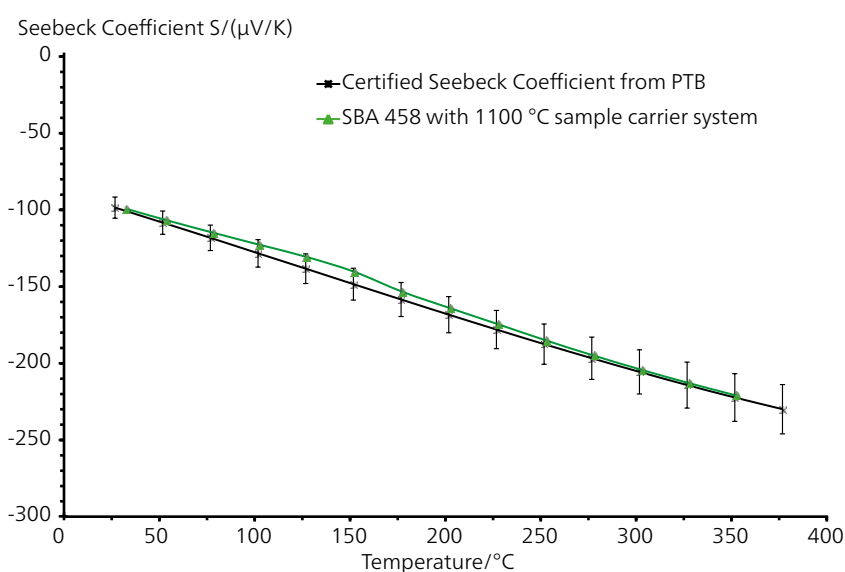


Figure 3. Measurement of the Seebeck coefficient of certified lead telluride, PbTe, with the SBA 458 in comparison with literature values

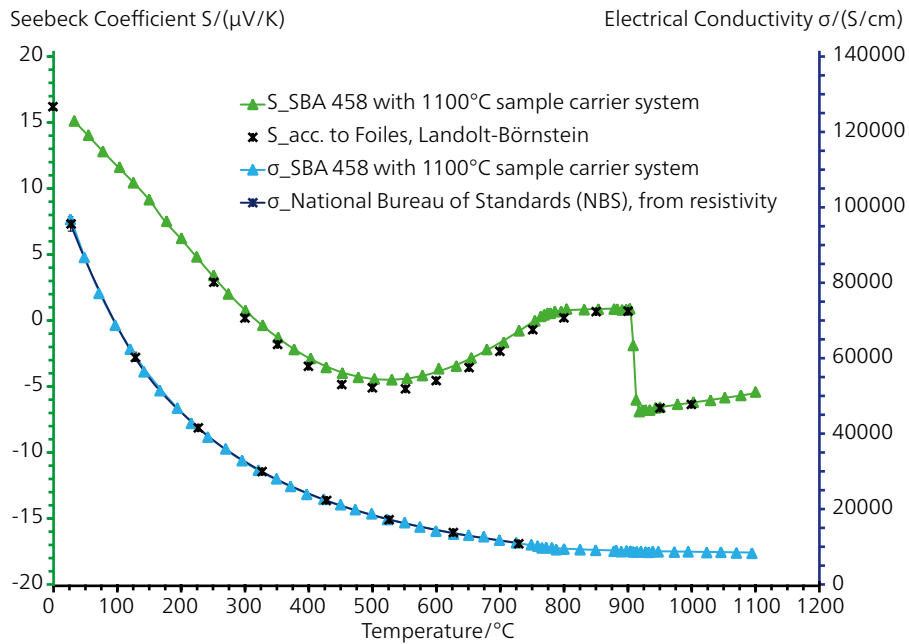


Figure 4. Measurement of the Seebeck coefficient and the electrical conductivity of pure iron in comparison with literature values

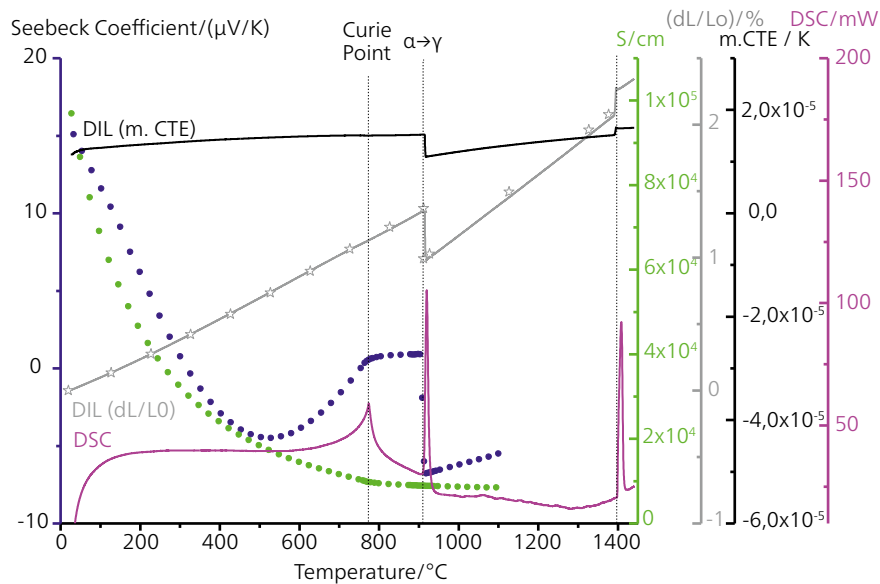


Figure 5. Measurement on pure iron with the SBA 458 Nemesis®, DIL 402 Expedis Supreme and DSC 404 F1 Pegasus®

# Ferrous Metals

## Energy Release of Cold-Forged Iron

### Introduction

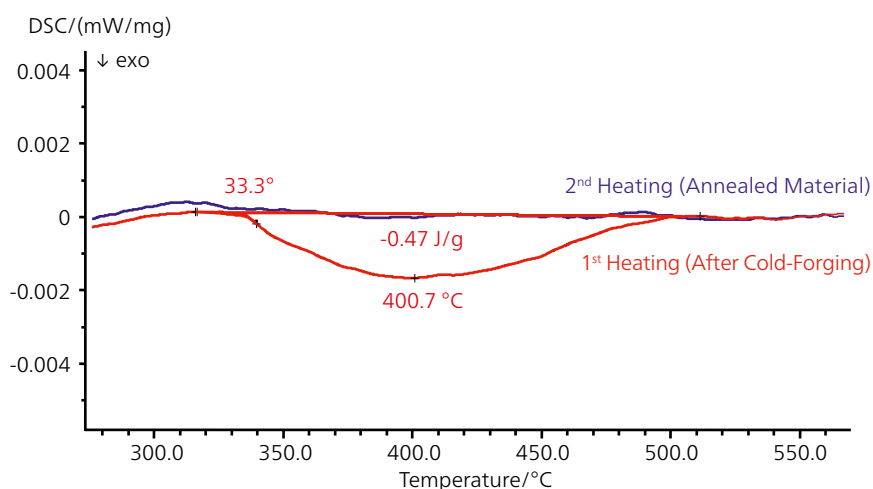
Forging is one way of shaping a metal by plastic deformation. The conventional forging process is done at high temperatures making metals easier to shape and less likely to fracture. Commonly, iron or steel parts are forged at temperatures where the metal becomes malleable (typically red hot). Cold forging is done at low temperatures. Once the final shape has been forged, iron and steel are often subjected to some type of heat treatment. This can result in various degrees of hardening or softening depending on the type the treatment. During heat treatment, defects in the crystal structure anneal or new phases are formed, resulting in a small energy release. This extremely weak exothermal effects can be analyzed with a NETZSCH DSC or STA system.

### Test Results

Presented in the plot is the specific heat-flow curve measured on a cold-forged iron sample. During the first heating run, an exothermal effect was detected at 335°C (extrapolated onset). The peak temperature was at 401°C. At approx. 500°C, the exothermal reaction was finished. The energy

Test Conditions	
Instrument	DSC 404 Pegasus®
Sample	Iron (Fe, cold forged)
Sample mass	335 mg
Temperature range	200°C to 600°C
Heating/cooling rate	20 K/min
Atmosphere	Argon (50 ml/min) – reference side used an annealed Ti sample
Crucible	Pt
Sensor	DSC, type S

release during this relaxation reaction was 0.47 J/g. The effect is not visible in the measurement of the annealed material. These tests require a vacuum-tight instrument and pure purge gases (to avoid oxidation effects which can occur in a similar temperature range), as well as a high-performance DSC sensor, with high sensitivity, low noise and good baseline stability. These requirements are standard features of the NETZSCH high-temperature DSC and STA systems.



Specific heat flow rate of cold-forged iron





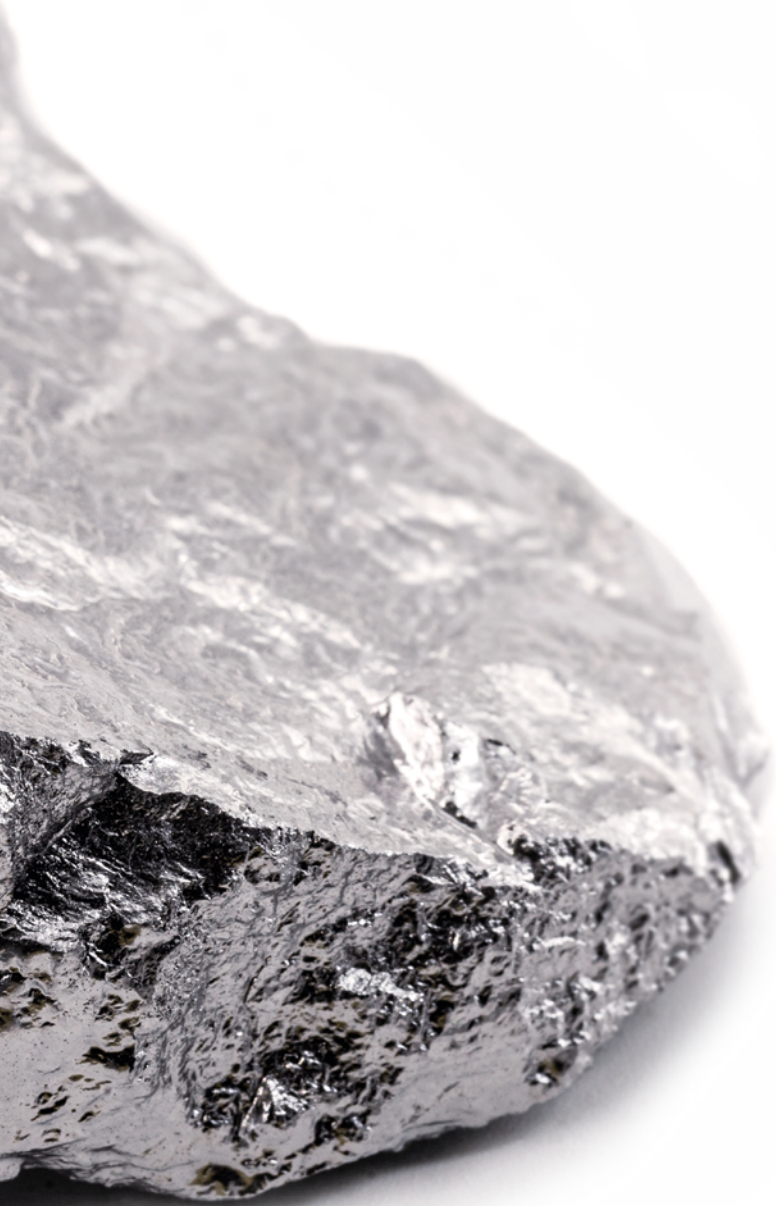
Steel ingot in a hydraulic forging processes







# Alloys



# Light Metal Alloys

## Thermophysical Properties of Aluminum Alloy in the Solid and Liquid State

### Introduction

Reduced development times and costs, optimization of the manufacturing processes and lower masses in spite of increasingly higher demands on thermally stressed components are important goals of the automotive industry. For example, numerical simulations were used to predict the temperature distribution within the engine components during the casting process. A basic necessity is the knowledge of the thermophysical properties (TPP) of the casting material over the entire temperature range. The measurement results of an aluminum alloy are presented in Figure 1. LFA tests were made using a special sapphire container, which maintains the dimension of liquids, for the measurement of metals into the liquid range (Figure 2).

### Test Results

The thermal diffusivity and thermal conductivity show a nearly linear decrease above room temperature (Figure 1). A typical

Test Conditions	
Instrument	LFA 457 <i>MicroFlash</i> <sup>®</sup>
Sample	Aluminum alloy
Sample thickness	1.454 mm
Temperature range	RT to 850°C
Sample holder	Sapphire-C, for liquid metals
Sample surface preparation	Sandblasted
$c_p$ from DSC	Corrected, without latent heat of melting

step in the thermal diffusivity/conductivity was detected for the phase transition (solid/liquid) above 550°C. This is due to the dissolution of the lattice structure during the phase transition and therefore a reduced electronic heat transfer. The example clearly demonstrates that the LFA method is not limited to solid materials with defined dimensions. The LFA 457 can analyze liquid metals without any problems.

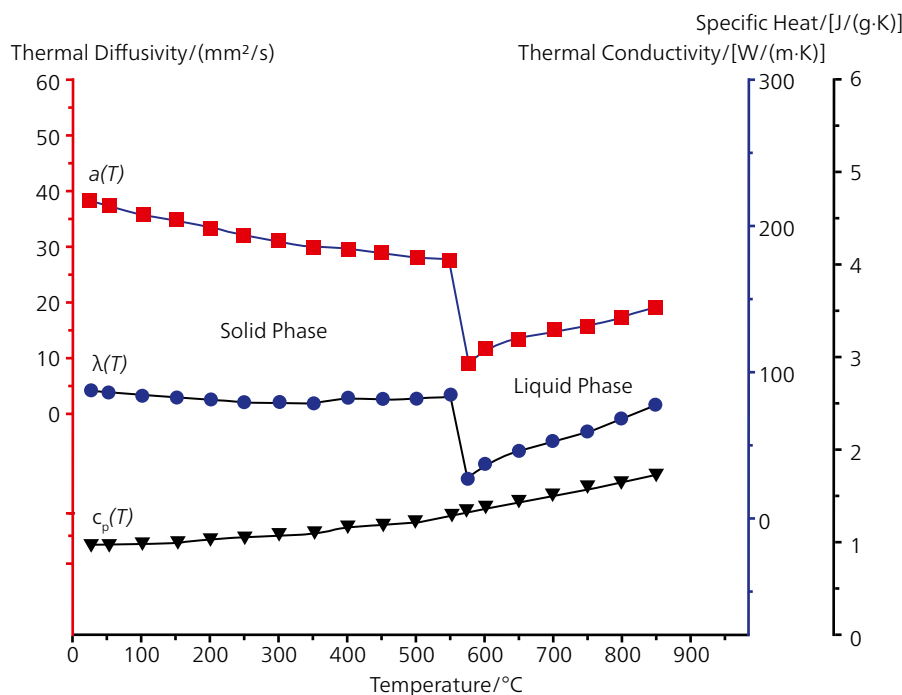


Figure 1. Thermal diffusivity (by means of LFA) and specific heat capacity (by means of DSC); the specific heat data was corrected by subtracting the latent heat of the melting.



Figure 2. Sample holder for liquid metals

## Volumetric Expansion of Aluminum Alloy into the Melt

### Introduction

The behavior of an aluminum-based alloy during heating is illustrated here. Displayed are the volumetric expansion ( $dV/V_0$ , black) and the density change (red) which can both be calculated from the measured thermal expansion data by using the NETZSCH *Density Determination* software.

### Test Results

After an initial linear expansion, the aluminum alloy starts to melt at 559°C (extrapolated onset temperature of the *c-DTA*<sup>®</sup>\* signal in dashed blue). For realizing such an experiment, a special container (Figure 2) is necessary.

During melting, a strong expansion occurs representing the "mushy region" in which liquid and solid state are present together (Figure 1). Above 622°C, the entire sample is molten.

While the volume increases, the initial density drops by about 10% (from 2.66 g/cm<sup>3</sup> to 2.40 g/cm<sup>3</sup>) until the end of the measurement.

The *c-DTA*<sup>®</sup> curve (blue) clearly shows the melting range by endothermal effects.

\* calculated DTA signal for temperature calibration and determination of endo-/exothermal effects

Test Conditions	
Instrument	DIL 402 <i>Expedis Select</i>
Sample	Aluminum alloy
Sample length	Approx. 12 mm
Temperature range	RT to 1000°C
Atmosphere	Helium
Heating rate	5 K/min
Sample holder	Alumina + alumina container
Contact force	250 mN, constant
Software	<i>Density Determination</i>



Figure 1. Containers for dilatometer measurements, made of alumina, fused silica, sapphire and graphite

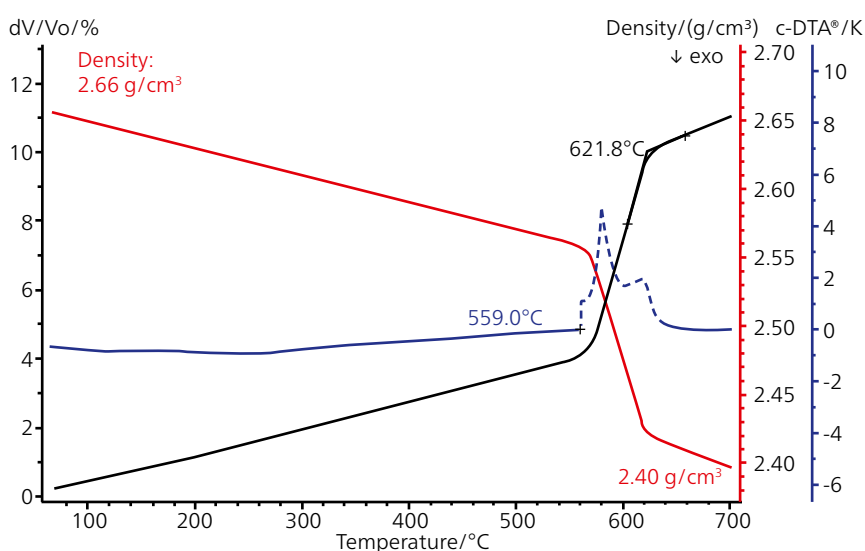


Figure 2. Volumetric expansion (black curve) and calculated density change (red curve) by means of dilatometry; melting by *c-DTA*<sup>®</sup> (blue curve).

# Light Metal Alloys

## Magnesium Alloy

### Introduction

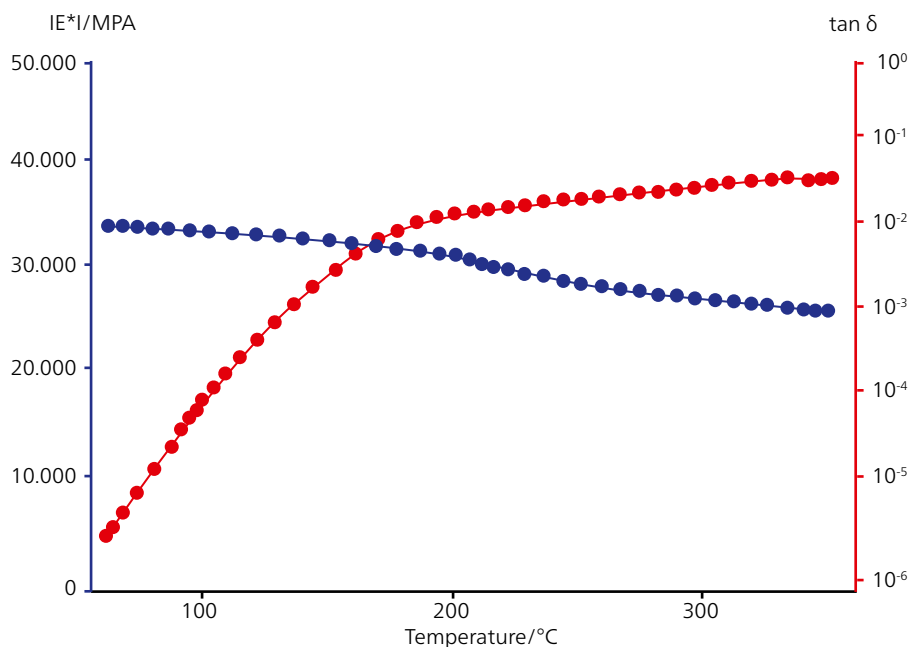
Magnesium alloys are mixtures of the lightest structural metal, magnesium, with other metals to improve the physical properties. These metals include manganese, aluminum, zinc, silicon, copper, zirconium, and rare-earth metals. Magnesium alloys have a hexagonal lattice structure, which affects the fundamental properties of these alloys. Magnesium's properties include low specific weight and a high strength-to-weight ratio. Plastic deformation of the hexagonal lattice is more complicated than in cubic latticed metals like aluminum, copper and steel; therefore, magnesium alloys are suitable as cast alloys in automotive, aerospace, industrial, electronic, biomedical, and commercial applications.

### Temperature Dependence of $E^*$ Modulus of Magnesium Alloy

The measurement presents the course of the complex modulus  $E^*$  (unilaterally tensioned bending beam: modified single-cantilever device) and the loss factor  $\tan \delta$  of a magnesium

Test Conditions	
Instrument	DMA EPLEXOR®
Sample	Magnesium alloy
Heating rate	2 K/min
Test frequency	10 Hz
Measurement mode	Tensile

alloy as a frequency of temperature. With increasing temperature, the modulus  $E^*$  decreases by approximately 20%. Significant is the extremely broad damping range through which the magnesium sample passes in the temperature sweep. On a logarithmic scale,  $\tan \delta$  changes by almost four decades. Such small damping can only be recorded by means of high-resolution measuring equipment such as the EPLEXOR®.



DMA measurement on a magnesium alloy

# Precise Determination of the the Thermal Expansion of Aluminum Alloy 6061

## Introduction

Al 6061 is a common aluminum alloy with magnesium and silicon as major components. Its combination of light weight, good mechanical strength, and high weldability makes it a popular choice for many transportation applications like airplanes, boats, automobiles, and bicycles. Besides dilatometry, thermomechanical analysis is ideally suited to measure the thermal expansion of Al 6061 and other metals or metal alloys .

Test Conditions	
Instrument	TMA 402 <b>F1</b> Hyperion®
Sample	Al 6061
Sample length	25 mm
Pushrod force	0.30 N
Temperature range	-20°C to 500°C
Heating rate	5 K/min
Atmosphere	Helium (20 ml/min)
Sample carrier	Fused silica
Measurement mode	Expansion

## Coefficient of Linear Thermal Expansion (CTE)



describes the length change of a material as a function of the temperature. The mean (average or technical) CTE is defined as the slope of a secant through two points of the curve of thermal expansion:

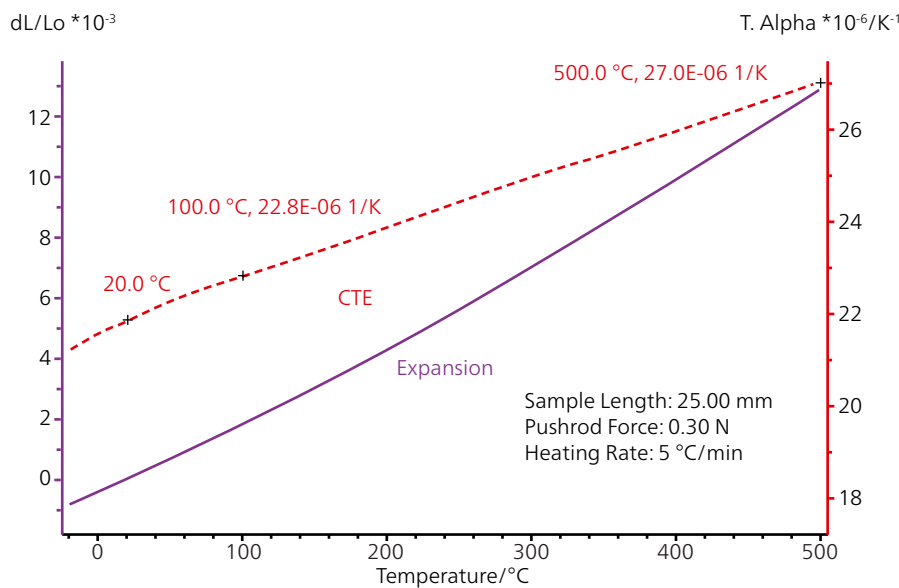
$$\alpha_1(T_0, T) = \frac{1}{l_0} \frac{l(T) - l(T_0)}{T - T_0} = \frac{1}{l_0} \frac{\Delta l}{\Delta T}$$

The physical (differential) CTE is the slope of the expansion curve at a given temperature. It thus corresponds to the first derivative of the curve of thermal expansion according to temperature:

$$\alpha_1(T) = \frac{1}{l_0} \left( \frac{dl}{dT} \right)_p$$

## Test Results

The plot shows a slightly bent thermal expansion curve of the Al alloy up to 500°C. The technical alpha value, CTE, between 20°C and 100°C was determined to be  $22.8 \cdot 10^{-6}$  1/K. This result is quite close to the CTE of about  $23.0 \cdot 10^{-6}$  1/K to  $23.6 \cdot 10^{-6}$  1/K which can be found in literature [1], [2]. The value of the mean coefficient of thermal expansion (technical alpha value) at 500°C, using 20°C as the reference point, was determined to  $27.0 \cdot 10^{-6}$  1/K.



Thermal expansion of aluminum alloy up to 500°C

## Literature

- [1] [www.smh-metalle.de/internet/media/smh/pdf/datenblatt\\_en\\_aw\\_6061.pdf](http://www.smh-metalle.de/internet/media/smh/pdf/datenblatt_en_aw_6061.pdf)
- [2] [www.vegasfastener.com/Aluminum-6061.php](http://www.vegasfastener.com/Aluminum-6061.php)



# Ferrous Alloys

## Oxidation and Corrosion Studies on Large Metal Surfaces

### Introduction

For oxidation and corrosion studies, it is preferable to have a large sample surface in order to maximize the accessibility to the gas. TGA and TGA-DTA sample holders are available which allow the sample to be attached in a hanging position. The samples can be a plate, mesh or a compact body which can be placed in a platinum basket

### Test Results

For the below TGA measurement on a sheet of steel, the TGA sample holder for hanging samples was used (Figure 1). The sample was subjected to several heating cycles at a heating rate of 5 K/min in a nitrogen atmosphere with 16% oxygen. Oxidation (mass increase) decreases with each subsequent heating cycle (Figure 2). At the beginning of the test, oxidation of the sheet surface occurs. This can be observed in the early onset and rapid mass increase for the first heating cycle (green curve).

After a couple of heating cycles, the oxide layer gets thicker with every heating and oxidation decreases due to hindered diffusion of the oxygen through the layer. The inner oxidation is indicated by a slower, diffusion-dependent mass increase.

Test Conditions	
Instrument	STA 409 <b>F1</b> Jupiter®
Sample	Sheet of steel
Sample mass	1.9 g
Heating/cooling rate	5 K/min
Atmosphere	16% O <sub>2</sub> in N <sub>2</sub> , 110 ml/min
Sample holder	For hanging samples

Hanging the sample in the special holder maximizes the accessible sample surface and therefore improves oxygen access to all sample sides. This is a prerequisite for certain analyses, such as kinetic studies of the oxidation behavior.



Figure 1. TGA sample holder for hanging samples

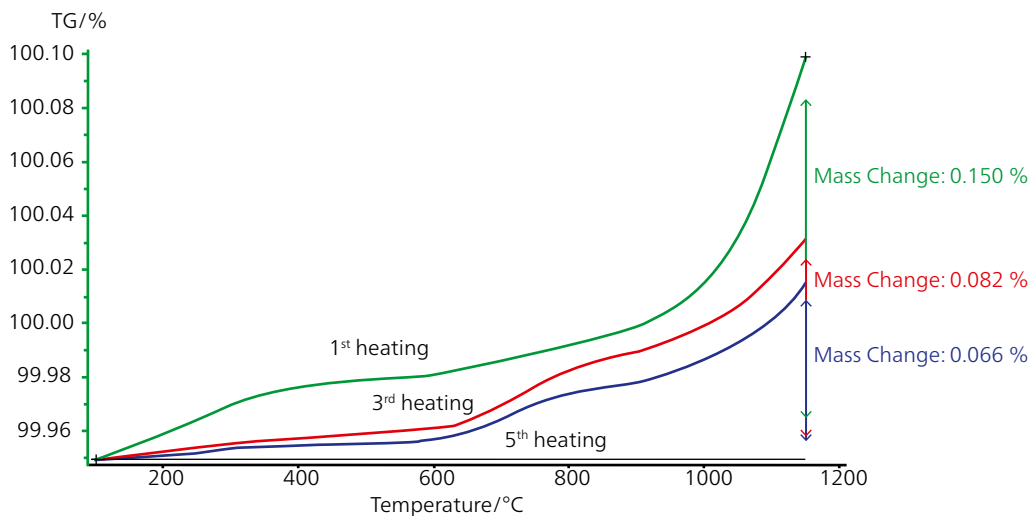


Figure 2. Oxidation of a steel sheet, increased sample surface by the hanging sample holder for oxygen access

## Melting and Mass Loss Behavior of a Steel Sample

### Introduction

The calculated DTA/DSC-signal, *c-DTA*<sup>®</sup>, is ideal for easy temperature calibration without the need for magnetic Curie Point standards, which would often necessitate partial disassembling of the thermobalance. In addition, mass change signals, along with endo- and exothermal behaviors (e.g., vaporization with mass loss or melting without mass change) can be obtained without any hardware add-ons. Thus, correlation of such results is not influenced by the hardware.

All TGA sample carriers of the NETZSCH TG 209 **F1/F3** and STA 449 **F1/F3/F5 Jupiter**<sup>®</sup> allow for *c-DTA*<sup>®</sup> determination. Ceramic and metallic crucibles are available to achieve optimum peak temperature results and caloric information.

### Test Results

In this example, a slip-on plate made of alumina (diameter 17 mm) was used to support the sample (Figure 1).

The *c-DTA*<sup>®</sup> curve (blue) shows an endothermic effect at 1362°C which corresponds to melting of the sample. In the same temperature range, the TGA curve (green) indicates some minor mass loss (0.02%) due to a small evaporation effect (Figure 2)..

Test Conditions	
Instrument	STA 449 <b>F1 Jupiter</b> <sup>®</sup>
Sample	Steel
Sample mass	1018.59 mg
Temperature range	RT to 1400°C
Atmosphere	Argon
Heating rate	20 K/min
Sample holder	TGA, slip-on plate made of alumina



Figure 1. Al<sub>2</sub>O<sub>3</sub> slip-on plates

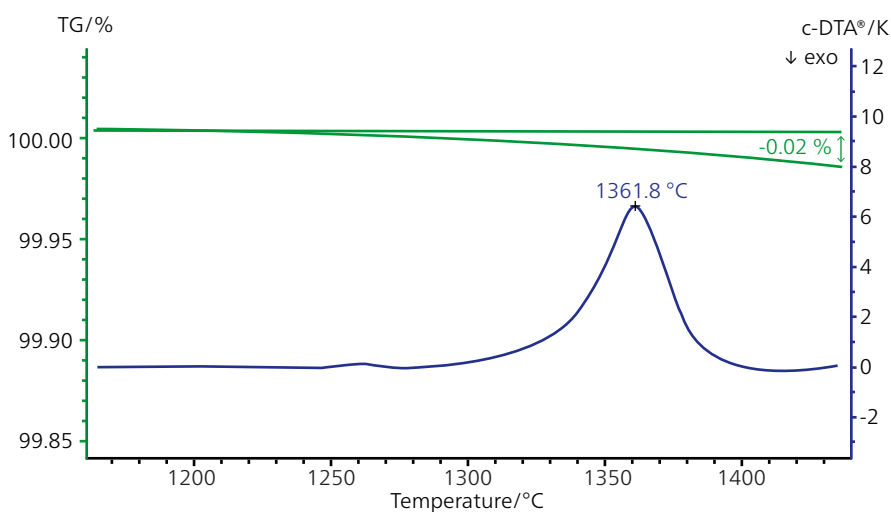


Figure 2. Measurement of large sample masses can be made with slip-on plates

# Ferrous Alloys

## Steel Corrosion under a Humid Atmosphere

### Introduction

Corrosion is a deterioration of intrinsic properties in a material due to reactions with its environment. Weakening of steel because of oxidation of the iron atoms is a well-known example of electrochemical corrosion. Most structural alloys corrode merely by exposure to moisture in the air, but the process can be strongly affected by exposure to certain substances like acids, bases, halogens, etc. Controlled corrosion treatments such as passivation and chromate conversion will increase a material's corrosion resistance. Stainless steel, for example, a ferrous alloy with a minimum of 10.5% chromium content, does not stain, corrode or rust as easily as ordinary steel.

Corrosion processes can be simulated and studied by means of thermogravimetry under defined temperature, gas and humidity conditions.

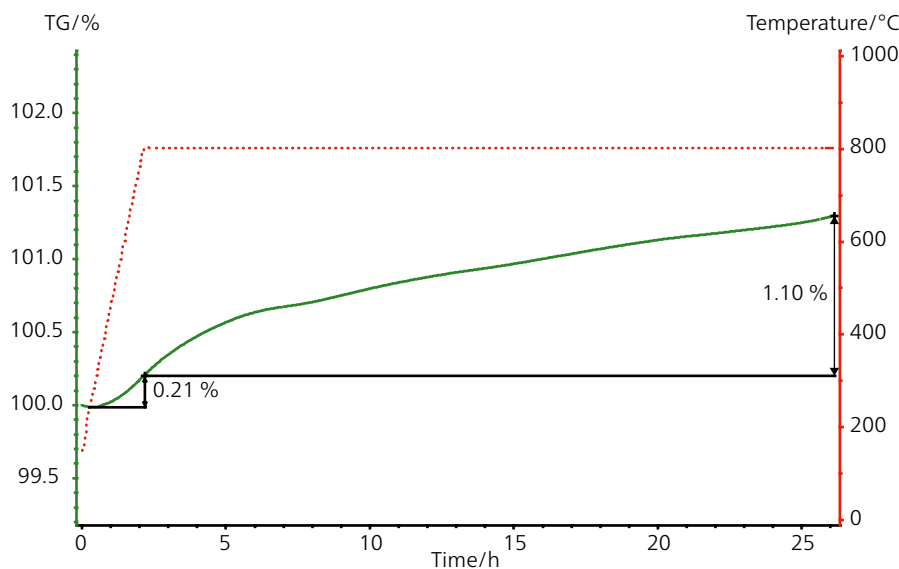
### Test Results

A steel sample was heated and isothermal at 800°C for more than 20 hours under a humid atmosphere. The observed increase in sample mass is due to corrosion of the steel

Test Conditions	
Instrument	STA 409
Sample	EM steel
Sample mass	303.12 mg
Temperature range	RT to 800°C, isothermal for 24 h at 800°C
Heating rate	10 K/min
Atmosphere	Air + 50% H <sub>2</sub> O at 160 ml/min
Crucible	TGA, slip-on plate made of Al <sub>2</sub> O <sub>3</sub>
Sensor	TGA, type S

sample. A humid atmosphere up to 100% absolute concentration can be created by a special water-vapor furnace which can also be coupled to evolved gas analysis.

Typical application fields of humid atmospheres are corrosion and scaling processes on steels, where the oxidation and decarbonization by means of the water vapor is especially important. The same applies to, e.g., the study of sintering processes in ceramic components, water gasification of petroleum coke and inorganic building materials.



STA measurements of steel under a humid atmosphere



# Precise Determination of the Thermal Expansion of Type 304 Stainless Steel

## Introduction

Type 304 stainless steel is a common austenite steel alloy composed of 18 to 20% chromium and 8 to 12% nickel. It features high resistance to corrosion and is widely used in the chemical, petroleum, and food industries. Type 304 stainless steel has good drawability and can be readily formed into complex shapes.

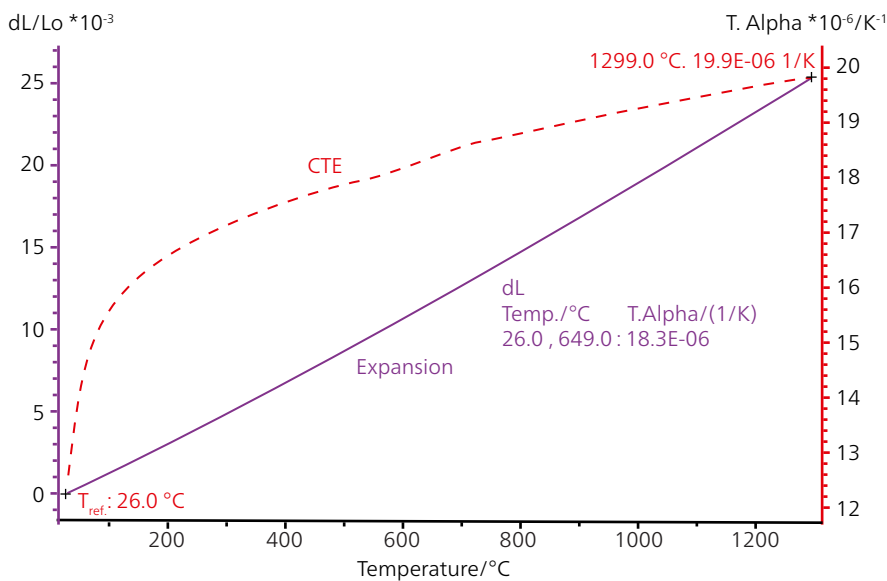
Besides dilatometry, thermomechanical analysis is ideally suited to measure the thermal expansion of 304 steel and other metals or metal alloys .

Test Conditions	
Instrument	TMA 402 <b>F1</b> Hyperion®
Sample	Type 304 stainless steel
Sample length	24.99 mm
Temperature range	RT to 1300°C
Atmosphere	Helium (20 ml/min)
Heating rate	5 K/min
Pushrod force	0.30 N
Sample carrier	Alumina
Measurement mode	Expansion

## Test Results

The below graphic shows an almost linear increase in relative length change up to 1300°C. The value of the coefficient of thermal expansion (technical alpha value, CTE) between 26°C and 649°C (79°F to 1200°F) was determined to be  $18.3 \cdot 10^{-6}$  1/K and corresponds well to the value of  $18.7 \cdot 10^{-6}$  1/K given in literature\* for a temperature interval between 0°C and 649°C (32°F to 1200°F). Finally, the CTE reaches a value of  $19.9 \cdot 10^{-6}$  1/K between 26°C and 1299°C (79°F to 2372°F).

\* Data sheet AK Steel – Stainless Steel 304/304L



Coefficient of thermal expansion (CTE, red dotted curve) of type 304 stainless steel and thermal expansion curve in purple

# Ferrous Alloys

## Low-Alloyed Steel

### Introduction

Steel is a metal alloy whose main component is iron, with carbon being the most important alloying element. Carbon acts as a hardening agent, preventing iron atoms, which are naturally arranged in a crystal lattice, from sliding past one another (dislocation). Varying the amount of carbon and the content of other possible additives (alloy components) will have a strong influence on the phase change behavior. When iron is extracted from its ore by commercial processes, it contains more carbon than desirable. To become steel, it must be melted and reprocessed to obtain the correct amount of carbon, at which point other elements can be added. High-temperature DSC can provide helpful information on whether the manufacturing process leads to the desired product quality.

### Test Results

Figure 1 presents the measured specific heat flow rate of a low-alloyed steel<sup>1</sup> between 400°C and 1550°C. At 734°C, the change in crystal structure (from body-centered to face-centered) can be seen.

This is probably the eutectic temperature and the  $\alpha$ - $\gamma$ -transition of the alloyed iron. This temperature range

Test Conditions	
Instrument	DSC 404
Sample	Low-alloy steel
Sample mass	173.24 mg
Temperature range	RT to 1550°C
Heating/cooling rate	20 K/min
Atmosphere	Argon (50 ml/min)
Crucible	Pt with liner and lid (Figure 2)
Sensor	DSC, type S

also includes the change in magnetic properties from a ferromagnetic to a paramagnetic material. This transition temperature is called the Curie temperature. At higher temperatures, a broader endothermic peak is observed, which reappears as a double peak in cooling with a small undercooling effect. This indicates the solid solution region of the Fe-C carbon phase diagram with the solidus temperature at 1411°C (heating curve, red) and a liquidus temperature at 1473°C (cooling curve, blue).

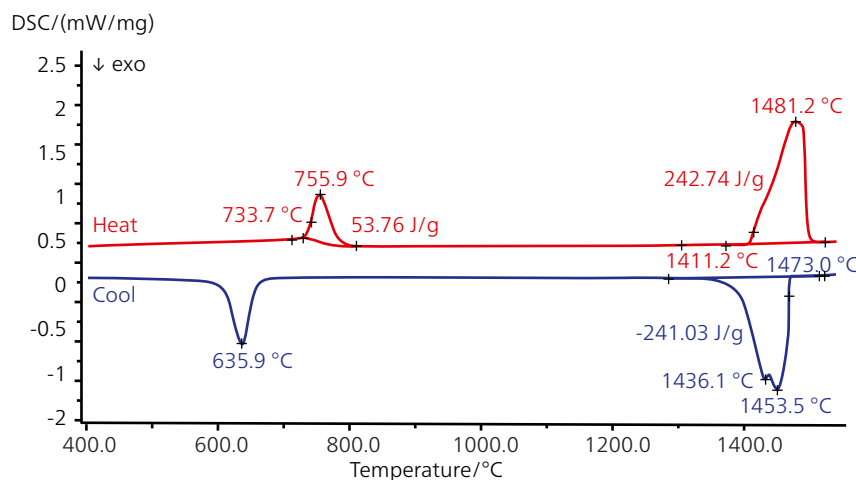


Figure 1. Heating and cooling run in the DSC; undercooling effects in the DSC cooling run can be observed for the crystallization effect and the transition.



### Low-Alloy Steel

Low-alloy steels have a much lower percentage of alloying elements, usually 1 to 5 percent. These steels have very different strengths and uses depending on the chosen alloy.

In high-alloy steels, the sum of total alloying elements is  $>5\%$ .



### Undercooling

The temperature to which the liquid metal must cool below the equilibrium freezing temperature before nucleation occurs.



Figure 2. The crucible combination of PtRh/ $\text{Al}_2\text{O}_3$  can be used for samples which may react with Pt up to  $1700^\circ\text{C}$ . MgO and  $\text{Y}_2\text{O}_3$  liners are also available.



# Ferrous Alloys

## Liquid Metals – Cast Iron

### Introduction

Knowledge of the thermophysical properties of the casting material over the entire temperature range is crucial for construction. In the automotive industry, reduced development times and costs, the optimization of manufacturing processes and lower masses in spite of increasingly higher demands on thermally stressed components are important. To predict the temperature distribution, numerical simulations are used. In the following, the results of LFA measurements on a cast iron sample carried out using a special sapphire container are presented (Figure 1).

Test Conditions	
Instrument	LFA
Sample	Cast iron
Sample thickness	1.5 mm
Density	7.2 g/cm <sup>3</sup> at RT
Temperature range	RT to 1400°C
Sample holder	Sapphire, for measurements on metals into the melt
Sample surface preparation	Sandblasted

### Test Results

The thermal diffusivity and specific heat capacity show a typical behavior with peaks at the Curie transition (2<sup>nd</sup> order phase transition). The thermal conductivity decreases nearly continuously up to the melt. A typical step in the thermal diffusivity/conductivity was detected for the phase transition (solid/liquid) above 1150°C. The reason is that the lattice structure collapses during the phase transition.



Figure 1. Sample holder for liquid metals

Using the sample holder for liquid metals, the measurement of iron alloys is possible also within the liquid phase.

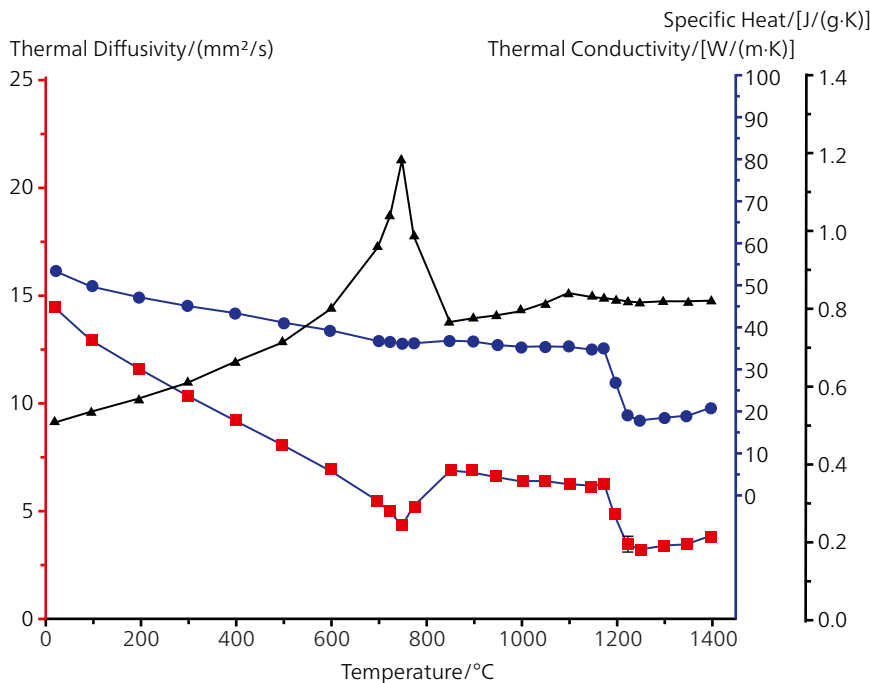
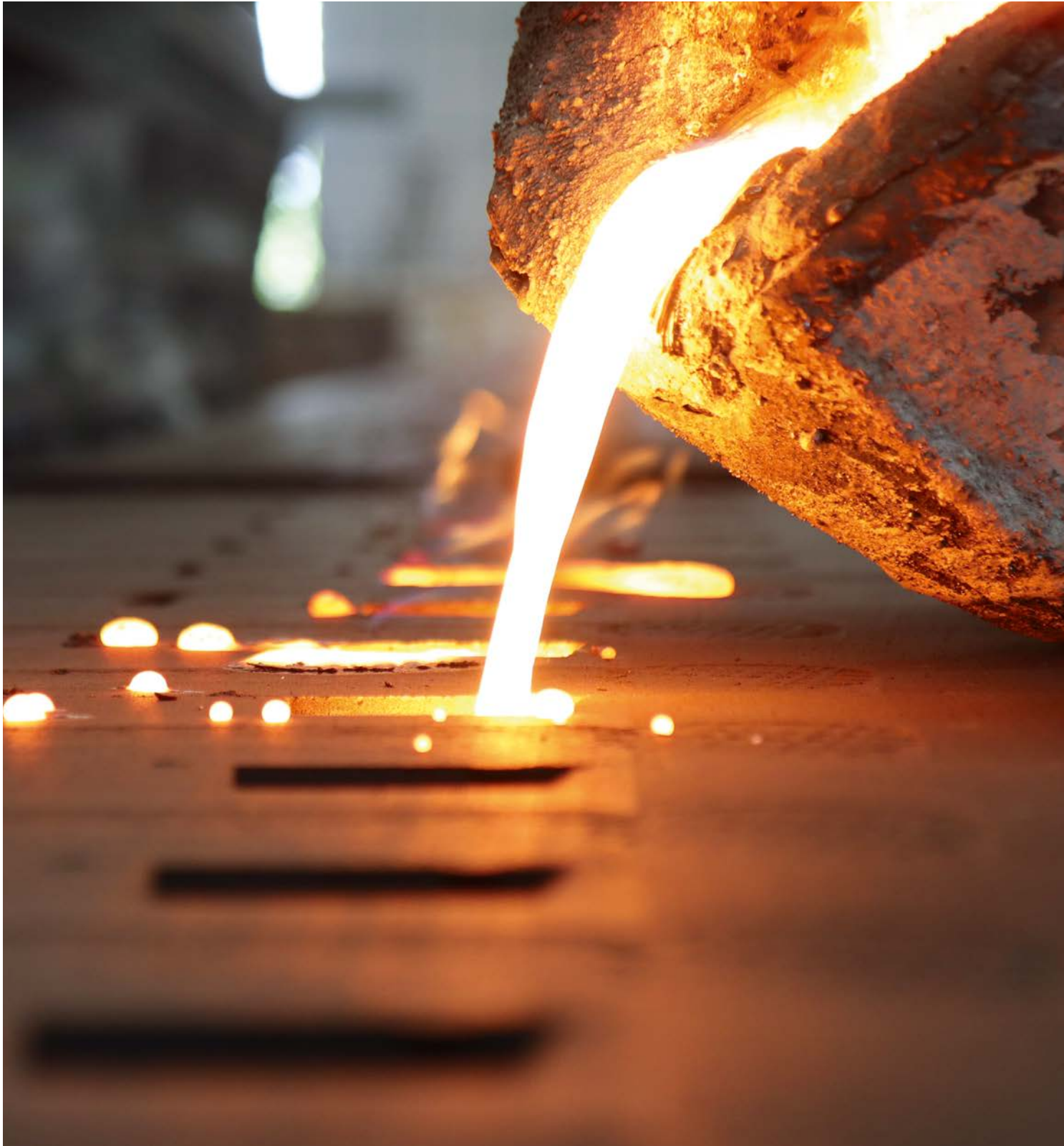


Figure 2. LFA results for cast iron, red: thermal diffusivity; blue: thermal conductivity; black: specific heat capacity



# High-Melting Alloys

## Dental Alloy

### Introduction

It is very difficult to obtain a general impression of metal alloys used in dentistry because of the large number currently present on the market. Several hundred dental alloys are available in the United States which have been registered by the American Dental Association.

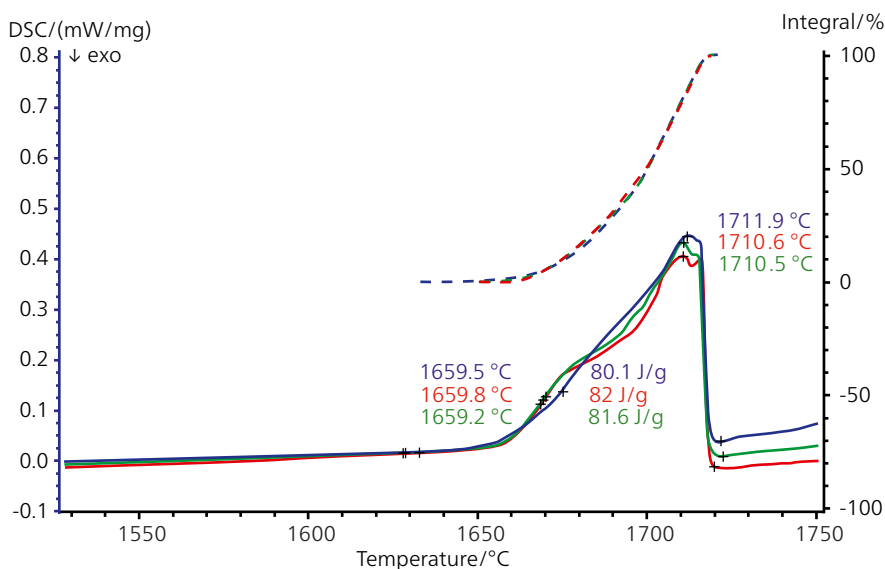
When two or three principal constituents of an alloy are known, it is possible to classify them into four groups: high-gold alloys, gold-reduced alloys, palladium-silver alloys and base metal alloys. The prerequisites of a dental alloy for dental applications are its bio-compatibility, malleability and resistance to corrosion. The requirement for good biocompatibility of a material is obviously closely related to the corrosion resistance. Thus, when the alloy is placed in contact with the body of the patient, there should be no detrimental harm to health. The aim is an alloy that is easy for the dentist to manipulate but is strong, stiff, durable and resistant to tarnish and corrosion. These alloys are used for inlays, crowns and bridges.

### Test Results

The heat-flow rate (DSC) of a dental alloy was measured to 1750°C (three samples were measured). At an extrapolated

Test Conditions	
Instrument	DSC 404 <i>Pegasus</i> ®
Sample	Dental alloy, Pt0.89Au0.11Ir0.01
Sample mass	83.06 mg
Temperature range	RT to 1750°C
Heating/cooling rate	20 K/min
Atmosphere	Argon (50 ml/min)
Crucible	Pt with liner and coating
Sensor	DSC, type B

onset temperature of ~1659°C, melting was observed. The melting peak occurred at ~1711°C. The melting enthalpy was ~81 J/g. The DSC integral curve sums the area of the melting peak so that small material variations can be neglected. In this example, the integral curves represent the melting peaks and the good reproducibility of the DSC measurements.



DSC heating runs on a dental alloy up to 1750°C; dashed lines represent the DSC integral curves

# Titanium Alloy

## Introduction

Titanium alloys are metallic materials which contain a mixture of titanium and other chemical elements. Such alloys feature very high tensile strength and toughness (even at extreme temperatures), are lightweight, and have extraordinary corrosion resistance. However, the high cost of both raw materials and processing, limit their use to military applications, aircraft, spacecraft, medical devices, and some premium sports equipment and consumer electronics.

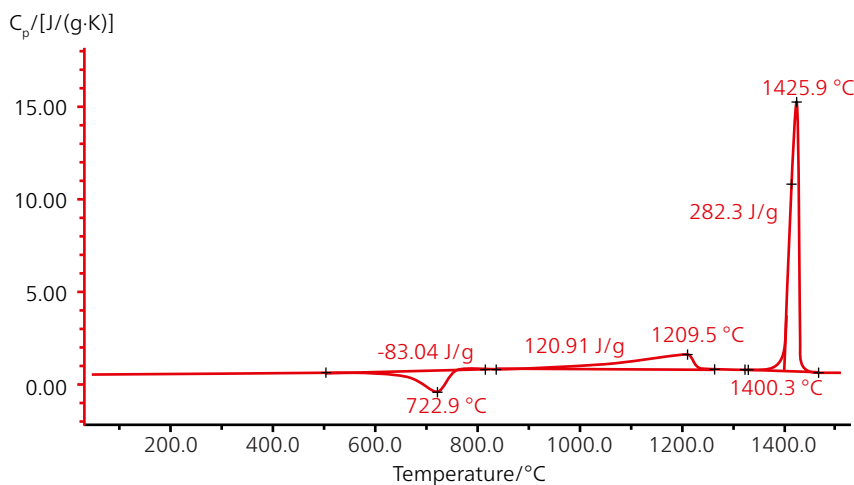
The addition of chromium to titanium in concentrations exceeding 10 wt% helps improve the burn-resistance of titanium alloys. Furthermore, such alloys can be solidified in the partially amorphous form by rapid cooling.

## Test Results

Presented in this plot is the apparent specific heat of a titanium chromium alloy between room temperature and 1525°C. At 723°C (peak temperature), the specific heat is overlapped by the cold-crystallization of amorphous contents. The broad endothermic effect at 1211°C (peak

Test Conditions	
Instrument	STA 409
Sample	TiCr alloy
Sample mass	approx. 200 mg
Temperature range	RT to 1750°C
Heating/cooling rate	10 K/min
Atmosphere	Argon, 5N (60ml/min)
Crucible	Pt/Rh with Al <sub>2</sub> O <sub>3</sub> liner with inner Y <sub>2</sub> O <sub>3</sub> coating
Sensor	TGA-DSC, type B

temperature) is due to the  $\alpha$ - $\beta$ -transition. Melting of the alloy starts at 1400°C. The heat of fusion amounts to 282.3 J/g. Even in the liquid region there is no overlapping oxidation and therefore, no decrease in the measured specific heat was observed. This, however, can only be realized if extremely pure purge gas (Ar 5N) and special crucible arrangement (yttria-coated crucibles) are used for the tests.



Apparent specific heat on a titanium chromium alloy between room temperature and 1525°C

# High-Melting Alloys

## Titanium Alloy $\gamma$ -TiAl

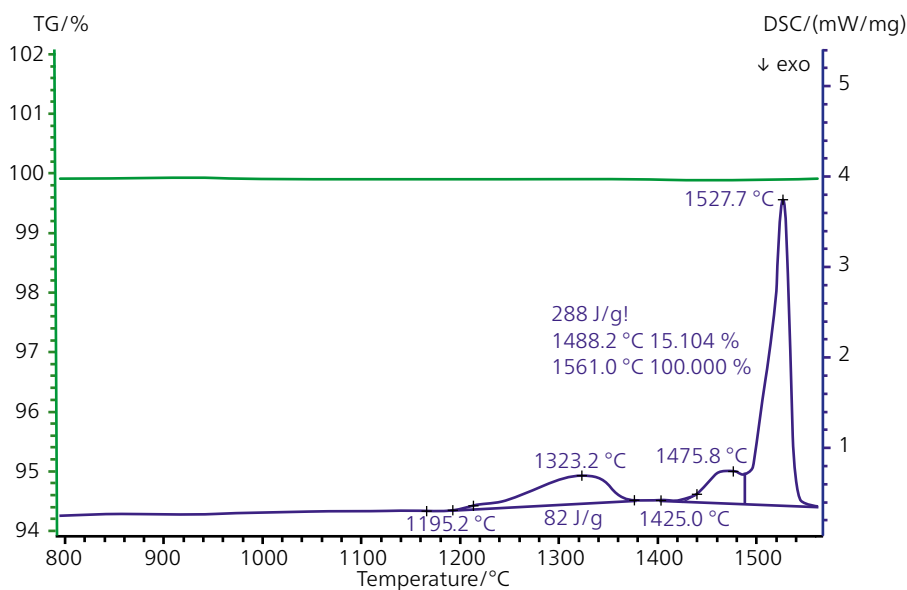
### Introduction

The high-performance metal  $\gamma$ -TiAl distinguishes itself through high temperature and corrosion resistance with a low specific weight. It is used, for instance, in turbochargers, turbines, and automotive motors as well as in aircraft and space applications. This material can be considered as an exemplary alloy when investigated by STA. Typically, phase transformations like melting, but also mass changes due to oxidation or reduction, can be observed.

### Test Results

The DSC signal shows an endothermic effect (1322°C peak temperature) beginning at an extrapolated onset temperature of 1195°C; this is due to the structural  $\alpha_2 \rightarrow \alpha$  transformation. At 1476°C (DSC peak temperature), the  $\alpha \rightarrow \beta$  transformation occurs. The endothermic DSC peak at 1528°C is due to melting of the sample (onset at approx. 1490°C, liquidus temperature at about 1560°C). No significant mass changes were detected during the experiment indicating that the sample did not oxidize during the experiment.

Test Conditions	
Instrument	STA 449 <b>F3</b> Jupiter®
Sample	$\gamma$ -TiAl
Sample mass	30.08 mg
Temperature range	RT to 1600°C
Heating rate	20 K/min
Atmosphere	Argon (70 ml/min)
Crucible	Pt+Al <sub>2</sub> O <sub>3</sub> liners
Sensor	TGA-DSC, type S



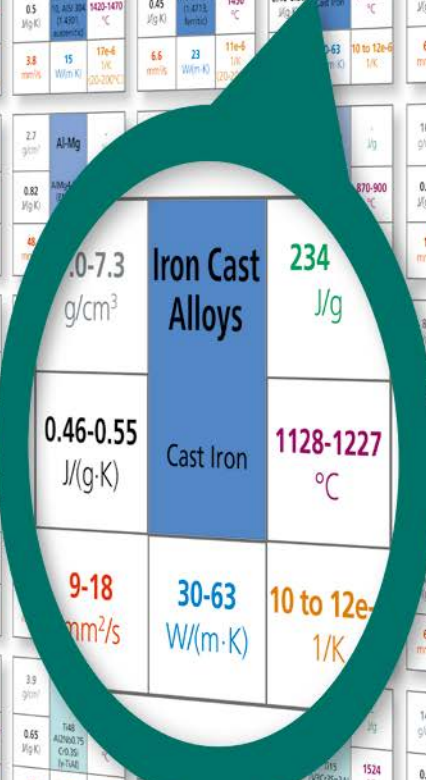
STA measurement in an Ar atmosphere not only proves the vacuum-tightness of the STA as no oxidation effects were detected (e.g., weight gain).



# Thermal Properties of Alloys

**NETZSCH**  
Proven Excellence.

<b>Low Alloyed Steels</b> 7.8 g/cm <sup>3</sup> 0.46-0.48 J/(g·K) 11-17 mm/s	<b>Alloyed Steels</b> 7.8 g/cm <sup>3</sup> 0.48 J/(g·K) 3.4 mm/s	<b>Alloyed Steels</b> 7.8 g/cm <sup>3</sup> 0.5 J/(g·K) 3.8 mm/s	<b>Alloyed Steels</b> 7.7 g/cm <sup>3</sup> 0.45 J/(g·K) 6.6 mm/s	<b>Iron Cast Alloys</b> 7.0-7.3 g/cm <sup>3</sup> 0.46-0.55 J/(g·K) 5-63 mm/s	<b>Al-Si</b> 2.44 g/cm <sup>3</sup> 0.85 J/(g·K) 64 mm/s	<b>Al-Si</b> 2.7 g/cm <sup>3</sup> 0.85 J/(g·K) 66 mm/s	<b>Al-Si</b> 2.7 g/cm <sup>3</sup> 0.83 J/(g·K) 53 mm/s	<b>Al-Mg</b> 2.4 g/cm <sup>3</sup> 0.93 J/(g·K) 38 mm/s
<b>Al-Mg</b> 2.4 g/cm <sup>3</sup> 0.96 J/(g·K) 38 mm/s	<b>Al-Mg</b> 2.4 g/cm <sup>3</sup> 0.8 J/(g·K) 36 mm/s	<b>Al-Mg</b> 2.7 g/cm <sup>3</sup> 0.82 J/(g·K) 48 mm/s	<b>Al-Mg</b> 2.7 g/cm <sup>3</sup> 0.82 J/(g·K) 48 mm/s	<b>Iron Cast Alloys</b> 7.0-7.3 g/cm <sup>3</sup> 0.46-0.55 J/(g·K) 5-63 mm/s	<b>Au-Pd</b> 16.2 g/cm <sup>3</sup> 0.16 J/(g·K) 17 mm/s	<b>Au-Ni</b> 14.7 g/cm <sup>3</sup> 0.25 J/(g·K) 8.5 mm/s	<b>Brass (Cu-Zn)</b> 8.9 g/cm <sup>3</sup> 0.38 J/(g·K) 72 mm/s	<b>Brass (Cu-Zn)</b> 8.8 g/cm <sup>3</sup> 0.38 J/(g·K) 48 mm/s
<b>Brass (Cu-Zn)</b> 8.6 g/cm <sup>3</sup> 0.38 J/(g·K) 38 mm/s	<b>Brass (Cu-Zn)</b> 8.4 g/cm <sup>3</sup> 0.38 J/(g·K) 37 mm/s	<b>Al-Mg</b> 2.7 g/cm <sup>3</sup> 0.82 J/(g·K) 48 mm/s	<b>Al-Mg</b> 2.7 g/cm <sup>3</sup> 0.82 J/(g·K) 48 mm/s	<b>Iron Cast Alloys</b> 7.0-7.3 g/cm <sup>3</sup> 0.46-0.55 J/(g·K) 5-63 mm/s	<b>Bronze (Cu-Sn)</b> 8.8 g/cm <sup>3</sup> 0.38 J/(g·K) 20 mm/s	<b>Bronze (Cu-Sn)</b> 8.8 g/cm <sup>3</sup> 0.38 J/(g·K) 20 mm/s	<b>Nickel Silver (Cu-Ni)</b> 8.7 g/cm <sup>3</sup> 0.38 J/(g·K) 13 mm/s	<b>Nickel Silver (Cu-Ni)</b> 8.7 g/cm <sup>3</sup> 0.38 J/(g·K) 10 mm/s
<b>Cu-Al</b> 7.6 g/cm <sup>3</sup> 0.41 J/(g·K) 11 mm/s	<b>Mg-Al</b> 1.8-1.9 g/cm <sup>3</sup> 0.95-1.06 J/(g·K) 17.42 mm/s	<b>Mg-Al</b> 1.8-1.9 g/cm <sup>3</sup> 0.95-1.06 J/(g·K) 17.42 mm/s	<b>Mg-Al</b> 1.8-1.9 g/cm <sup>3</sup> 0.95-1.06 J/(g·K) 17.42 mm/s	<b>Iron Cast Alloys</b> 7.0-7.3 g/cm <sup>3</sup> 0.46-0.55 J/(g·K) 5-63 mm/s	<b>Mg-Ag-Rare Earth-Zr</b> 8.0 g/cm <sup>3</sup> 0.9 J/(g·K) 62 mm/s	<b>Ni-X</b> 7.6-9.0 g/cm <sup>3</sup> 0.41-0.52 J/(g·K) 2.3-5.8 mm/s	<b>Ni-Cr</b> 8.2 g/cm <sup>3</sup> 0.44 J/(g·K) 3.2 mm/s	<b>Ni-Cr</b> 8.3 g/cm <sup>3</sup> 0.44 J/(g·K) 3.5 mm/s
<b>Ni-Cu</b> 8.8 g/cm <sup>3</sup> 0.43 J/(g·K) 5.8 mm/s	<b>Ti-Al</b> 4.4 g/cm <sup>3</sup> 0.58 J/(g·K) 2.6 mm/s	<b>Ti-Al</b> 4.4 g/cm <sup>3</sup> 0.58 J/(g·K) 2.6 mm/s	<b>Ti-Al</b> 4.4 g/cm <sup>3</sup> 0.58 J/(g·K) 2.6 mm/s	<b>Iron Cast Alloys</b> 7.0-7.3 g/cm <sup>3</sup> 0.46-0.55 J/(g·K) 5-63 mm/s	<b>Mo-W</b> 14.8 g/cm <sup>3</sup> 0.20 J/(g·K) 34 mm/s	<b>Iron Alloys (Cu-Al)</b> 8.8 g/cm <sup>3</sup> 0.43 J/(g·K) 5.8 mm/s	<b>Aluminum Alloys (Al-Si, Al-Mg)</b> 2.7 g/cm <sup>3</sup> 0.83 J/(g·K) 53 mm/s	<b>Gold Alloys (Au-Ag)</b> 19.3 g/cm <sup>3</sup> 0.125 J/(g·K) 10 to 12e-6 1/K



Iron Alloys (Cu-Al)	Aluminum Alloys (Al-Si, Al-Mg)	Gold Alloys (Au-Ag)
Copper Alloys (Ni-Cu-Zn, Ni-Si, Ni-Co)	Magnesium Alloys (Mg-Al, Mg-Ag-Rare Earth-Zr)	Nickel Alloys (Ni-Cr, Ni-Cu)
Titanium Alloy (Ti-Al)	Molybdenum-Tungsten-Alloy (Mo-W)	

Density	Alloy	Melting Enthalpy
Specific Heat Capacity		Melting Range
Thermal Diffusivity	Thermal Conductivity	Coefficient of Thermal Expansion

GET YOUR FREE POSTER  
[www.netzsch.com/tpoa](http://www.netzsch.com/tpoa)

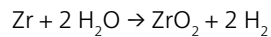


# High-Melting Alloys

## Hydrogen Emission from Zircaloy BCR-276 Under Water Vapor

### Introduction

Zircaloy BCR-276 (Zirc-4) is a certified European Commission reference material. Zircalloys are common cladding materials in nuclear reactors because of their low thermal neutron absorption cross-section and their excellent thermal and mechanical properties. During the earthquake/tsunami-related accident at the Fukushima-Daiichi nuclear plant in Japan, hydrogen accumulated under the roof of the building and was ignited. One way to produce hydrogen under these extraordinary conditions could follow this relative simple chemical reaction (1):



To confirm this reaction, some preliminary experiments were carried out and are described below.

### Experimental

A NETZSCH STA 449 **F3 Jupiter**<sup>®</sup> was equipped with a water-vapor furnace and a QMS 403 **Aëolos**<sup>®</sup> mass spectrometer. Three cylinders of BCR-276 (sample weight approx. 600 mg) were placed on an alumina slip-on plate on a TGA

Test Conditions	
Instrument	STA 449 <b>F3 Jupiter</b> <sup>®</sup> with water-vapor furnace, coupled to a QMS 403 <b>Aëolos</b> <sup>®</sup>
Sample	Zircaloy BCR-276
Sample mass	Approx. 600 mg
Temperature range	RT to 1100°C
Heating/cooling rate	5 and 10 K/min
Atmosphere	N <sub>2</sub> / water vapor (60 ml/min)
Sample carrier	TGA, type S

sample carrier. The samples were heated to 1050°C at 5 and 10 K/min under N<sub>2</sub> and water vapor. The intensities of water and hydrogen were monitored with the mass spectrometer.

### Test Results

Figure 1 depicts the TGA curve (mass change) and the intensities of hydrogen and water versus temperature for the measurement at 10 K/min. After the start of the weight increase due to oxidation the hydrogen level increases.

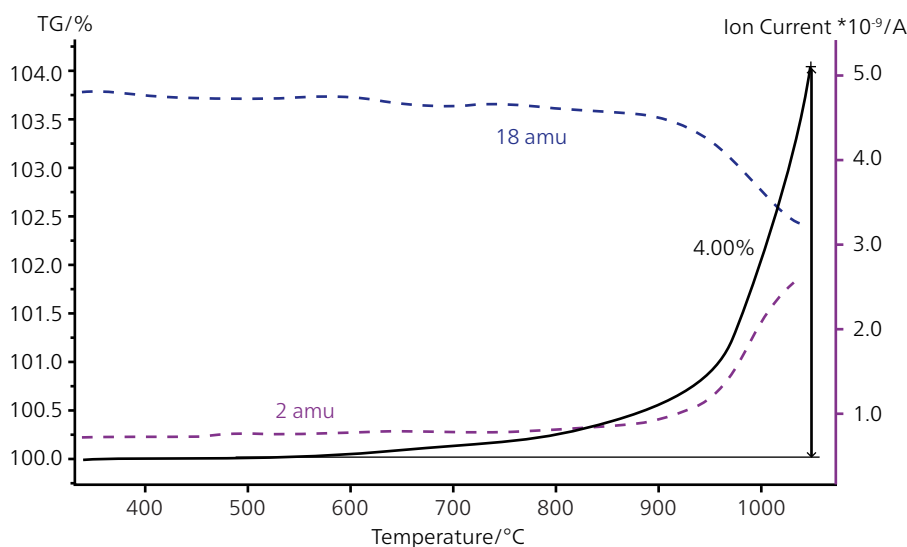


Figure 1. TGA curve and mass intensities of hydrogen (2 amu) and water (18 amu) of BCR-276 in water vapor and nitrogen

Simultaneously to the hydrogen increase, the water intensity decreases. The weight increase up to 1050°C was 4 wt%. In Figure 2, the TGA curves and the intensities of hydrogen for the two measurements at 5 K/min and 10 K/min were compared. At a heating rate of 5 K/min, the oxidation and the hydrogen evolution starts earlier than at 10 K/min. At about 950°C, the hydrogen evolution goes into a stable saturated state (constant level).

### Literature

(1) M. Steinbrück, Hydrogen absorption by zirconium alloys at high temperatures. Journal of Nuclear Materials 334, p. 58-64

Figure 3 shows the sample before and after the measurement.

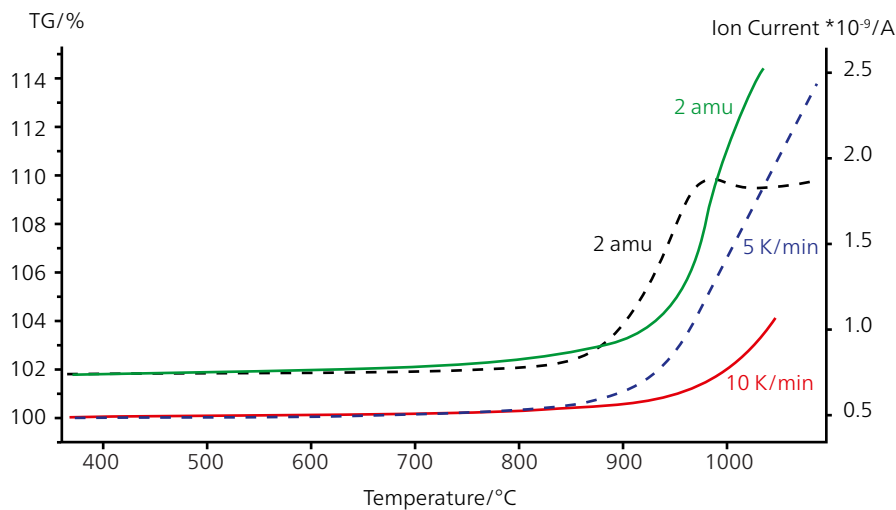


Figure 2. TGA curves and H<sub>2</sub> intensities of Zircaloy BCR-276 at a heating rate of 5 K/min and 10 K/min

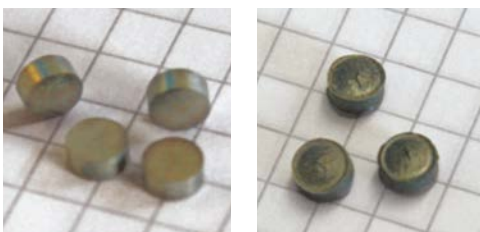


Figure 3. BCR-276 "original" and after the measurement

# High-Melting Alloys

## Copper Alloy

### Introduction

Copper and copper alloys are essential for a broad range of applications, e.g., for the electronic and electrical industry, for automotive (bearing bushes for powertrains and brakes, high-performance heat exchangers for oil coolers, etc.). For optimization of the manufacturing processes and for the later application of the copper alloys, knowledge of the thermophysical properties is necessary.

The thermal diffusivity and specific heat were measured using the LFA. The thermal conductivity was calculated by multiplying the measured properties with the room temperature bulk density. For comparison of the specific heat results, additional DSC measurements were carried out.

### Test Results

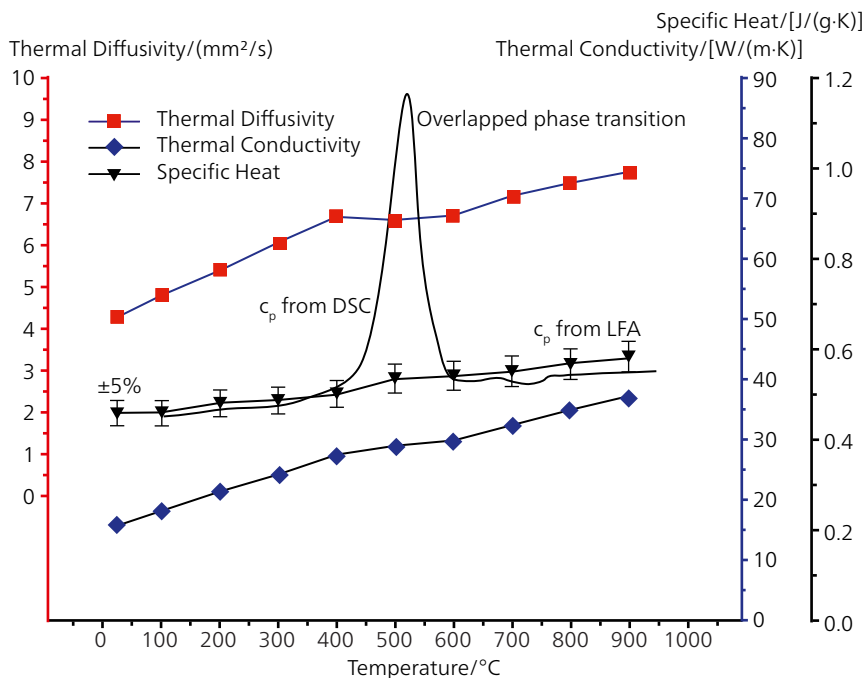
The thermophysical properties increase with temperature. Between 500°C and 600°C, a step in the thermal diffusivity was detected. In the same temperature range, an overlapping endothermic effect is visible ( $c_p$  from DSC) due to the phase transition. The differences in the specific heat, measured with different methods (LFA and DSC), are quite small (<5%). The thermal conductivity continuously increases.

Test Conditions	
Instruments	LFA 457 <i>MicroFlash</i> <sup>®</sup> , DSC 404 <i>Pegasus</i> <sup>®</sup>
Sample	Copper alloy
Sample thickness	3.04 mm
Temperature range	RT to 900°C
Density	8.253 g/cm <sup>3</sup> at RT
Sample holder (LFA)	12.7 mm diameter
Sample surface preparation (LFA)	Graphite
$c_p$ from LFA, standard	Pure copper
Sensor (DSC)	DSC, type S



### Difference Between Thermal Conductivity ( $\lambda$ ) and Thermal Diffusivity ( $a$ )

$\lambda$  (W/m·K) of a material is a measure of the ability of that material to conduct heat through it. On the other hand, a (mm<sup>2</sup>/s) of a material is the thermal inertia of that material. This value describes how quickly a material reacts to a temperature change.



Thermophysical Properties of a copper alloy between room temperature and 1000°C

## Silver Alloy SF928CH

### Introduction

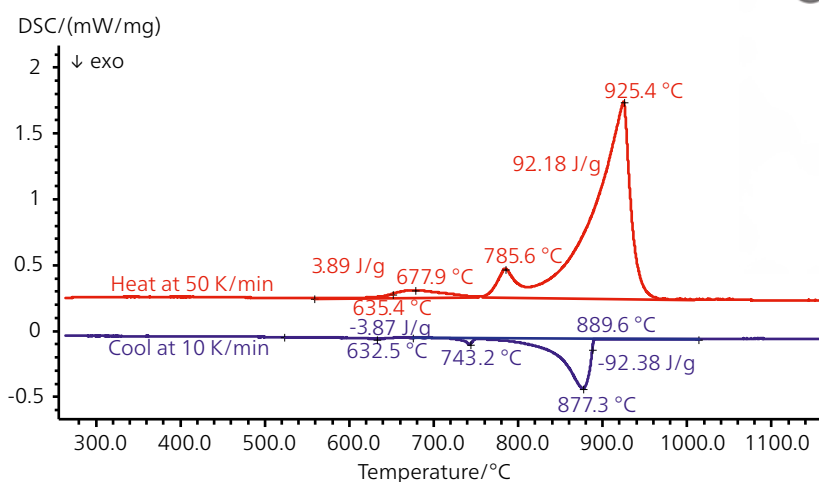
Silver is a precious metal well-known for its high thermal and electrical conductivity. It is therefore used in many electrical and electronic products. Printed circuits, for example, are made using silver paints, and computer keyboards using silver electrical contacts. Silver is also used in high-voltage contacts because it is the only metal that will not arc across contacts, hence it is extremely safe. Fine silver (99.9% pure) is generally too soft for producing large functional objects. Therefore, it is generally alloyed with other metals (e.g., copper) to give strength whilst preserving the ductility of the silver and a high precious metal content. Silver alloy SF928CH contains 92.5% pure silver and 7.5% other elements, which are composed of copper (72%) and zinc (28%).

### Test Results

The specific heat-flow rate was measured at a high heating rate of 50 K/min up to 1150°C and during cooling at 10 K/min. Due to the high heating rate at 50 K/min, melting is shifted to higher temperatures. Melting of the alloy occurs in three steps (peak temperatures at 678, 786 and 925°C

Test Conditions	
Instrument	DSC 404 Pegasus®
Sample	Silver alloy SF928CH
Sample mass	57.42 mg
Temperature range	RT to 1150°C
Heating/cooling rates	50 K/min (↑) and 10 K/min (↓)
Atmosphere	Argon (50 ml/min)
Crucible	Pt with liner and lid
Sensor	DSC, type S

during heating). The entire heat of fusion was 96.1 J/g (3.89+92.18 J/g). Solidification of the alloy was measured at 890°C (endset). Three separate peaks occurred again during the solidification process. The enthalpy change during solidification was 96.2 J/g (3.87+92.38 J/g) and therefore, nearly the same as during heating. The onset temperature of melting (635°C) was close to the last solidification peak (at 633°C), even though a very high heating rate was employed during the heating cycle.



DSC results on silver alloy SF928CH

# Superalloys

## Nickel-Based Superalloy (Inconel 600) – DSC Measurements

### Introduction

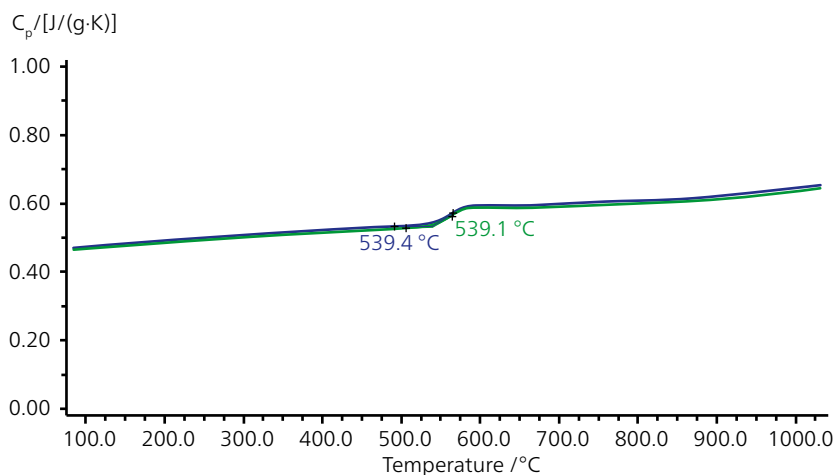
Inconel alloys are a family of non-magnetic nickel-based superalloys. Inconel 600 alloy consists of 72% nickel, 16% chromium, 8% iron and 4% further minor metal amounts. The high chromium content of Inconel 600 raises its oxidation resistance considerably above that of pure nickel while its high nickel content provides good corrosion resistance under reducing conditions. Therefore, Inconel 600 offers high oxidation and corrosion resistance, even at very high temperatures, and also retains a high mechanical strength under these conditions. It is therefore often used under extreme conditions, such as aircraft engine parts, turbocharger turbine wheels, chemical processing and pressure vessels. Inconel 600 & 800 are also used in the pressure tubes of CANDU nuclear reactors. Furthermore, Inconel 600 is a certified reference material for the determination of the thermal conductivity by means of LFA (Laser Flash Analysis).

### Test Results

Presented in the below plot are the results of six different DSC runs on an Inconel superalloy. The differences between the individual runs are in the range of  $\pm 2\%$  which corresponds

Test Conditions	
Instrument	DSC 404 Pegasus®
Sample	Inconel 600
Sample mass	Approx. 195 mg
Temperature range	RT to 1000°C
Heating/cooling rate	20 K/min
Atmosphere	Argon (60 ml/min)
Crucible	Pt with lid
Sensor	DSC, type S

to the typical reproducibility of this DSC instrument. At lower temperatures, the specific heat capacity shows a nearly linear increase. Between 550°C and 700°C, an endothermic step can be observed in the measured specific heat. This step can be explained by an additional contribution to the specific heat capacity; the true specific heat is overlapped by an enthalpy change caused by a phase transition (formation of  $\text{NiCr}_3$  clusters). Therefore, the measured data represents the apparent specific heat capacity in this temperature range.



Six different DSC runs on Inconel 600 superalloy

## Nickel-Based Superalloy (Inconel 600) – DIL Measurements

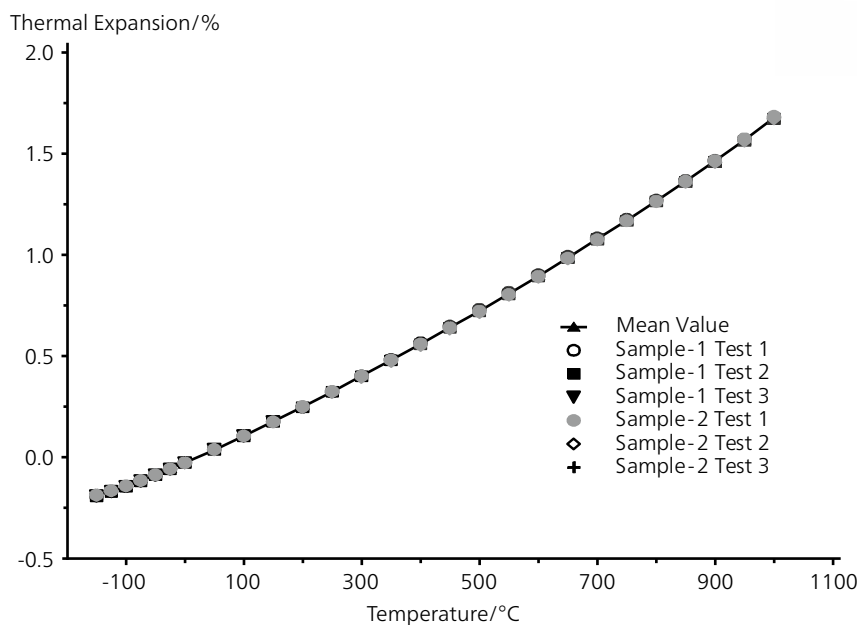
### Introduction

Thermal expansion is a very important parameter to know for the construction arrangement and consideration of the "free space" between the components.

### Test Results

Presented in the plot are the results of six different runs on an Inconel superalloy between room temperature and 1000°C. Additional measurements were carried out between -150°C and 50°C using a low temperature furnace. The differences between the individual runs are in the range of ±0.5% which corresponds to the typical accuracy of the Dilatometer DIL 402 C. At lower temperatures, a nearly linear increase in the thermal expansion results can be seen. Between 500°C and 600°C, a slight slope change is visible. This effect can be explained by a structural change in the material (formation of NiCr<sub>3</sub> clusters) leading to a slightly different rate of expansion at higher temperatures.

Test Conditions	
Instrument	DIL 402 C
Sample	Inconel 600
Sample length	Approx. 25 mm
Temperature range	-150°C to 1000°C
Heating rate	5 K/min
Atmosphere	Helium (100 ml/min)
Sample holder	Fused silica
Calibration	Platinum / fused silica



DIL measurements on nickel-based Inconel 600 superalloy



# Superalloys

## Nickel-Based Superalloy (Inconel 600) – LFA Measurements, Thermal Diffusivity

### Introduction

The thermal diffusivity is a measure of how fast heat is transferred within the material. This data is very important and many simulation programs use it.

### Test Results

Figure 1 presents the results for six different LFA runs on Inconel 600 superalloy between -125°C and 1000°C. Two different furnace systems were employed for the tests (-125°C ... 25°C and 25°C ... 1000°C). The differences between the individual runs are in the range of ±2% which corresponds to the typical accuracy of the unit. A minimum was obtained in the thermal diffusivity curve slightly below 0°C. This might be due to a change in magnetic properties. Between 500 and 700°C, a step overlaps the thermal diffusivity. This step is caused by the formation of NiCr<sub>3</sub> clusters. Outside the transition range, a nearly linear increase was obtained in the thermal diffusivity.

Test Conditions	
Instrument	LFA 457 <i>MicroFlash</i> ®
Sample	Inconel 600
Sample thickness	Approx. 3 mm
Temperature range	-125°C to 1000°C
Sample holder	12.7 mm
Sample surface preparation	Sandblasted

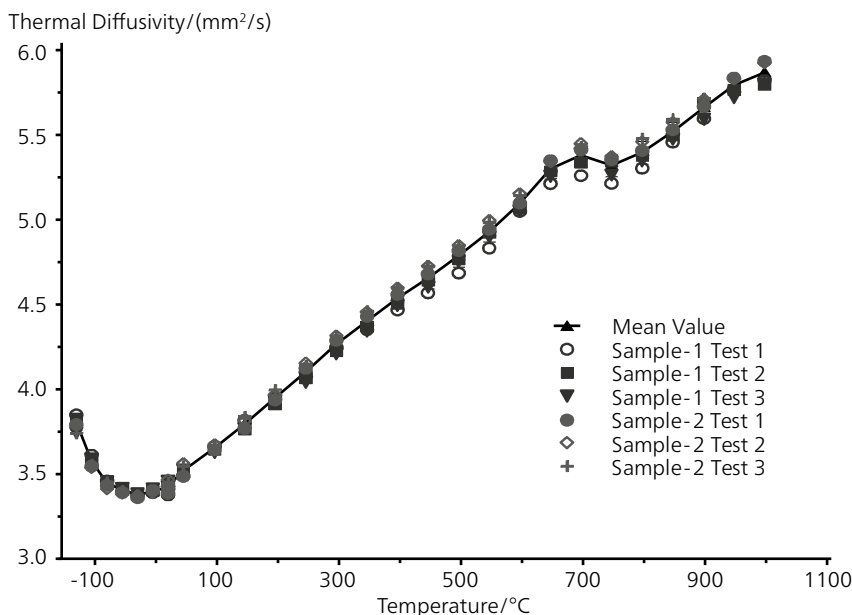


Figure 1. LFA measurements on nickel-based Inconel 600 superalloy

## Highly Corrosion-Resistant Metal Alloy – Hastelloy

### Introduction

Hastelloy is a nickel-chromium-molybdenum-tungsten alloy with outstanding high-temperature stability as evidenced by high ductility and corrosion resistance. It has excellent resistance to stress-corrosion cracking and to oxidizing atmospheres up to 1038°C. It is used in combustion gas desulfurization plants, the chemical industry and incineration plants, etc.

### Test Results

The STA measurement was carried out between room temperature and 1450°C. The DSC curve (blue) depicts the melting of a hastelloy sample (alloy 22) at 1358°C (extrapolated onset) with an enthalpy of 165 J/g. During cooling, crystallization occurred at 1351°C (extrapolated endset) with nearly the same enthalpy change (red DSC curve). During heating and cooling, neither a mass loss nor an increase due to oxidation was observed (TGA signals).

### Conclusion

Investigation of the melting and crystallization behavior of metal alloys is possible with the STA 449 **F5 Jupiter**<sup>®</sup>. The vacuum-tight design allows for measurements under

Test Conditions	
Instrument	STA 449 <b>F5 Jupiter</b> <sup>®</sup>
Sample	Hastelloy
Sample mass	39.02 mg
Temperature range	RT to 1450°C
Heating/cooling rate	20 K/min
Atmosphere	Argon (70 ml/min)
Crucibles	Platinum with Al liners
Sample holder	TGA-DSC, type S

defined atmospheres improving the test results in terms of repeatability and accuracy. In addition, the risk of misinterpretation of the results due to oxidation effects can be minimized.

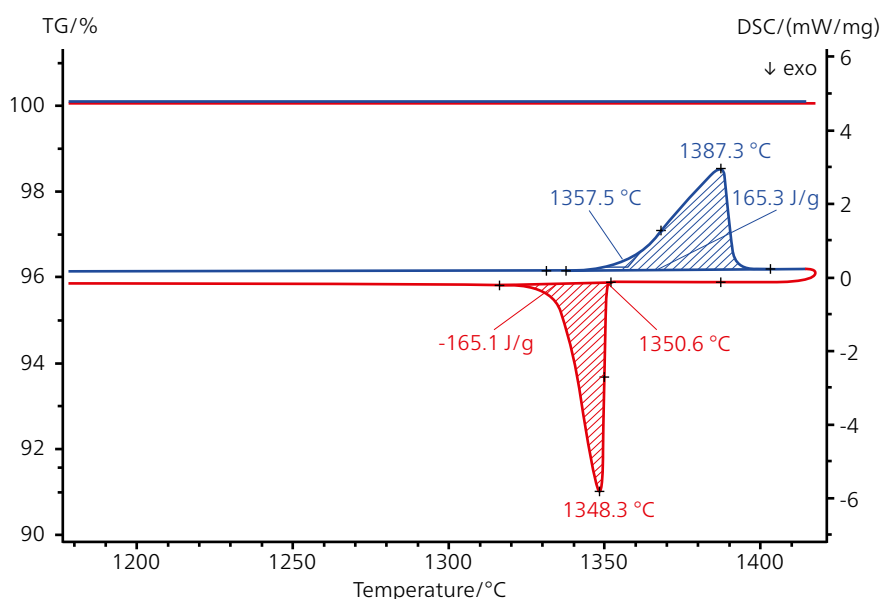


Figure 1. Heating (blue curve) and cooling (red curve) of the STA measurement on hastelloy in argon atmosphere

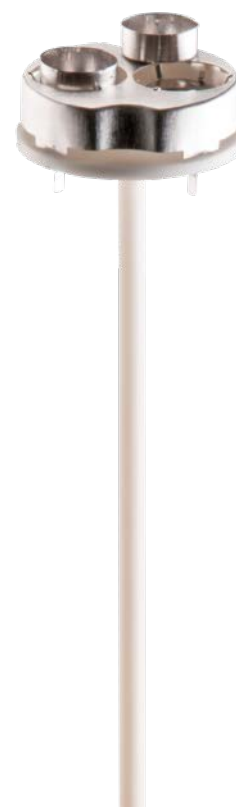


Figure 2. DSC sensor in round design with Pt crucibles

# Shape Memory Alloys

## TiNiPd Alloys

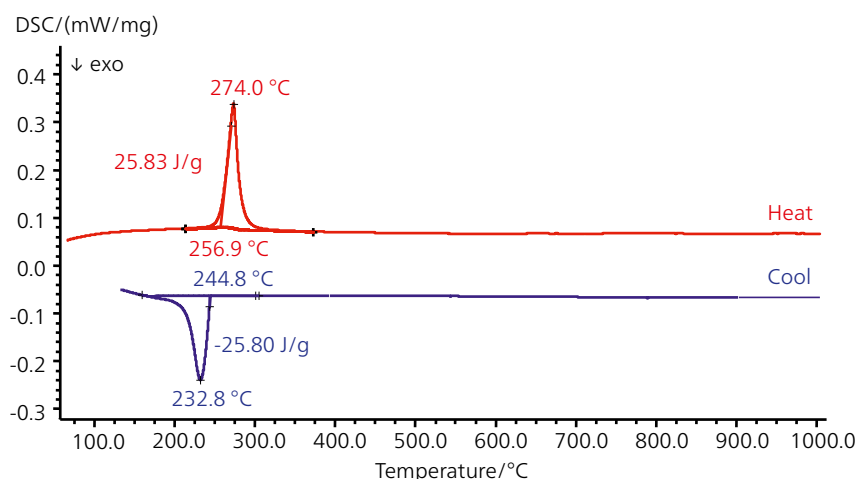
### Introduction

The exciting field of smart materials is expanding rapidly, with one of the most interesting areas being that of shape memory alloys. A shape memory alloy (SMA) can undergo substantial plastic deformation, and then be triggered into returning to its original shape by the application of heat. From early applications such as greenhouse window openers in which an SMA actuator provided temperature-dependent ventilation, through to mobile phone antennas made of a super-elastic SMA, the list of applications has increased enormously throughout the 1990s to the modern day. Medical applications of SMAs, using their superelastic and shape recovery properties, are particularly interesting and are growing rapidly.

### Test Results

Using DSC systems capable of operation under pure atmospheres and up to high temperatures, solid-solid transitions occurring in shape memory alloys at elevated temperatures can be studied without the influence of oxidation. In the below alloy, the solid-solid transition is visible at 257°C during heating and at 245°C during cooling. The enthalpy change connected with the transition amounts to 25.8 J/g

Test Conditions	
Instrument	DSC 404 Pegasus®
Sample	Ti <sub>50.5%</sub> Ni <sub>24.5%</sub> Pd <sub>25%</sub>
Sample mass	194.4 mg
Temperature range	RT to 1000°C
Heating/cooling rate	10 K/min
Atmosphere	Argon (50 ml/min)
Sample mass	194.4 mg
Crucible	Pt with alumina liner
Sensor	c <sub>p</sub> type S



Heating and cooling segment of the DSC measurement on TiNiPd alloys

# NiTiNOL

## Introduction

After a sample of SMA (shape memory alloy) has been deformed from its "original" conformation, it regains its original geometry by itself during heating (one-way effect) or, at higher ambient temperatures, simply during unloading (pseudo-elasticity). These extraordinary properties are due to a temperature-dependent martensitic phase transformation from a low symmetry to a highly symmetric crystallographic structure.

These materials are used in, e.g., the development of dental braces that exert a constant pressure on the teeth. However, these materials are not currently appropriate for applications such as robotics or artificial muscles, due to energy inefficiency, slow response times, and large hysteresis.

## Test Results

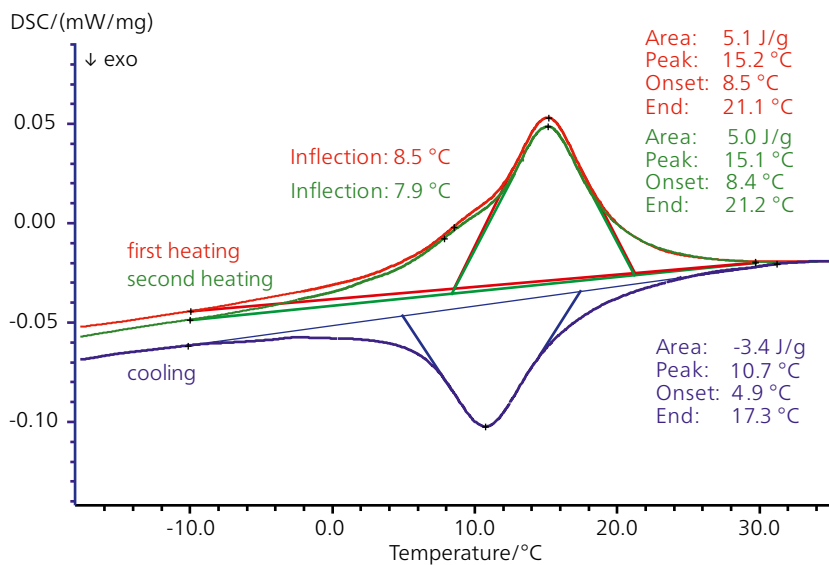
The extraordinary properties of SMAs are based on the structural changes. Every phase transition is associated with a heat exchange and can therefore be studied by means of DSC. The analysis of SMAs with several heating and cooling cycles can not only determine the phase transition temperature, but also prove the reversibility of these phase transitions. Comparing the results of the 1<sup>st</sup> and 2<sup>nd</sup> heatings, the results confirm an identical peak shape and reversible values for the transition temperatures as well as for the transition enthalpy.

Test Conditions	
Instrument	DSC 204 <b>F1</b> Phoenix®
Sample	NiTiNOL
Sample mass	5.34 mg
Temperature range	-50°C to 50°C
Heating rate	10 K/min
Atmosphere	Nitrogen (40 ml/min)
Crucible	Aluminum, pierced lid



### Martensitic Phase Transformation

It is a 1<sup>st</sup> order solid-solid and displacive phase transition (without atomic diffusion) consisting of a homogeneous lattice deformation leading to the new crystal structure (martensite). Due to the displacive character, the transformation proceeds by small cooperative movements of the atoms, keeping the same chemical composition and atomic order of the parent phase (austenite). It can be induced by changing the temperature (on cooling) or by applying an external stress. It is reversible by heating from the martensitic state or by releasing the stress, but it proceeds at higher temperatures or lower stresses than the direct transformation, thus the transformation cycle exhibits hysteresis.



1<sup>st</sup> heating (red), cooling (blue) and 2<sup>nd</sup> heating segment (green) of the DSC measurement on a shape memory alloy

# Shape Memory Alloys

## Shape Memory Alloy – Viscoelastic Behavior

### Introduction

Among shape memory alloys, shape-memory materials have gained high interest due to their large strain recovery capability. This can be up to 8% in metals and up to 800% in polymers.

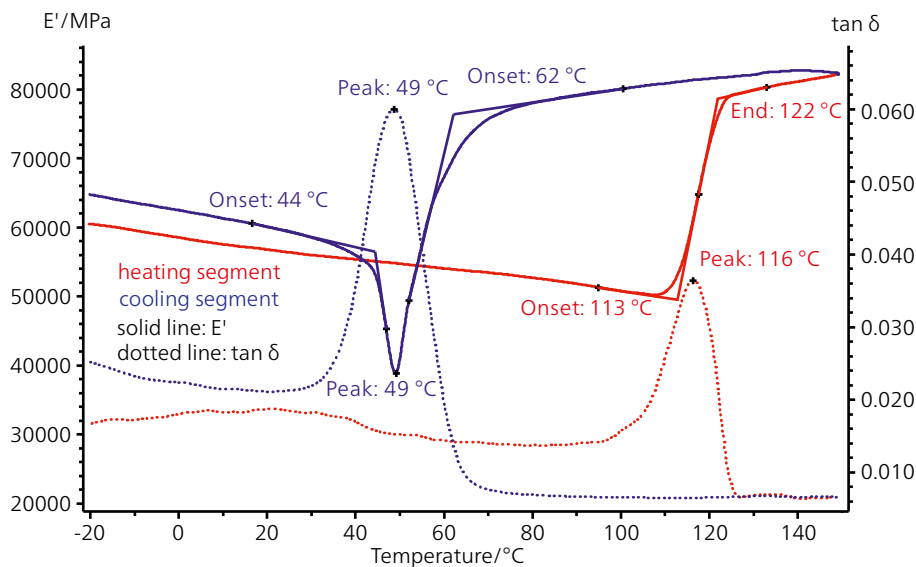
Dynamic mechanical analysis (DMA) can be used to characterize the thermal and mechanical properties of shape memory alloys. In the thermally induced phase transformation of austenite to martensite (or vice versa), the modulus changes and a peak appears each time in the  $\tan \delta$  curve during the phase change. In addition, a hysteresis effect can be observed between heating and cooling.

Test Conditions	
Instrument	DMA 242
Sample	Shape memory alloy
Temperature range	-20°C to 150°C
Heating rate	3 K/min
Amplitude	$\pm 20 \mu\text{m}$
Sample holder	3-point bending, 10 mm
Frequency	1 Hz
Proportional factor	1.3
Max dynamic force	6.1 N

### Test Results

The dynamic thermomechanical properties of a shape memory alloy between -20°C and 150°C are displayed in this figure. At the beginning, the storage modulus  $E'$  decreases with increasing temperature in the heating segment (red curve). Between 113°C (extrapolated onset) and 122°C (extrapolated end), a sharp increase in  $E'$  was

detected which can be related to the phase transition. The corresponding maximum in the  $\tan \delta$  curve was at 116°C. During cooling (blue curve), the phase transition was found between 44°C and 62°C (extrapolated onset). Furthermore, the storage modulus  $E'$  curve exhibits a minimum at 49°C. The effect can also be evaluated as a peak in the loss factor curve at 49°C.



Heating (red curve) and cooling (blue curve) segment of the DMA measurement on a shape memory alloy



## TiNi Memory Metal

### Introduction

DMA determines the ratio of the amplitude of the excitation (e.g., force) to the magnitude of the sample response (e.g., deformation), as well as the time delay with which the response is delayed relative to the excitation. This analysis can also be applied to memory metals that structurally reorganize at certain temperatures. If one changes the sample temperature (temperature sweep) during such a series of measurements, the transformation temperatures can be detected via the associated modulus changes.

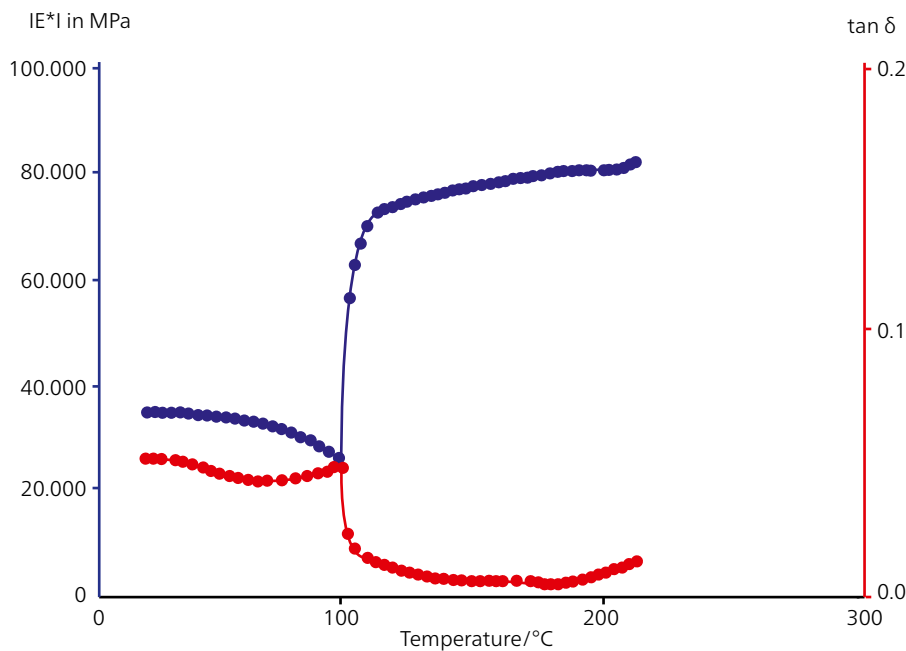
Besides the detection of the phase transition from austenite to martensite phase, the reversal shape memory effect and the super-elasticity can also be studied.

### Test Results

The measurement plot shows the temperature-dependent course of  $E^*$  (dynamic tensile test) and loss factor  $\tan \delta$  (inner damping) of a NiTi.

Test Conditions	
Instrument	DMA GABO EPLEXOR®
Sample	TiNi
Heating rate	3 K/min
Test frequency	10 Hz
Measurement mode	Tensile

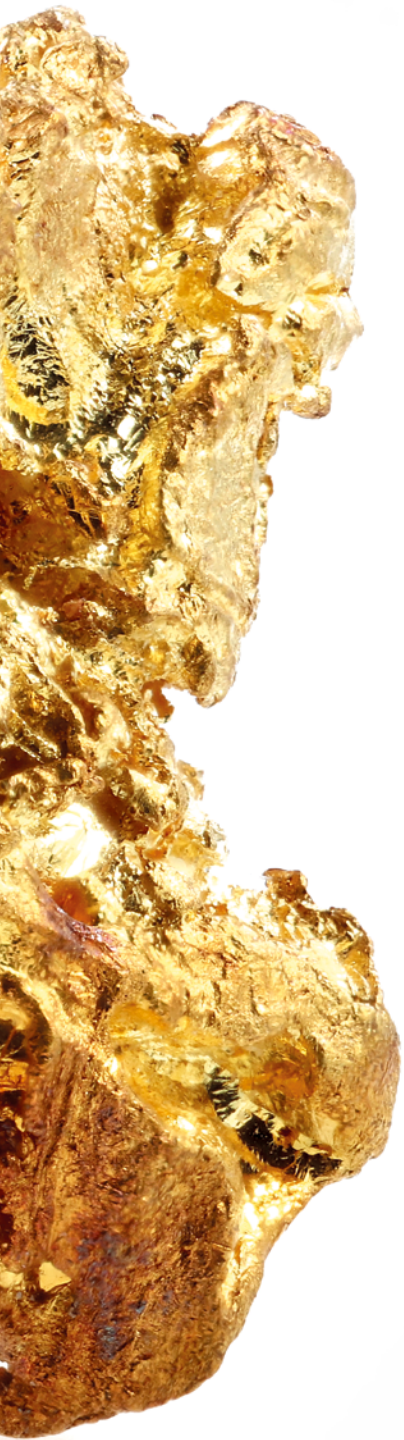
At about 100°C, the alloy shows the martensite-austenite transformation. This transformation is reversible. In the transition, a sudden increase in modulus  $E^*$  can be observed. At the same time, significant reduction of the inner material damping takes place.



Viscoelastic behavior of TiNi during heating and cooling in the DMA GABO EPLEXOR®



# Related Materials and Other Applications



# Related Materials and Other Applications

## Metallic Foams – Al Foam

### Introduction

Closed-cell metal foams have been developed since about many years, and are commonly made by injecting a gas or foaming agent into molten metal. Closed-cell metal foams are primarily used as impact-absorbing material. For optimization of the manufacturing process and/or for the later application (e.g., car manufacturing), the mechanical and thermophysical properties are important.

For LFA measurements, a homogeneous sample surface of the aluminum foam sample is necessary. Therefore, the porous surface structure was closed using a special SiC paste. Concerning the heat transfer through the sample, no significant influence of the additional SiC material was expected due to the fact that only the free space within the surface structure was filled.

Test Conditions	
Instrument	LFA 447 NanoFlash
Sample	Aluminum foam with closed cell structure
Sample thickness	8.150 mm
Density	0.549 g/cm <sup>3</sup> at RT
Temperature range	RT to 300°C
Sample holder	25.4 mm diameter
Sample surface preparation	SiC / graphite
Specific heat	By means of LFA measurement on standard pure aluminum (w/o porosity)

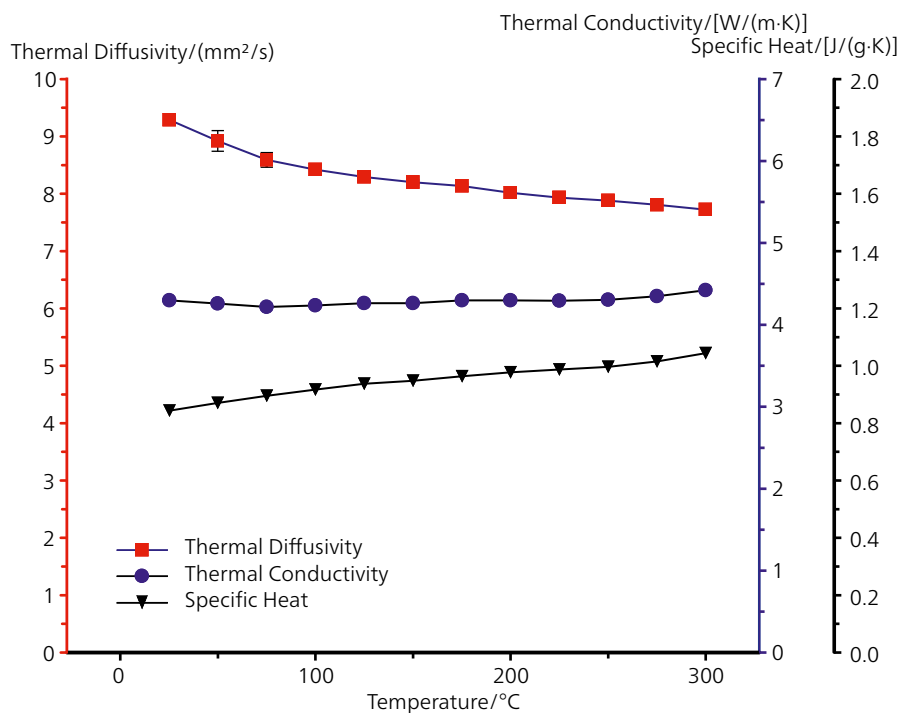


Figure 1. LFA measurements on an Al foam





## Test Results

The thermal diffusivity of the aluminum foam sample decreases with increasing temperature (Figure 1). The specific heat increases over the entire temperature range as expected from the Debye theory. However, the thermal conductivity shows only slight changes up to 300°C.

## Debye Model

The Debye model (by Peter Debye, 1912) estimates the phonon contribution to the specific heat in a solid. It treats the vibrations of the atomic lattice (heat) as phonons in a box, in contrast to the Einstein model, which treats the solid as many individual, non-interacting quantum harmonic oscillators. The Debye model correctly predicts the low temperature dependence of the heat capacity, which is proportional to  $T^3$  – the Debye  $T^3$  law.



# Related Materials and Other Applications

## Amorphous Metals – Amorphous Fe Alloy

### Introduction

An amorphous metal is a metallic material with a disordered atomic-scale structure and, in contrast to “normal” crystalline metals or alloys, it is in a glassy, non-crystalline state. Amorphous metals are usually alloys which were cooled very rapidly from the melt (vapor deposition, spinning, etc.). Iron-based amorphous alloys (Fe-Ni-Co-Si-B) show a higher strength than steel but are not ductile and can show a sudden failure.

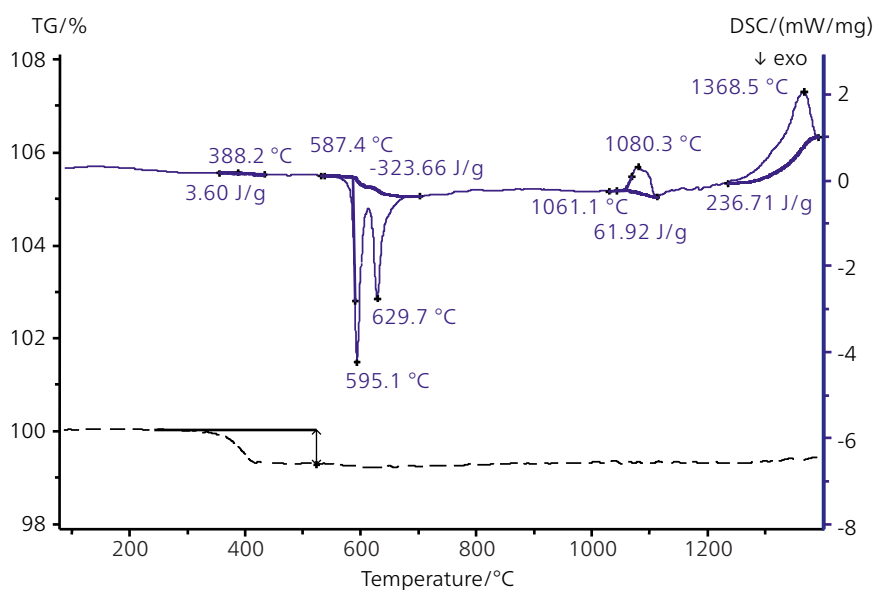
These materials are also used in civil applications, for example, as sensors in safety systems because of their magnetic properties.

### Test Results

This iron-based amorphous alloy shows a small mass-loss step of 0.7% between 300°C and 400°C (probably evaporation of organic contamination). At 587°C (extrapolated onset), the alloy crystallizes in two steps. The exothermal

Test Conditions	
Instrument	STA 449 Jupiter®
Sample	Fe alloy, amorphous
Sample mass	23 mg
Temperature range	RT to 1400°C
Heating/cooling rate	10 K/min
Atmosphere	Argon (40 ml/min)
Crucible	Pt with alumina liner
Sensor	TGA-DSC, type S

enthalpy is relatively high with 323 J/g. At 1061°C (extrapolated onset), an endothermic DSC peak was detected which could be due to a phase transition. Melting of the substance started around 1250°C with a peak temperature at 1368°C. The melting enthalpy was determined to 237 J/g. However, the melting process is not yet finished at 1400°C which could explain the difference between the enthalpies of cold-crystallization and melting.



STA measurement on an amorphous Fe alloy: The DSC curve shows endo- and exothermal effects and the TGA curve demonstrates the mass-loss behavior.



## Minerals – High-Performance Material for Thermoelectrical Applications – Skutterudite

### Introduction

Optimization of energy efficiency is one of the major challenges of the 21<sup>st</sup> century. In many industrial applications, huge amounts of unused thermal energy is generated. Such waste heat is produced by melting furnaces, incineration plants, power plants and even motor vehicles – and could all be used for the generation of electrical energy.

Thermoelectric generators can be employed in all areas where usable temperature differences are available. Such applications require the development of thermoelectric materials with high efficiency.

For the development and optimization of thermoelectric materials, knowledge of the thermophysical and thermoelectric properties is essential. For assessment of the efficiency, the figure of merit ( $ZT$  value) is used. This thermoelectric figure describes how well, or poorly, suited a special material is for use in a thermoelectric generator. The  $ZT$  value thus yields information on the material's efficiency.

The objective is to develop materials exhibiting low thermal conductivity,  $\lambda$ , with simultaneously high electrical conductivity,  $\sigma$ , and a high Seebeck coefficient,  $S$ . The difficulty here is in the fact that these three properties can only be influenced independently of one another under certain conditions.

With the SBA 458 *Nemesis*<sup>®</sup>, the Seebeck coefficient,  $S$ , and electrical conductivity,  $\sigma$ , can be determined simultaneously. Using the LFA, the specific heat capacity,  $c_p$ , and thermal diffusivity,  $a$ , can be measured directly. Along with the density,  $\rho$ , the thermal conductivity,  $\lambda$ , can be calculated.

$$ZT = \left( \frac{S^2 \cdot \sigma}{\lambda} \right) T \qquad \lambda = \rho \cdot c_p \cdot a$$

$\lambda$  = thermal conductivity  
 $a$  = thermal diffusivity  
 $\sigma$  = density  
 $c_p$  = specific heat capacity

Test Conditions	
Instruments	SBA 458 <i>Nemesis</i> <sup>®</sup> LFA 467 <i>HyperFlash</i> <sup>®</sup>
Sample	Skutterudite
Sample length/ $\emptyset$	12.7 mm
Temperature range	0°C to 400°C

Skutterudite in particular has the potential for excellent electrical properties. It is a material consisting of cobalt and arsenic, often contaminated by rare earths. Skutterudite features a very high charge carrier mobility and a medium-sized Seebeck coefficient. Its thermal conductivity, on the other hand, is high. The crystal structure can optimally be modified. Two voids in the elementary cell can be filled by the insertion of foreign atoms. This way, the thermal conductivity of skutterudite can be reduced. Therefore, skutterudites are potential candidates for more efficient thermoelectric converters with which, for example, waste heat from the exhaust systems of automobiles could be directly converted into electricity.

### LFA Measurements

For calculation of the dimensionless  $ZT$  value of skutterudite, the thermal diffusivity (Figure 1, red curve) and the specific heat capacity (Figure 1, black curve) were determined by an LFA in the temperature range between 0°C and 400°C.

Calculation of the thermal conductivity  $\lambda$  is based on the equation on the left and considered in the  $ZT$  calculation in Figure 4 (page 73).

### SBA Measurement

With the SBA 458 *Nemesis*<sup>®</sup>, the Seebeck coefficient and electrical conductivity of the sample already used for the LFA measurement was determined between RT and 350°C. The Seebeck coefficient increased from 100  $\mu\text{V/K}$  to almost 160  $\mu\text{V/K}$  while the electrical conductivity decreased from approx. 1300 S/cm to 1000 S/cm.

# Related Materials and Other Applications

The measurement results exhibit excellent reproducibility ( $\pm 2\%$ ) for both parameters (see Figure 2).

## ZT Value

The ZT value is calculated by means of the results obtained with the LFA and SBA on the same sample (see Figure 3) using the equation on the previous page.

The plot in Figure 4 represents the increase in the ZT value between room temperature and 400°C reaching a maximum value of 0.75.

## Summary

The thermophysical properties – including thermal diffusivity and thermal conductivity, specific heat capacity, Seebeck coefficient and electrical conductivity – can be determined using only one sample.

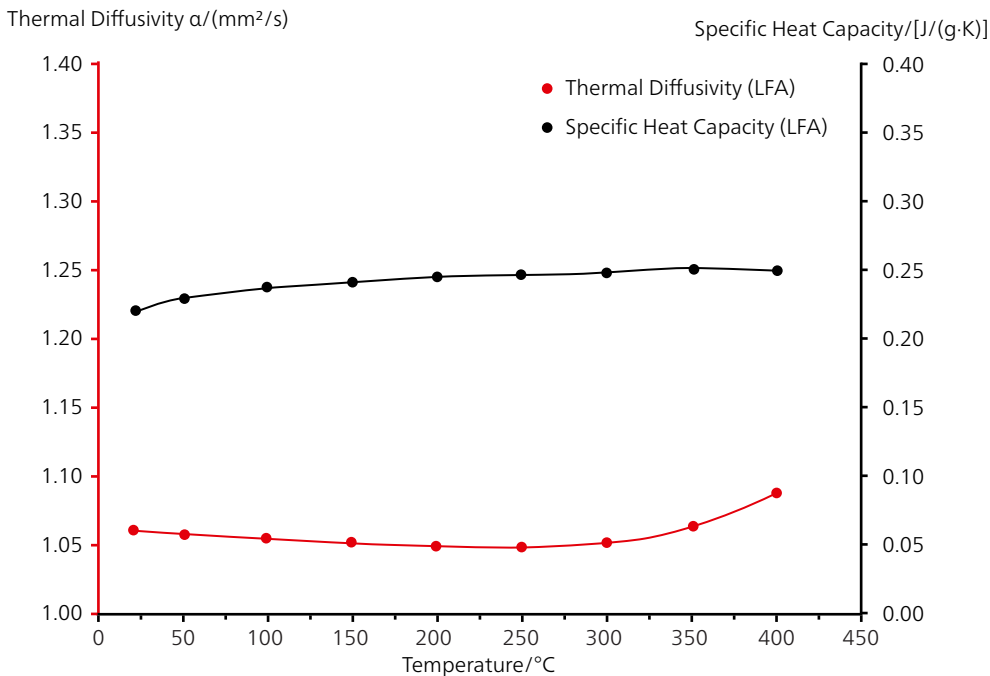
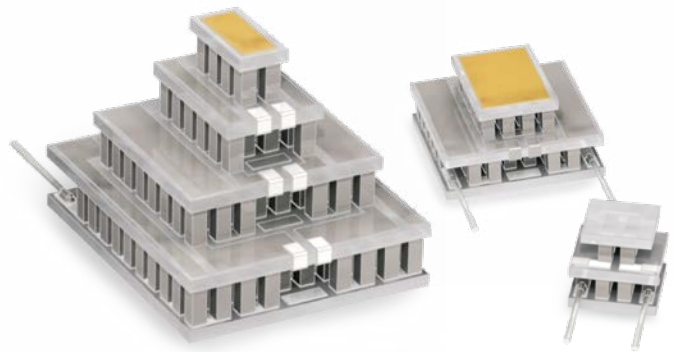


Figure 1. Measurement of the thermal diffusivity (red curve) and the specific heat capacity (black curve) of Skutterudite by means of LFA

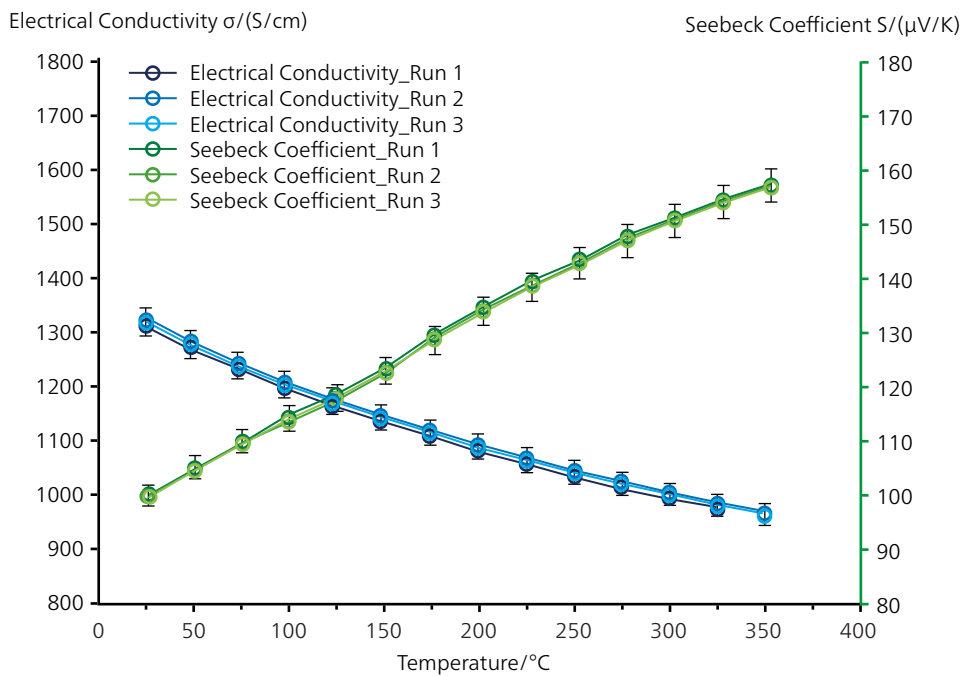


Figure 2. Determination of the Seebeck coefficient and electrical conductivity between RT and 350°C with the SBA 458 *Nemesis*®



Figure 3. Only one sample is required for the demonstration of the  $ZT$  value

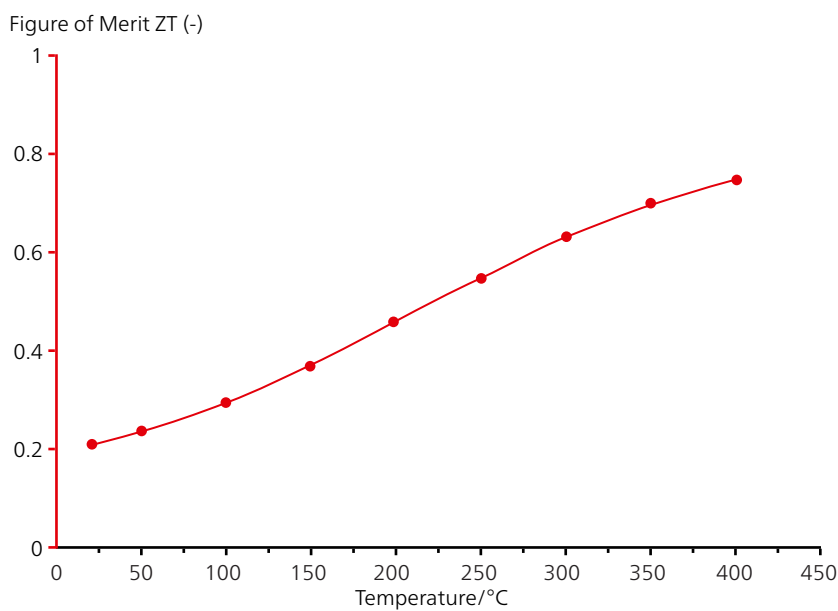


Figure 4. Temperature-dependence of the  $ZT$  value of Skutterudite

# Related Materials and Other Applications

## Metal Injection Molding (MIM) – Optimization of the Debinding Process of a Metal Green Body for Highest Product Quality

### Introduction

Within the realm of metal powder injection (Metal Injection Molding – MIM), the organic binder present must be removed after molding without influencing the component's geometry. Debinding can be carried out via catalytic methods, with the help of solvents or by thermal treatment. A combination of different methods is often applied in order to achieve debinding as gently as possible with short processing times. The resulting porous brown body is very sensitive and usually contains only enough binder for the component to be sufficiently stable for handling during the subsequent sintering process.

To avoid cracking or blistering during the molding, high demands are made via process management during thermal debinding. It is important to adjust the process parameters selected to the binder system used. In this case, the NETZSCH Kinetics Neo software can deliver valuable information for optimization of the temperature profile and save much time over lengthy practical tests.

### Test Results: Decomposition Behavior

Thermogravimetry is an established method for the analysis of the decomposition behavior of thermoplastic components in organically bound metal or ceramic powders.

Test Conditions	
Instrument	TG 209 <b>F1</b> Libra®
Sample	Metal powder (MIM green body)
Sample mass	approx. 20 mg
Temperature range	RT to 475°C
Heating rates	0.1, 0.3, 1, 3, 5 and 10 K/min
Atmosphere	Nitrogen
Crucible	Pt

If multiple TGA investigations are carried out on the same material at different heating rates, these curves can be subjected to a kinetic evaluation. If a suitable formal model for the description of all experimental curves is found, almost any temperature-time-course can be derived.

Figure 1 shows six TGA measurements on a powder metal green body carried out at six different heating rates. In the temperature range up to approx. 475°C, several steps with a total mass loss of more than 9% each – a typical value for MIM green bodies – can clearly be seen. At an increasing heating rate, a significant shift of the TGA curves to higher temperatures also occurs.

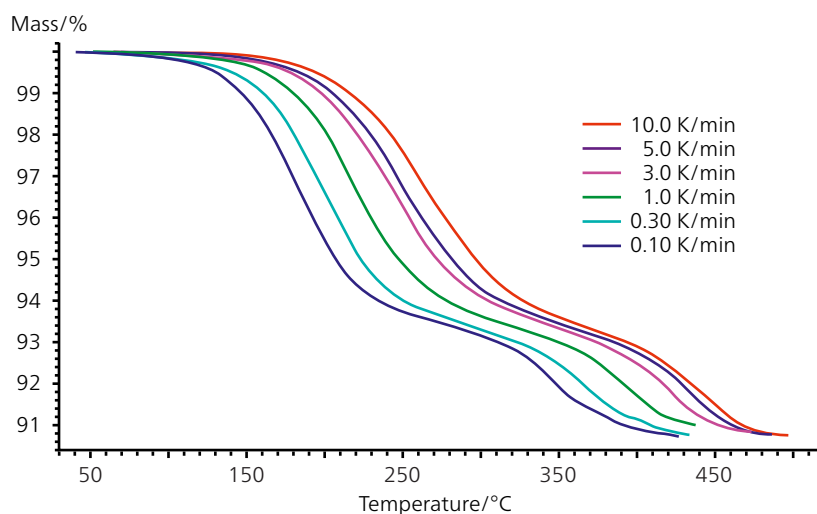


Figure 1. TGA measurement on an MIM green body at different heating rates in an N<sub>2</sub> atmosphere

Since the total mass changes observed are approximately the same in all cases, it is presumably very likely that no competing reactions were involved in the pyrolysis of the binder.

### Test Results: Kinetic Evaluation and Simulations

In a second step, the measuring data from Figure 1 was entered into the NETZSCH Kinetics Neo software and processed. Figure 2 shows the calculated kinetic model and compares the measured TGA curves with the calculated TGA curves using the kinetics software. The graphs reveal good correlation of the experimental data (colored symbols) with the calculated curves (black lines).

The best fit was achieved with a 4-step follow-up model under consideration of a diffusion reaction (3-dimensional according to Ginstling-Brownstein included in the software Kinetics Neo) as a first step. It was possible to depict the three following steps as a reaction of  $n^{\text{th}}$  order. The correlation coefficient of the fits amounts to 0.99994.

Based on the proposed kinetic model, it was then possible to make various predictions. Figure 3 shows the calculated temperature profile (red) for the realization of a constant mass decrease of 0.05% (blue) in the temperature range between 30°C and 475°C. The maximum allowable heating rate was assumed to be 50 K/min, which was also used within the first 5 minutes. The calculated heating rate decreases around 200°C to values below 1 K/min, only to increase again in two steps to about 5 K/min each.

The reverse path, however, is also possible. The objective in Figure 4 was to simulate the mass loss in a zone furnace. The calculated TGA signal is again depicted in blue; the stepwise temperature program in red. The individual temperature steps were 180°C, 200°C, 230°C, 290°C and 400°C. The isothermal phases in between were each 30 minutes long; for the heating from 30°C to 180°C, a heating rate of 50 K/min was defined. During the first two temperature steps, the calculated TGA signal exhibits almost linear behavior.

At higher temperatures, the mass losses actually increase when the defined temperature is reached.

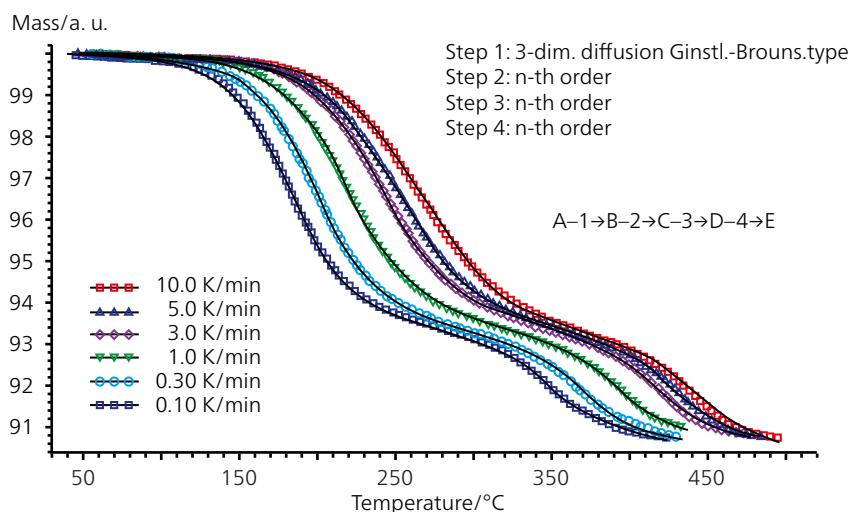


Figure 2. Comparison of the original TGA measurement data of an MIM green body (measured in an  $N_2$  atmosphere at different heating rates – colored symbols) with the curve fit (black lines), calculated by means of the NETZSCH Kinetics Neo software

# Related Materials and Other Applications

## Summary

Thermogravimetry (and simultaneous thermal analysis, STA) are ideal for analyzing the binder burnout from a green

body. Combined with thermokinetic analysis, this data can then be used to simulate different scenarios, determining optimal temperature profiles to increase and maintain product quality.

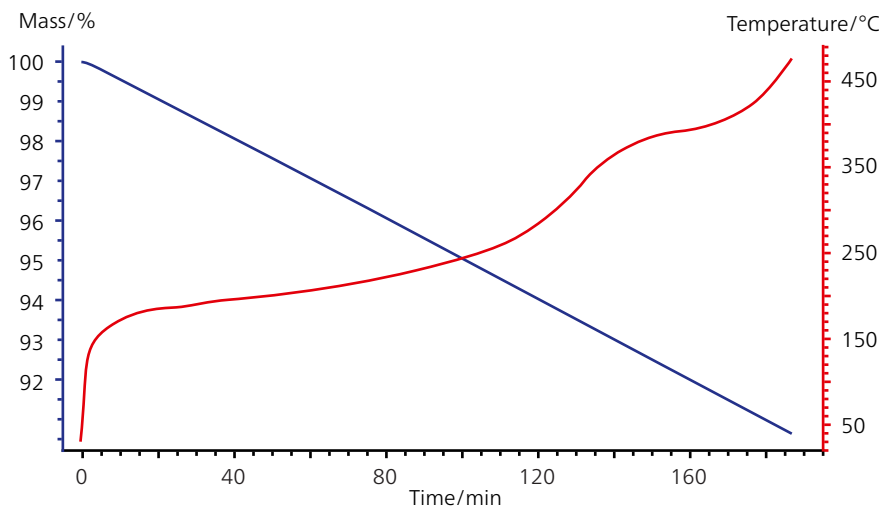


Figure 3. Prediction of the temperature profile (red) for a constant mass change of 0.05% (blue) on the basis of the kinetic model from Figure 2

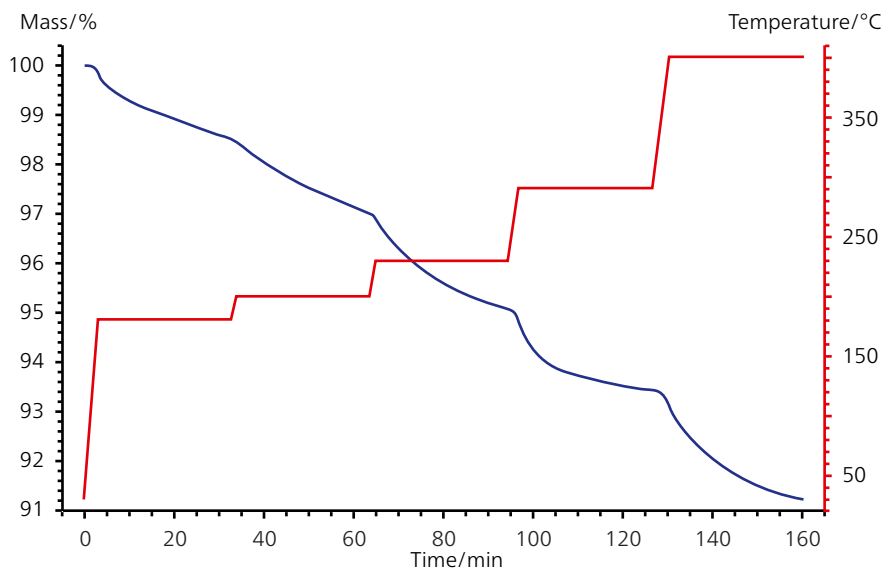


Figure 4. Prediction of the mass-change behavior (blue) by using a stepwise temperature program (red)







NETZSCH-Gerätebau GmbH  
Wittelsbacherstraße 42  
95100 Selb  
Germany  
Tel.: +49 9287 881-0  
Fax: +49 9287 881 505  
at@netzsch.com

Copyright © 2022 by NETZSCH-Gerätebau GmbH

All rights reserved. No part in this book may be reproduced in any form without written permission of the copyright owner.

Disclaimer of liability:  
NETZSCH-Gerätebau GmbH can make no guarantees for any of the information provided here nor claim any responsibility for its accuracy.



**NETZSCH®**

[www.netzsch.com](http://www.netzsch.com)

